

Design of gas bearing systems for precision applications

Citation for published version (APA):

Wang, J. (1993). *Design of gas bearing systems for precision applications*. [Phd Thesis 1 (Research TU/e / Graduation TU/e), Mechanical Engineering]. Technische Universiteit Eindhoven.
<https://doi.org/10.6100/IR391172>

DOI:

[10.6100/IR391172](https://doi.org/10.6100/IR391172)

Document status and date:

Published: 01/01/1993

Document Version:

Publisher's PDF, also known as Version of Record (includes final page, issue and volume numbers)

Please check the document version of this publication:

- A submitted manuscript is the version of the article upon submission and before peer-review. There can be important differences between the submitted version and the official published version of record. People interested in the research are advised to contact the author for the final version of the publication, or visit the DOI to the publisher's website.
- The final author version and the galley proof are versions of the publication after peer review.
- The final published version features the final layout of the paper including the volume, issue and page numbers.

[Link to publication](#)

General rights

Copyright and moral rights for the publications made accessible in the public portal are retained by the authors and/or other copyright owners and it is a condition of accessing publications that users recognise and abide by the legal requirements associated with these rights.

- Users may download and print one copy of any publication from the public portal for the purpose of private study or research.
- You may not further distribute the material or use it for any profit-making activity or commercial gain
- You may freely distribute the URL identifying the publication in the public portal.

If the publication is distributed under the terms of Article 25fa of the Dutch Copyright Act, indicated by the "Taverne" license above, please follow below link for the End User Agreement:

www.tue.nl/taverne

Take down policy

If you believe that this document breaches copyright please contact us at:

openaccess@tue.nl

providing details and we will investigate your claim.

**Design of Gas Bearing Systems
for Precision Applications**

Junming Wang

Design of Gas Bearing Systems for Precision Applications

PROEFSCHRIFT

ter verkrijging van de graad van doctor aan de
Technische Universiteit Eindhoven, op gezag van
de Rector Magnificus, prof. dr. J.H. van Lint,
voor een commissie aangewezen door het College
van Dekanen in het openbaar te verdedigen op
donderdag 7 januari 1993 om 16.00 uur

door

JUNMING WANG

geboren te Acheng, Heilongjiang (China)

Dit proefschrift is goedgekeurd
door de promotoren

prof. dr. ir. P. H. J. Schellekens
prof. dr. ir. M. J. W. Schouten

en de copromotor

dr. ir. J. W. M. C. Teeuwsen

ISBN 90-386-0112-3

To Xiao-Wei and
our parents

ACKNOWLEDGEMENT

First of all, I would like to express my great thanks to Prof. dr. ir. P. H. J. Schellekens and Prof. dr. ir. A. C. H. van der Wolf for the detailed financial and technical arrangements of the project and to the firm BOTECH, Helmond for his continuous funding and Mitutoyo Nederland R & D, for his financial contribution to the project. Without their supports, this project could not have been completed.

Next, I would like to express my gratitude to the staff and students who have, in one way or another, helped me through the course of this project, especially to Klaas Struik, Frits Theuws, Harry Sonnenmans, and Adriaan de Gilde, Metrology Laboratory, for their practical supports, to Jaap Snip and Eric Driessen, master students, Jinghan Yang, AIO, for their positive contributions to the work, and to Theo Maas, CTD, for his great help with the test set-ups.

I also wish to state my great appreciation to the promotors Prof. dr. ir. P. H. J. Schellekens and Prof. dr. ir. M. J. W. Schouten, the co-promotor dr. ir. J. W. M. C. Teeuwssen, and the other members of the reading committee, Prof. dr. ir. A. C. H. van der Wolf and Prof. dr. ir. A. A. van Steenhoven for their fruitful discussions and critical readings of this thesis.

I am also obliged to ing. P. L. Holster, Philips Research Laboratories, for his helpful discussions, to Mr. Tim Bell and Mr. Nigel Moody for correcting my English and to P. Mulders (TUE) for his carefully reviewing the thesis.

Finally, to Xiao-wei, my wife, for her patience, encouragement, and love throughout the endeavor.

CONTENTS

Contents	i
Nomenclatures	iv
Acknowledgements	vii
Chapter 1. General Introduction	1
1.1. Gas bearings and their history	1
1.2. Applications	2
1.3. Advantages and limitations	3
1.4. The scope of the present research	4
PART ONE: DESIGN OF EPG BEARING PADS	
Chapter 2. Theory of Externally Pressurized Gas Bearings	7
2.1. Introduction	7
2.2. The basic equations	7
2.2.1. The equation of motion	7
2.2.2. The energy equation for gas lubrication	9
2.2.3. The Nusselt number in gas lubrication	11
2.2.4. The continuity equation for EPG bearings	12
2.2.5. The Reynolds equation for EPG bearings	13
2.3. Special aspects	15
2.3.1. Gap shape	15
2.3.2. Bearing body tilt	16
2.3.3. Surface imperfections	17
2.4. Overall characteristics	19
2.4.1. Load capacity	19
2.4.2. Stiffness	20
2.4.3. Possible methods to achieve high stiffness	21
2.4.4. Damping stiffness	22
2.5. Refinement of restrictor flow model	23
2.5.1. Principles of orifice/inherent restrictors	23
2.5.2. Refinement	24
Chapter 3. Numerical Calculations and Experimental Verifications	26
3.1. Introduction	26
3.2. Numerical methods	26
3.2.1. Linearization	27
3.2.2. FEM formulations	28

3.2.3. Bearing design software	31
3.3. Experimental systems	32
3.3.1. The mechanical structure	32
3.3.2. The instrumentation	37
3.3.3. The test set-up for wall temperature	39
3.4. Tri-conical gap shaped EPG bearings	39
3.5. The effect of bearing body tilt	44
3.5.1. Higher supply pressure and lower working gap height	45
3.5.2. Higher supply pressure and higher working gap height	47
3.5.3. Lower supply pressure and higher working gap height	48
3.5.4. Lower supply pressure and lower working gap height	48
3.5.5. Rectangular pads	50
3.5.6. Effects of dimensions	50
3.5.7. Experimental verifications	51
3.5.8. Tilt effects on the dynamic performance	51
3.6. Effect of surface imperfection	52
3.6.1. Effect of waviness	53
3.6.2. Effect of roughness	56
3.7. Wall temperature	57
3.8. Effects of bearing motion velocity	61
3.9. Conclusions	62
PART TWO: DESIGN OF EPG BEARING SYSTEMS	
Chapter 4. Modeling of Linear Guides with EPG bearings	65
4.1. Introduction	65
4.2. Linear guides	66
4.2.1. Kinematical mounting	66
4.2.2. Loop stiffness	68
4.2.3. Symmetrical arrangement	69
4.2.4. Kinematical driving	69
4.2.5. Preloading	69
4.3. Model to describe the real bearing gap height	70
4.4. Idealization of gas film stiffness	73
4.4.1. The description of displacement dependence	74
4.4.2. The description of frequency dependence	75
4.5. Dynamic model	78

Contents

iii

4.5.1. The equation of motion	78
4.5.2. The natural frequency	79
4.5.3. Solution methods	82
4.5.4. Determination of vibration modes	84
4.6. Effects of non-linearity of film stiffness	85
4.7. Conclusions	86
Chapter 5. Experiments on a Linear Guide with EPG Bearing Pads	87
5.1. Introduction	87
5.2. Design of the linear guide	88
5.2.1. Mechanical structure	88
5.2.2. Analysis	92
5.3. Experiments	96
5.3.1. Experimental set-up	96
5.3.2. The identification of vibration modes	98
5.3.2.1. Fully symmetrical configuration (I)	99
5.3.2.2. Partially symmetrical configuration(II)	100
5.3.2.3. Influence of eccentric mass	103
5.4. Discussions	104
5.4.1. Symmetry	104
5.4.2. Influence of the support of the guide beam	104
5.5. Conclusions	105
Chapter 6. Conclusions and Recommendations	106
6.1. Conclusions	106
6.2. Recommendations	108
Appendix 1. The simplification of the equation of motion	109
Appendix 2. The simplification of the energy equation	112
Appendix 3. The Joule-Thomson coefficient	113
Appendix 4. The FEM formulation of the Reynolds equation	114
Appendix 5. The analysis of ball-cone pair	117
Appendix 6. The analysis of rigid-flexible mounting pair	120
Appendix 7. The equations of the vibration motion of the slide	122
Appendix 8. Test results of vibration of the slide	125
References	128
Summary	134
Samenvatting	136
Curriculum Vitae	138

NOMENCLATURES

English letters

A	: bearing area	m^2
A _d	: restrictor hole area	m^2
C _J	: the reduced Reynolds number	-
C _{Jo}	: the specific reduced Reynolds number	-
C _m	: reduced Mach number	-
c _d	: discharge coefficient	-
c _p	: heat capacity at constant pressure	$J\ kg^{-1}K^{-1}$
div	: divergency	-
dd	: restrictor diameter	m
DD	: bearing pad diameter	m
DC	: diameter of conical region of tri-/bi-conical pads	m
e	: eccentricity	m
E	: elasticity	$N\ m^{-2}$
f	: the vector of body force	N
f	: frequency	s^{-1}
F _d	: dynamic force (moment)	N (Nm)
F _m	: mass force (inertial moment)	N (Nm)
grad	: gradient	-
h	: bearing gap height	m
h'	: dynamic change of bearing gap height	m
h ₀	: reference gap height	m
h _e	: average gap height in an element	m
h _t	: gap height change due to tilt at edge of a pad	m
h _w	: working gap height	m
Im	: imaginary	-
J, j	: the moment of inertia	Nm
j	: $j = \sqrt{-1}$	-
k	: ratio of specific heat, c_p/c_v	-
k _i	: permeability of porous materials	m^2
K	: correction factor for turbulent restrictor	-
K	: complex stiffness	$N\ m^{-1}$
K _n	: the Knudsen number, l_p/h	-
l _p	: molecular free path	m
L	: reference dimension	m

L_x, L_z	: half-wave length of a surface wave	m
\dot{m}	: mass flow	kg s ⁻¹
m_b	: mass of a pad	kg
M_x, M_z	: moment capacity	N m
M_c	: the reference Mach number	-
M_a	: the Mach number	-
M	: mass or inertial moment	kg (kg m)
$N\mu$: viscosity number	-
Nu	: the Nusselt number	-
P_e	: environmental pressure	Pa
P_0	: the pressure in the upstream of the restrictor	Pa
P, p	: pressure	Pa
Pr	: the Prandtl number, $\kappa/\mu c_p$	-
r	: coordinate	m
R	: gas constant	m ² s ⁻² K ⁻¹
Re	: the Reynolds number, $\rho Vh/\mu$	-
Re'	: the reduced Reynolds number, ψRe	-
S	: stiffness	N m ⁻¹
S_b	: average bulk stiffness	N m ⁻¹
T_1	: temperature in surface 1	K
T_2	: temperature in surface 2	K
T	: temperature	K
T_0	: stagnation temperature or reference temperature	K
T_s	: static temperature	K
t	: time	s.
U	: vector form of velocity in the bearing surface	m s ⁻¹
V	: vector form of velocity	m s ⁻¹
u, v, w	: velocity components	m s ⁻¹
W	: load capacity	N
\bar{W}	: load capacity per unit area	N m ⁻²
U, V, W	: reference velocities	m s ⁻¹
U', V', W'	: slip velocities	m s ⁻¹
x, y, z, X, Z	: coordinates	m

Greek letters

α, β	: initial phase angles of waviness	rad.
ϵ	: amplitude ratio of waviness,	-

δ	: $\delta=1$ in restrictor area, $\delta=0$ others	-
ϕ	: wave orientation angle	rad.
γ	: exponent concerning heat transfer process,	-
ψ	: the ratio of bearing gap and length or porosity	-
θ	: coordinate	rad.
θ, η	: tilt angles	rad.
ζ	: distance to tilt axis	m
λ	: ratio of bearing length and width	-
κ	: the coefficient of heat conductivity	$\text{W m}^{-1}\text{K}^{-1}$
μ	: viscosity of gas	Pa s
μ'	: apparent viscosity	Pa s
μ_0	: reference viscosity	Pa s
μ_J	: Joule-Thomson coefficient	Pa K^{-1}
ρ	: density of gas	kg m^{-3}
ρ'	: gas density near the bearing surface	kg m^{-3}
Δ	: change	-
ω	: angle frequency	rad. s^{-1}
α, β, γ	: rotation of slides	rad.

superscripts

o	: initial
i	: in-phase part
u	: out-of-phase part

footnotes

d	: downstream restrictor / dynamic	
e	: entrance	
f	: film	
h	: surface connected to the bearing pads	
i	: index	
in	: inlet	
J	: Joule-Thomson effect	Pa K^{-1}
0	: static or reference condition or specific	
R	: restrictor	
r	: restrictor	
m	: mass	
w	: wave	
x, y, z, r	: coordinates	

CHAPTER 1.

GENERAL INTRODUCTION

1.1. GAS BEARINGS AND THEIR HISTORY

An Externally Pressurized Gas (EPG) bearing is a kind of gas bearings in which gas is used as a lubricant. Like other fluid lubricated bearings, it serves two purposes: one is to support an external load; the other is to lubricate a pair of surfaces. In principle, load capacity of gas bearings can be provided by several physical phenomena, such as by external pressurization, relative shear motion, squeeze motion, supersonic effect, jet effect, Bernoulli effect, stretching and thermal effects. The EPG bearings are commonly used in the field of Precision Engineering so that they are dealt with in this thesis. In elements with externally pressurized gas lubrication, any relative motion across the film thickness is compensated by squeeze effects in the film and by restriction effects in the bearing gap and inlet restrictor(s). The first investigation into EPG bearings was the experimental work on the gas flow between two parallel surfaces [Willis, 1828]. Twenty-six years later, Hirn [Hirn, 1854] further stated that the gas might be used as a lubricant, but unfortunately gas bearing technology was limited by the general technological level of that time. The important theoretical breakthrough was the derivation of the pressure equation for thin fluid films [Reynolds, 1886]. Thereafter, with the advancement of the industrial revolution, the fluid film bearings began to appear in machines, as well as gas bearings. The practical use of EPG bearings did not emerge until W. H. Wood [Wood, 1890] patented the counterbalance system using externally pressurized gas. The early application to metrology systems was the work at NPL (National Physics Laboratory, UK) in the 1930s. However, the EPG bearings (generally speaking all the gas bearings) were not taken seriously until 1959 when the First International Gas Bearing Symposium was opened [Fuller, 1959]. Thereafter, gas bearings have been applied in all the fields of engineering. In the field of Precision Engineering, EPG bearings are more popular because they provide better performance than the other types of gas bearings.

1.2. APPLICATIONS

Applications of EPG bearings may be found in all the engineering fields, especially in the field of Precision Engineering. EPG bearings (strictly speaking, externally pressurized gas lubricated elements) are mainly used for four purposes, i.e. motion supports (including journal and thrust bearings in spindles, guideways and leadscrews), actuators, fluid sealings and mechanical couplings, which are illustrated in Fig. 1.1.

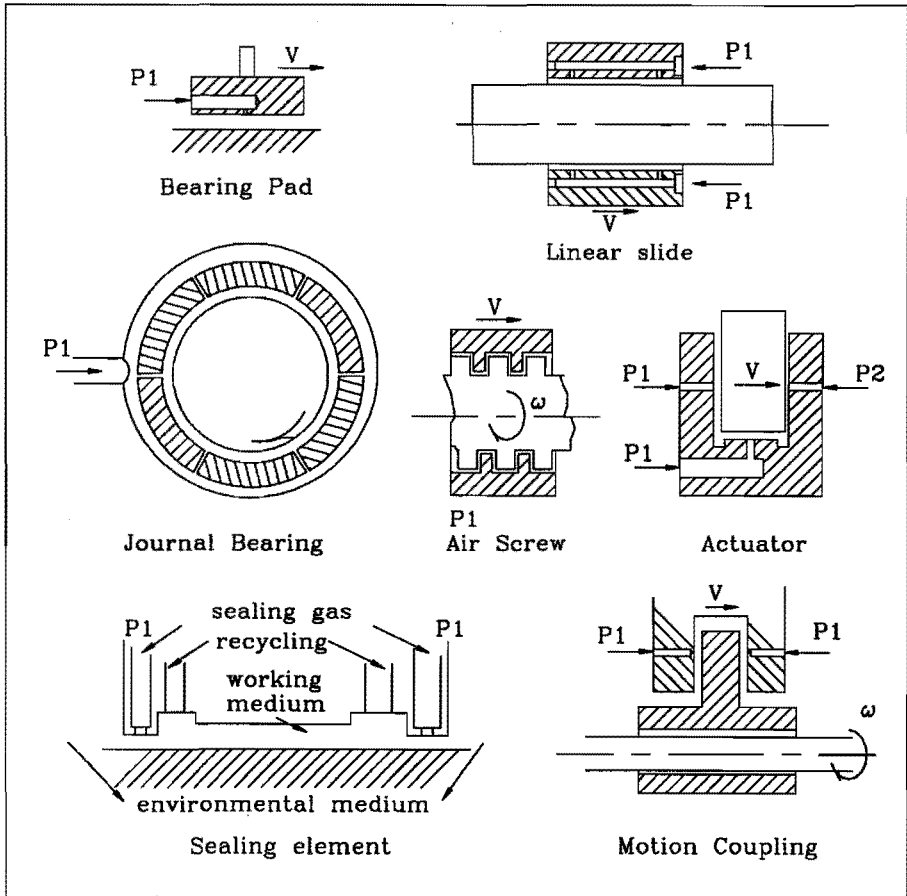


Fig. 1.1. Schematic illustration of EPG bearing family

The practical examples can be found in the following machines :

* metrology systems, e.g. :

-- coordinate measuring machines

- roughness and roundness measuring machines
- torque measuring systems
- probe systems
- * cutting systems, e.g. :
 - diamond turning and milling machines
 - grinding machines
 - print-board drilling machines
- * lithographical systems, e.g. :
 - optical exposure instruments
 - pattern writing and inspection instruments
 - silicon waver cutting and polishing machines
- * astronomical purposes, e.g. :
 - interferometers
 - gyrometers
- * turbomachinery, e.g. :
 - turbocompressor
 - steam lubricated blower

1.3. ADVANTAGES AND LIMITATIONS

Because gases are used as lubricant, EPG bearings have the following distinguishing characteristics:

1). Low and near constant friction: Because gases have very low values of viscosity and less sensitive to temperature and pressure change, the friction coefficients of EPG bearings are very low and are nearly constants, e.g. the reduction of residual friction torques to 10^{-6} of that of the ball bearings was achieved in the dynamometer used in the cage support of guidance gyros for rocket vehicles [Rothe, 1959].

2). No metal contact during operation: This is because the gas film separates the two bearing surfaces, which makes such bearings have a very low level of wear and mechanical noise.

3). Very high accuracy and very long accuracy life: The distributively pressurized gas presents averaging effects on bearing surface imperfections, e.g. roundness of a shaft. Therefore, very high accurate axis definition can be easily achieved [Li and Wang, 1983].

4). Wide working temperature range: In high temperature lubricated applications, the working temperature of gas bearings is limited by the solid

components in a machine. However, at the lower end, the temperature scale condensation of the gas may become a limitation. Complex gases on the other hand will have decomposition limitations at the upper end of their usable temperature range.

5). Environmental friendliness: The gases used in EPG bearings are the same as the environmental media, e.g. air in workshops and measuring rooms. Therefore, no pollution is introduced.

6). Micro-displacement feature: Although it is not really separable, this is quite useful in precision applications. The difference of supply pressures in two opposite directions is used to adjust a rotor position. For instance, it has been used as an actuator for high accuracy positioning mechanism [Kanai and Miyashita, 1983] and for motion error correcting systems [Shimokohbe et al, 1986].

There are some necessary conditions in order to make EPG bearings work properly. The specifications of these conditions depend on the requirements of a machine. In general, the following conditions are essential:

1). Continuous supply of externally pressurized gas with reasonable stabilization of pressure and filtration of dust, oil, water and other harmful matter.

2). Carefully prepared bearing surfaces with acceptable waviness and roughness.

3). Proper selection of heat expansion coefficients of bearing wall materials in the cases of high speed motion or of having a big change of environmental temperature.

4). Correct design of mechanical connections with sufficient mounting stiffness and possibility of self-alignment.

5). Taking care of gas temperature and temperature change through restriction process.

1.4. THE SCOPE OF THE PRESENT RESEARCH

The development of gas bearings follows the general trend of technological progress. With ever increasing machine accuracy, the EPG bearings have to provide better performance. In the field of gas bearing technology, there are still less understanding and poor quantification on the various subjects, such as:

1). accurate and correct modeling of the restrictor flow;

- 2). detailed study into the electronically controlled restrictor;
- 3). transient behaviours;
- 4). various subjects related to the application in precision engineering.

The following topics closely related to the applications in Precision Engineering will be discussed in this thesis:

- 1). influences of gap shape on the bearing performance;
- 2). effects of bearing body tilt on the bearing performance;
- 3). influences of bearing surface imperfections on bearing performance;
- 4). temperature drops in EPG bearings in quasi-stationary conditions;
- 5). the optimal use of multiple bearings in a mechanical system;
- 6). the use of EPG bearing damping characteristics in the design;
- 7). effects of motion velocity.

The aim of the research is to provide the up-to-date knowledge and the efficient tools to design better EPG bearing systems, including the design of individual bearings and to arrange all the bearings used in an optimal way. Both circular and rectangular EPG pads with rigid bearing surfaces and rigid inlet restrictors will be used in this research.

This thesis consists of two parts: Part one presents the design methods of single pads, as well as the numerical and experimental research on the above-mentioned special aspects. Part two gives the principles to design more accurate EPG bearing systems, as well as simulation and experiments on linear motion systems.

PART ONE
DESIGN OF EXTERNALLY PRESSURIZED GAS BEARINGS

CHAPTER 2.

THEORY OF EXTERNALLY PRESSURIZED GAS BEARINGS

2.1. INTRODUCTION

From a theoretical viewpoint, gas lubrication is concerned with the study of gas flow between two surfaces, the distance between these two surfaces being very small both in absolute value (less than 20 μm in most applications) and in comparison with the bearing dimensions (10^{-3} - 10^{-4}). Nevertheless, under those conditions, it is reasonable to neglect the molecular characteristics of the flow in the lubricant film of Externally Pressurized Gas (EPG) bearings and to consider the motion of gas as that of continuous fluid. However, if the permeability of a surface is high, e.g. bearings with porous walls [Majumder, 1988 & Sparrow et al, 1972] or the Knudsen number is greater than unity [Fukui and Kaneko, 1987], such as self-acting bearings used in the magnetic driver of information storage systems, the slip velocity at the bearing walls should be taken into account. In this chapter, we first discuss basic equations for gas lubrication, particularly in the EPG lubrication. Furthermore, the pressure equation, known as the Reynolds equation will be discussed in detail with consideration of bearing gap shape, bearing body tilt and surface imperfections. Afterwards, the overall characteristics will be described, with special attention to the relationship between basic concepts in gas dynamics and fluid mechanics, which can reveal ways to improve bearing characteristics. Finally, the models for bearing wall temperature and the refinement of inlet restrictor flow will be presented.

2.2. THE BASIC EQUATIONS

The equations used in the EPG bearings are adopted from the equations for viscous compressible fluids which are derived from the physical properties of gases and from the general equations of mechanics and thermodynamics.

2.2.1 The equation of motion

The equation of motion can be derived by characterizing the dynamic equilibrium between the inertia forces, the mass forces and the stresses in the fluid. By comparing the relative order of various terms in the equation of motion, it can be taken as a simple form in the gas lubrication (the simplification of the equation of motion will be given in Appendix 1) :

$$\rho \frac{Du}{Dt} = -\frac{\partial p}{\partial x} + \frac{\partial}{\partial y} \left(\mu \frac{\partial u}{\partial y} \right)$$

$$0 = -\frac{\partial p}{\partial y} \quad (2.1)$$

$$\rho \frac{Dw}{Dt} = -\frac{\partial p}{\partial z} + \frac{\partial}{\partial y} \left(\mu \frac{\partial w}{\partial y} \right)$$

where

$$\frac{D}{Dt} = \frac{\partial}{\partial t} + u \frac{\partial}{\partial x} + v \frac{\partial}{\partial y} + w \frac{\partial}{\partial z}$$

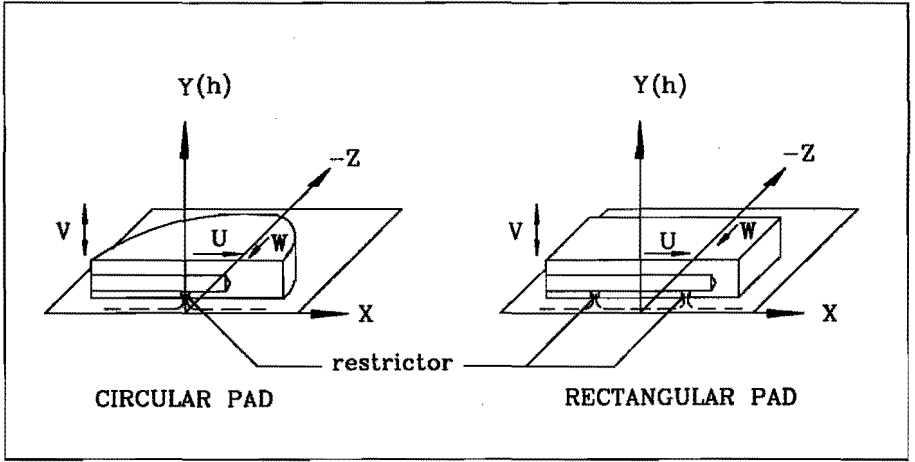


Fig. 2.1. Illustration of the coordinate system

From the reference [Wang, 1990], the dimensionless form reads :

$$k M_a^2 \frac{D\bar{u}}{D\bar{t}} = -\frac{\partial \bar{p}}{\partial \bar{x}} + N\mu \frac{\partial}{\partial \bar{y}} \left(\bar{\mu} \frac{\partial \bar{u}}{\partial \bar{y}} \right)$$

$$0 = -\frac{\partial \bar{p}}{\partial \bar{y}} \quad (2.2)$$

$$k (\lambda M_a)^2 \frac{D\bar{w}}{D\bar{t}} = -\frac{\partial \bar{p}}{\partial \bar{z}} + N\mu \frac{\partial}{\partial \bar{y}} \left(\bar{\mu} \frac{\partial \bar{w}}{\partial \bar{y}} \right)$$

where k : ratio of specific heat, $k = 1.4$ for air,

R : gas constant,

M_a : the Mach number, $U_0/(kRT_0)^{1/2}$, note that $\rho/P_0 = 1/(RT_0)$

U_0 : reference velocity,

T_0 : reference temperature,

$N\mu$: the viscosity number, $N\mu = \mu_0/\mu'$,

μ' : the apparent viscosity, $\mu' = (h_0/L)P_0h_0/U$ which is a measure of the combination of the operation parameters of a bearing.

$$\begin{aligned}
 x &= L \bar{x}, \quad y = h_0 \bar{y}, \quad z = \lambda L \bar{z}, \\
 u &= U \bar{u}, \quad v = \varphi U \bar{v}, \quad w = U \lambda \bar{w}, \\
 t &= (L/U) \bar{t}, \quad p = P_0 \bar{p}, \quad \mu = \mu_0 \bar{\mu}, \quad \varphi = h_0/L, \quad \lambda = L_w/L, \\
 L, L_w &: \text{reference dimensions in two coordinate directions separately} \\
 h_0, T_0, P_0, \mu_0 &: \text{reference values.}
 \end{aligned}$$

The reference parameters should be carefully selected, otherwise the dimensionless form will lead to the wrong result. The reference velocity for EPG bearings should take the gas flow velocity not that of the bearing motion velocity as it is used in the self-acting bearings. This is because the pressure is generated by bearing motion. From the dimensionless form of the equation of motion, it can be seen that the inertia force term in the left-hand side of the equation of motion is governed by a specific form of the Mach number, $k(M_a)^2$. The Mach number is the ratio of the gas velocity over the velocity of sound, its physical meaning can be interpreted as a measure of the weight between the inertia force and the pressure force. In linear motion systems, the optimal working gap height varies between the 10 ~ 15 μm for parallel gap shaped EPG bearings and around 5 μm for conical or tri-conical gap shaped bearings. From the observation on the flow phenomena of EPG bearings, given in Fig 2.2, it can be seen that the specific Mach numbers are negligible in the range of the optimal working gap height. This suggests that we can even take a simpler form of the equation of motion, i.e. without concerning the inertia effect :

$$\begin{aligned}
 0 &= -\frac{\partial p}{\partial x} + \frac{\partial}{\partial y} \left(\mu \frac{\partial u}{\partial y} \right) \\
 0 &= -\frac{\partial p}{\partial y} \tag{2.3} \\
 0 &= -\frac{\partial p}{\partial z} + \frac{\partial}{\partial y} \left(\mu \frac{\partial w}{\partial y} \right)
 \end{aligned}$$

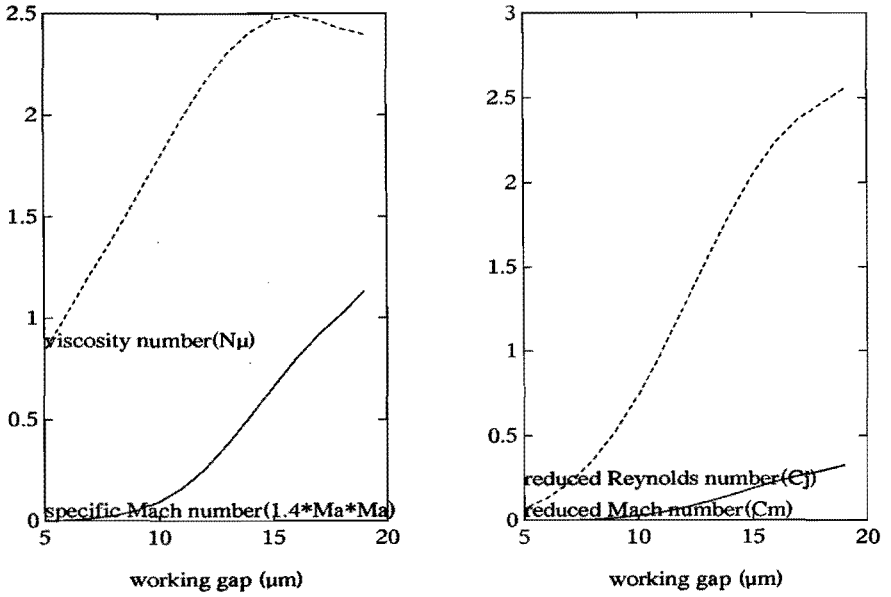
2.2.2. The energy equation for gas lubrication

Estimation of the relative order in the energy equation yields the following form for gas lubrication(the derivation will be given in Appendix 2)

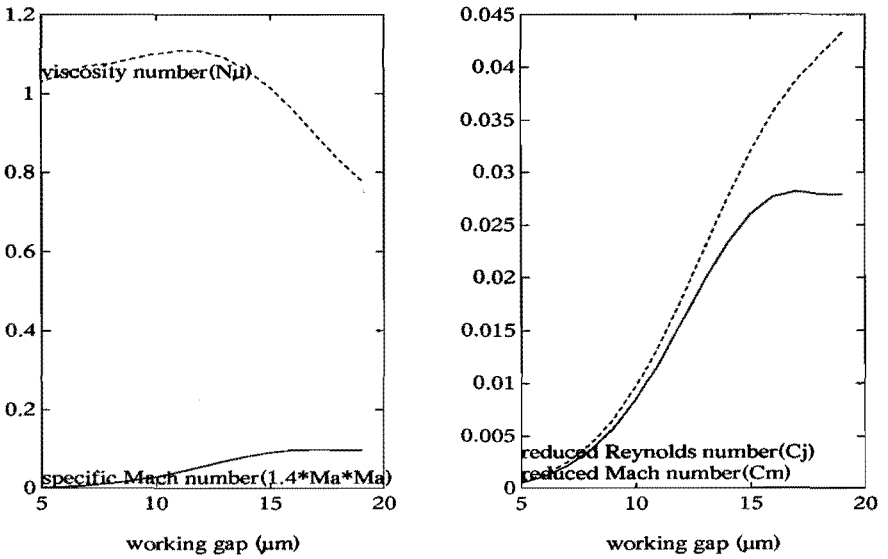
$$\rho c_p \frac{DT_0}{Dt} = \frac{\partial}{\partial y} \left(\kappa \frac{\partial T_s}{\partial y} \right) + \frac{\partial p}{\partial t} + \frac{\partial}{\partial y} \left[\mu u \frac{\partial u}{\partial y} \right] + \frac{\partial}{\partial y} \left[\mu w \frac{\partial w}{\partial y} \right] \tag{2.4}$$

The dimensionless form can be written as :

$$C_J \frac{D\bar{T}_0}{D\bar{t}} = \frac{\partial}{\partial \bar{y}} \left(\bar{\kappa} \frac{\partial \bar{T}_s}{\partial \bar{y}} \right) + C_{J_0} \left(\frac{\partial \bar{p}}{\partial \bar{t}} \right) + C_m \left[\frac{\partial}{\partial \bar{y}} \left(\bar{\mu} \bar{u} \frac{\partial \bar{u}}{\partial \bar{y}} \right) + \frac{\partial}{\partial \bar{y}} \left(\bar{w} \bar{\mu} \frac{\partial \bar{w}}{\partial \bar{y}} \right) \right] \tag{2.5}$$



(a) tri-conical gap shaped circular EPG bearing pads



(b) rectangular EPG pads with orifice restrictors

Fig. 2.2. The reduced Reynolds number (C_j), the reduced Mach number (C_m), the specific Mach number (kMa^2) and the viscosity number ($N\mu$)

where

- Re : the Reynolds number, $Re = \rho u h/\mu$,
- Pr : the Prandtl number, $Pr = c_p \mu/\kappa$
- C_J : the reduced Reynolds number, $C_J = Re Pr \varphi$, $\varphi = h/L$
- C_{J0} : the specific reduced Reynolds number, $C_{J0} = Re_0 Pr \varphi$
- Re₀ : the specific Reynolds number, $Re_0 = \rho_0 u_0 h_0/\mu_0$
- C_m : the reduced Mach number, $(k-1) M_a^2$
- $\bar{T}_s = T_s/T$, $\bar{T}_0 = T_0/T$, $\bar{\kappa} = \kappa/\kappa_r$, T_0, κ_r : reference parameters

In cases where the inertia effect can be ignored, the gas stagnation temperature on the left-hand side of the energy equation can be replaced by the gas static temperature.

From Fig. 2.2b, one can see that both the reduced Mach number and the reduced Reynolds number are much smaller than the unit for the bearings with the orifice restrictor. Hence, the energy equation in this situation is reduced to the conduction term alone. It is also true for the conical gap shaped pad at the optimal working gap height. However, the convection term still remains for the conical gap shaped bearings in higher working gap height :

$$\frac{\partial}{\partial \bar{y}} (\bar{\kappa} \frac{\partial \bar{T}_s}{\partial \bar{y}}) + C_{J0} \left(\frac{\partial \bar{p}}{\partial \bar{t}} \right) = \begin{cases} C_J \frac{D\bar{T}_0}{D\bar{t}} & \text{for conical/triconical bearings} \\ 0 & \text{for bearings with orifice restrictor} \end{cases} \quad (2.6)$$

2.2.3 The Nusselt number in gas lubrication

The integral of the equation (2.6) with the consideration of the boundary conditions yields the Nusselt number in two bearing walls. The geometrical meaning of the Nusselt number is the dimensionless temperature gradient at the wall. Physically, it is a measure of the weight between the heat conduction and the convection. Hence, the energy equation can be written as :

$$N_{uh} + N_{u0} = \begin{cases} C_J \left[\int_0^h \frac{\partial \bar{T}_0}{\partial \bar{t}} d\bar{y} + \int_0^h \bar{u} \frac{\partial \bar{T}_0}{\partial \bar{x}} d\bar{y} + \frac{1}{\lambda} \int_0^h \bar{w} \frac{\partial \bar{T}_0}{\partial \bar{z}} d\bar{y} + \int_0^h \bar{v} dT_0 \right] - C_{J0} \int_0^h \frac{\partial \bar{p}}{\partial \bar{t}} d\bar{y} \\ C_{J0} \int_0^h \frac{\partial \bar{p}}{\partial \bar{t}} d\bar{y} \end{cases} \quad (2.7)$$

In the heat equilibrium condition, it is much simplified :

$$N_{uh} + N_{u0} = \begin{cases} C_J \left[\int_0^h \bar{u} \frac{\partial \bar{T}_0}{\partial \bar{x}} d\bar{y} + \frac{1}{\lambda} \int_0^h \bar{w} \frac{\partial \bar{T}_0}{\partial \bar{z}} d\bar{y} + \int_0^h \bar{v} dT_0 \right] \\ 0 \end{cases} \quad (2.8)$$

2.2.4. The continuity equation for EPG bearings

By denoting the components of the velocity V of a fluid particle with u , v , w , the equation of continuity in a cartesian coordinate system (x,y,z) reads :

$$\frac{\partial \rho}{\partial t} + \text{div}(\rho V) = 0 \quad (2.9)$$

or the expansion form :

$$\frac{\partial \rho}{\partial t} + \frac{\partial(\rho u)}{\partial x} + \frac{\partial(\rho v)}{\partial y} + \frac{\partial(\rho w)}{\partial z} = 0 \quad (2.10)$$

For the thin film problem, it is convenient to consider the integral form of the continuity equation :

$$\int_0^h \frac{\partial \rho}{\partial t} dy + \int_0^h \frac{\partial(\rho u)}{\partial x} dy + \int_0^h \frac{\partial(\rho v)}{\partial y} dy + \int_0^h \frac{\partial(\rho w)}{\partial z} dy = 0 \quad (2.11)$$

Using the mathematical formula [Constantinescu, 1967] :

$$\int_0^h \frac{\partial}{\partial x} [f(x,y)] dy = \frac{\partial}{\partial x} \int_0^h f(x,y) dy - f(x,h) \frac{\partial h}{\partial x} \quad (2.12)$$

the continuity equation becomes :

$$\frac{\partial(\rho h)}{\partial t} + \frac{\partial}{\partial x} \int_0^h \rho u dy + \frac{\partial}{\partial z} \int_0^h \rho w dy = -(\rho V_h + \sum \delta \rho_i V_{r_i}) + \rho (U_h \frac{\partial h}{\partial x} + W_h \frac{\partial h}{\partial z} + \frac{\partial h}{\partial t}) \quad (2.13)$$

where:

footnotes for U , V , W have the following meanings: h stands for the velocity of the surface h and o for the velocity of the surface in X - Z plane shown in Fig. 2.1; r indicates velocity at the restrictor. In fact, $\partial h / \partial t = V_h$, the bearing body motion along the y -axis. For an EPG bearing with impermeable walls and one surface slow motion (U_h and $W_h \Rightarrow 0$), only one term remains on the right-hand side of the continuity equation, i.e. $\sum \delta \rho_i V_{r_i}$, where V_{r_i} is the function of ρ_i , the \sum stands for the sum of all the inlet restrictors and δ is an operational factor to indicate whether the restrictor is included or not.

If the gas film is bounded by permeable materials, the velocity in the bearing surface h is equal to the slip velocity, so that the terms on the right-hand side of the continuity equation read :

$$\rho [U_h \frac{\partial h}{\partial x} + W_h \frac{\partial h}{\partial z} + V_h] + \sum \delta \rho_i V_{r_i} \quad (2.14)$$

For the non-permeable bearing walls, the components of slip velocity

disappear and the continuity equation becomes :

$$\frac{\partial(\rho h)}{\partial t} + \frac{\partial}{\partial x} \int_0^h \rho u \, dy + \frac{\partial}{\partial z} \int_0^h \rho w \, dy + \sum \rho_i \delta V_{r_i} = 0 \tag{2.15}$$

The term $\rho_i V_{r_i}$ represents the unit area mass flow from a restrictor in the perpendicular direction to the gas film. Mathematically, it is a remaining term from the equation of continuity to describe the mass flow from a restrictor which cannot be indicated by the two dimensional Reynolds equation.

In order to derive the pressure equation - the Reynolds equation, the velocity terms in the continuity equation must be replaced by the pressure terms. The equation of motion gives the relationship between the pressure and the velocity.

2.2.5 The Reynolds equation for EPG bearings

This type of equation is so called due to the fact that Lord Reynolds first derived it for a thin oil film [Reynolds, 1886]. The Reynolds equation is derived by introducing the expression of velocity into the continuity equation while the velocity expression can be found by solving the equation of motion. The Reynolds type of equation was also given in general form by several authors [Cope, 1949] [Dowson, 1962] for lubrication problems. However, the commonly used Reynolds equation for EPG bearings is adapted from that for hydrodynamic gas or aerodynamic bearings. The problem is that the entrance effect is difficult to incorporate because there is no description in the region between the outlet of the restrictor and the entrance of the bearing gap. The attempt to solve this problem was to introduce the entrance correction factor [McCabe et al, 1969] [Vorh, 1969] [Bennett et al, 1976] [Pan 1980] [Wen et al, 1983] [Scharrer and Hibbs 1990] or to modify the "common" form of the Reynolds equation by solving the equation of motion with inertia terms [Mori and Mori, 1981]. In fact, the entrance can be incorporated in the Reynolds equation by introducing the outlet boundary condition of the inlet restrictor during the derivation of the Reynolds type of equation from the equation of continuity.

In cases where the inertia effects can be neglected, the velocity distribution across the film thickness as the function of x or z can be found by integrating the equations of motion (4). i.e. :

$$V = \text{grad} (p) [I^{1y} - I^{1h} (I^{0y}/I^{0h})] + U (I^{0y}/I^{0h}) \tag{2.16}$$

where

$$I^{1y} = \int_0^y \frac{y}{\mu} dy, \quad I^{0y} = \int_0^y \frac{dy}{\mu}, \quad I^{1h} = \int_0^h \frac{y}{\mu} dy, \quad I^{0h} = \int_0^h \frac{dy}{\mu} \quad (2.17)$$

By introducing the velocity distributions into the continuity equation, the corresponding Reynolds equation can be found :

$$\text{div} [-\Pi^1 \rho \text{grad}(p) + \rho U \Pi^0] + \frac{\partial h \rho}{\partial t} + \sum \delta \rho_i V_{r_i} = 0 \quad (2.18)$$

where

$$\Pi^1 = [I^{1y} - I^{1h} (I^{0y}/I^{0h})], \quad \Pi^0 = (I^{0y}/I^{0h}) \quad (2.19)$$

Investigations [Kao, 1963][Constantinescu, 1969] showed that the Reynolds type equation in cases where two walls have different temperature values can be replaced by the "normal" Reynolds equation with the average temperature of two walls. Therefore, only the Reynolds equation under isothermal conditions is more interesting in detail :

$$\text{div} [-\frac{h^3}{12\mu} p \text{grad}(p) + phU/2] + \frac{\partial hp}{\partial t} + f(p) = 0 \quad (2.20)$$

where

h is the bearing gap height. In general, it is a function of coordinates, i.e. $h = h(x, z)$, which includes the contribution from bearing float height {defined as working gap height (h_w)}, gap shape (h_g), surface imperfection (h_s) and pad body tilt (h_t). In some designs, it is also a function of pressure (h_p), where bearing surfaces are flexible. It can be written as :

$$h(x, z) = h_w + h_g(x, z) + h_t(x, z) + h_s(x, z) + h_p(x, z) \quad (2.21)$$

$$f(p) = \sum \delta p_i V_{r_i} (T_i/T_i) \quad (2.22)$$

The relationship between the entrance temperature (T_i) and the film temperature (T_f) can be found through the conservation law of mass flow, i.e. the mass flow at the exit of the restrictor must be equal to the mass flow at the entrance of bearing gap :

$$\dot{m}_e = \dot{m}_f \quad (2.23)$$

$$\text{or } V_e p_e A_e / RT_e = V_f p_f A_f / RT_f \quad (2.24)$$

Introducing the expressions for the areas $A_f = \pi d h$ and $A_e = \pi d^2/4$ yields :

$$V_e p_e (T_e/T_e) = V_f p_f 4h_e/d \quad (2.25)$$

Eventually, the term $f(p)$ reads:

$$f(p) = \sum \delta p_{fi} V_{fi} (4he/d) \tag{2.26}$$

where d : restrictor diameter; he : entrance gap height

In general, for the circular pads with rotation, it is convenient to use the expanded form of the Reynolds equation in the cylindrical coordinate system. In this coordinate system, the film thickness direction takes the height direction (z). The Reynolds equation for journal bearings takes radial direction as the film thickness direction in the cylindrical coordinate system. The Reynolds equation for the rectangular pads and the circular pads with linear motion is expanded in the Cartesian coordinate system and the z -direction is the film thickness. For the spherical bearings, the Reynolds equation is expanded in the spherical coordinate system and the radial direction is the film thickness direction. For bearings in linear motion systems, the expanded form of the Reynolds equation in the rectangular coordinate system is more convenient :

$$\frac{\partial}{\partial x} \left(\frac{ph^3}{12\mu} \frac{\partial p}{\partial x} \right) + \frac{\partial}{\partial z} \left(\frac{ph^3}{12\mu} \frac{\partial p}{\partial z} \right) = \frac{\partial ph}{\partial t} + \frac{\partial phU}{2\partial x} + \frac{\partial phW}{2\partial z} + f(p) \tag{2.27}$$

2.3. SPECIAL ASPECTS

2.3.1. Gap shape

Traditionally, the bearing gap shape is a linear line with zero slope, formed by two parallel surfaces. Research revealed that the modified gap shape can provide better overall characteristics, such as linear surface with a non-zero slope (conical gap shape) [Blondeel et al, 1976], multi-linear pieces with different slopes, two different slopes (bi-conical gap shape) [Blondeel et al, 1976] and three different slopes (tri-conical gap shape) [Wang, 1990] and flat surface with grooves (so called surface restriction). The gap shape of a multi conical circular pad can be described in the following way, the definitions of the terms are given in Fig. 2.3 :

$$h_{g_i} = \alpha_i hv_i + \sum_{j=i+1}^n hv_j \tag{2.28}$$

where

$\alpha_i = (r_i - r) / (r_i - r_{i-1})$ when $r_i > r > r_{i-1}$,
 r_0 : restrictor radius, hv_i : characteristic gap difference,
 r_i : characteristic radius, i : the index of conical parts.

2.3.2. Bearing body tilt

The bearing pad body may be rigidly tilted due to the errors of manufacturing and assembly, as well as the distortion caused by unsymmetrical loading and/or thermal loading. As a result, the bearing gap will be changed by the tilt, the change due to tilting can be expressed as :

$$h_t = x \theta + y \eta \tag{2.29}$$

where

$$\eta, \theta : \text{the tilt angles, } \theta = h_{tx}/(DD/2), \quad \eta = h_{tz}/(DD/2) \tag{2.30}$$

DD : the pad diameter, h_{tx} , h_{tz} : gap height change due to tilt

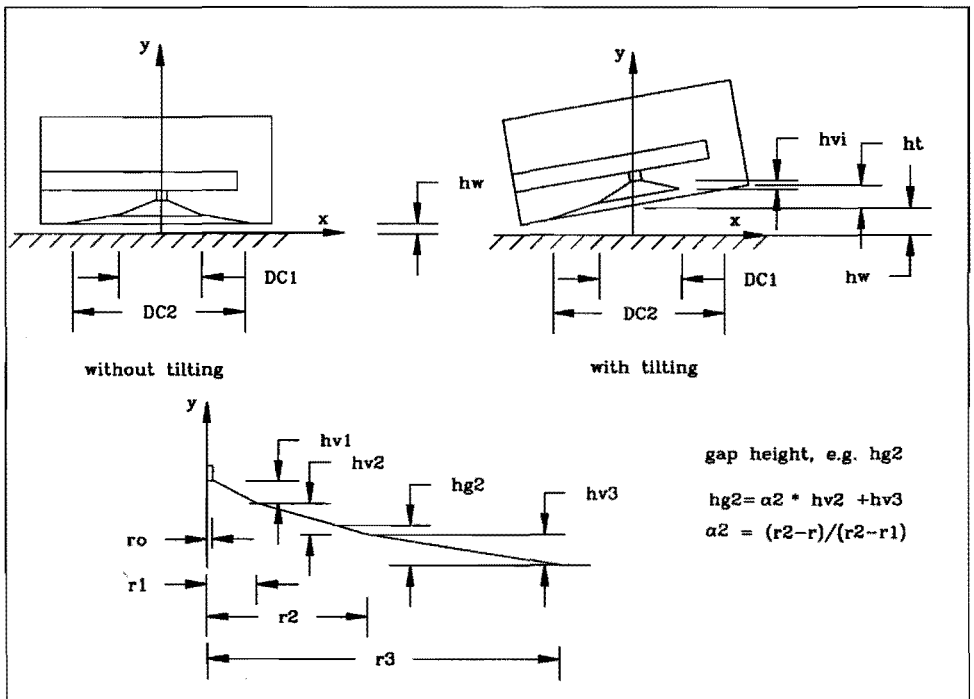


Fig. 2.3. Illustration of multi-conical circular EPG pads

For circular pads, tilting direction can be easily assigned to one set of coordinates. Therefore, the change of gap height due to tilt can be simplified as follows :

$$h_t = x \theta \tag{2.31}$$

Because the order of the tilt angle is less than 10^{-3} , the influences of it on the reference coordinate can be ignored. The theoretical study on a particular example was reported [Pande, 1985], later these types of bearing pads were more extensively studied under one dimensional model [Al-Bender and Brussels, 1992]. However, this thesis presents the comparative study on the different types of EPG bearing pads based on two dimensional model.

2.3.3 Surface imperfections

Typical discussions on the roughness effects [Mitsuya et al, 1989] [Tønder, 1984] [Raad and White, 1989] and waviness effects [Hayage, 1990] in hydrodynamic lubrication can be found in the literature. However, no related publication has been found for EPG lubrication. Reviewing the derivation of the Reynolds equation, it is found that the Reynolds equation is valid only when the inertia effect is neglected and the dimension ratio (the gap height over a reference length) is very small. Engineering surfaces always have certain imperfections due to errors of manufacturing and assembling, as well as the distortions of structures. The use of the Reynolds equation in such surfaces still requires those two conditions. One should note that in such a condition, the local dimension ratio (the roughness/waviness amplitude over the half wave-length) has to be considered. When this local dimension ratio meets the requirement, the Reynolds equation can be used to solve rough surface bearings with real gap shapes. If a surface can be considered as a sum of sine waves, the gap height contributed from surface imperfection can be written as :

$$h_s = h_0 \sum \epsilon_i \sin[\pi(x+X)/L_{xi} + \pi(z+Y)/L_{zi} + \alpha_i + \beta_i] \quad (2.32)$$

where

- h_0 : reference gap height
- ϵ_i : relative amplitude of *ith* wave
- α_i, β_i : initial phases of *ith* wave
- x, z : local coordinates, fixed on an EPG bearing
- X, Y : reference coordinates, fixed on the reference
- L_{xi}, L_{zi} : half-wavelength in X- and Z-direction

For the clearness and simplicity in the theoretical investigation into the effect of wave length and initial phase, one wave is considered. Furthermore, the surface waves may have their orientations. In order to

calculate the imperfection effect, the following form can be used :

$$h_s = h_0 [\varepsilon \sin(\pi (x+X) \cos\phi/L)] \quad (2.33)$$

where

ϕ : the orientation angle.

When the direction of motion is different from the wave direction, the apparent wave length will differ from the actual one. In the special case, when the moving direction is perpendicular to the wave direction, the position change will not change the moving body's behaviour. However, as expected, in the non-perpendicular direction, the performance of a moving body will change with the position change. For circular pads, the orientation of the surface wave will mean that flow in the gap takes a different pattern in the different radial direction.

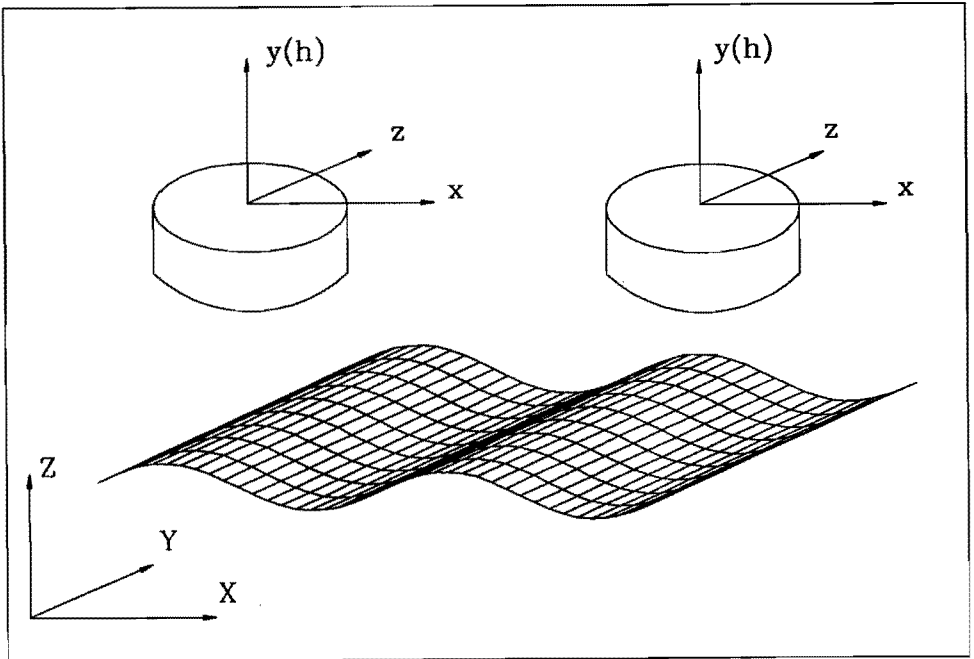


Fig. 2.4. Illustration of the coordinate systems for waviness study

Because the study on roughness effects is closely associated with the solution methods, it will be treated in Chapter 3. The references [Gans, 1987] [Patir and Cheng, 1984] [Wang, 1990] present the treatments for the random pattern of surfaces.

2.4. OVERALL CHARACTERISTICS

Because EPG bearings as mechanical elements are used to support moving bodies, the users of EPG bearings are more interested in the overall characteristics, such as the load capacity, stiffness, mass flow rate and damping. This section will present the general concepts of the global characteristics and some common ways to express them.

2.4.1. Load Capacity

The load capacity may be further divided into the bearing carrying force (W) and moment (M). The bearing carrying force is the integral of pressure distribution (p) over the whole bearing area (A). The bearing load capacity can be expressed as follows :

$$W = \int_A p \, dA \quad (2.34)$$

Using the relationship $p = \rho RT$, $\rho = dM/dV$ and $dV = h \, dA$, the load capacity reads :

$$W = RT M/h \quad (2.35)$$

where R : gas constant, T : temperature, M : mass content of gas

h : average gap height

The load per unit area can then be written as the following :

$$\bar{W} = W/A = \frac{1}{A} \int_A P \, dA = \frac{1}{A} \int_A K_T \, dA = \bar{K}_T \quad (2.36)$$

Which means that the load per unit area equals to the average isothermal bulk modulus (\bar{K}_T) of gas in a bearing. K_T is the local isothermal bulk modulus.

The bearing moment relative to the rotation axis of tilt reads :

$$M = \int_A \zeta P \, dA \quad (2.37)$$

The net load capacity and moment capacity of circular EPG pads with atmosphere as environmental pressure have the following forms :

$$W = \int_{-R}^R \int_{-xx}^{xx} (P-P_e) \, dz \, dx \quad (2.38)$$

$$M_x = \int_{-R}^R \int_{-xx}^{xx} (P-P_e) \, z \, dz \, dx \quad (2.39)$$

$$M_z = \int_{-R}^R \int_{-xx}^{xx} (P-P_e) \, x \, dz \, dx \quad (2.40)$$

where $xx = (R^2 - x^2)^{1/2} \quad (2.41)$

and rectangular EPG pads have the forms :

$$W = \int_{-a}^a \int_{-b}^b (P-P_e) \, dx \, dz \tag{2.42}$$

$$M_z = \int_{-a}^a \int_{-b}^b (P-P_e) \, x \, dx \, dz \tag{2.43}$$

$$M_x = \int_{-a}^a \int_{-b}^b (P-P_e) \, z \, dx \, dz \tag{2.44}$$

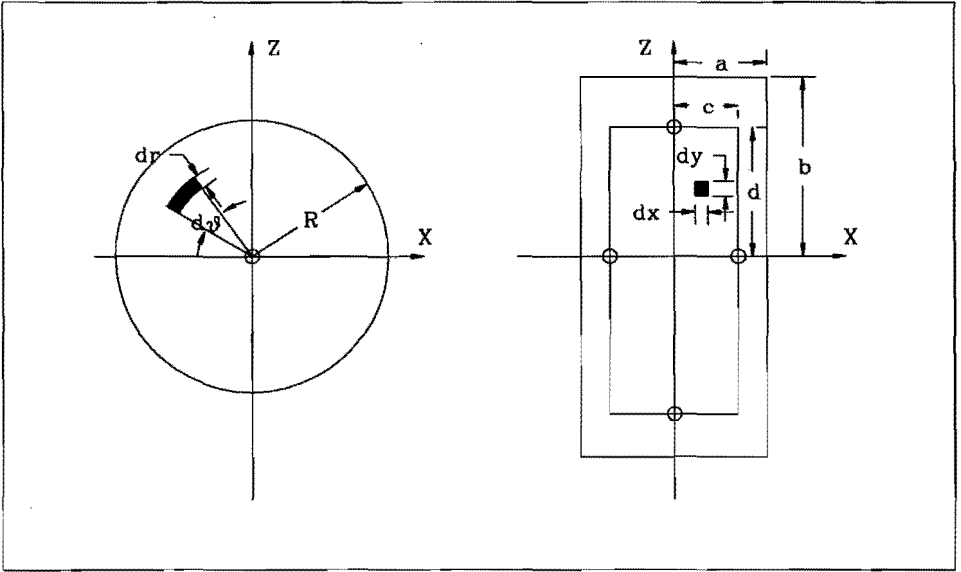


Fig. 2.5. Illustration of pad dimensions

2.4.2. Stiffness

The stiffness is the derivative of the load with respect to the working gap change which can be expressed as follows :

$$S = - \, dW/dh_w = - \int_A d/dh_w \, dA \tag{2.45}$$

The negative sign indicates that the change of the bearing working gap has an opposite direction to the load change. Using the relationship (2.35), the stiffness can be expressed as follows [Wang et al, 1988] :

$$S = \frac{RT}{h} \left(\frac{M}{h} - \frac{dM}{dh} \right) = \frac{RT}{h} \left(\frac{M}{h} + \frac{dM_{out}}{dh} - \frac{dM_{in}}{dh} \right) \tag{2.46}$$

$$S = S_b + S_{Mi} - S_{Mo} \tag{2.47}$$

Where M_{out} : amount of gas flowing out of a bearing

- M_{in} : amount of gas flowing into a bearing
 S_b : average bulk stiffness, $S_b = \bar{K}_T A/h = W/h$
 S_{Mi} : inlet stiffness due to mass content change caused by mass flow into the bearing
 S_{Mo} : outlet stiffness due to mass content change caused by mass flow out of the bearing.

This stiffness expression reveals the design principle for high stiffness, and infinite stiffness bearings. For the bearings with rigid bearing surfaces and a rigid restrictor, the stiffness takes average bulk stiffness as the highest limit which can not be achieved in the finite frequency range because the domination of inlet restriction effect. In principle, stiffness can be enhanced by designing a bearing with the dominant effect of outlet restriction. On the other hand, it can be seen that very high stiffness can be achieved by controlling the restriction effect in a correct way. For instance, the bearing with the membrane provides a negative outlet stiffness. When bearing load increases, the working gap decreases, at the same time, the membrane is deformed towards more concave. A suitable design of the membrane can provide the increased net change of mass flow content, i.e. negative change of mass flow content with respect to the working gap height. Therefore, the static stiffness can be much enhanced.

2.4.3. Possible methods to achieve high stiffness

The restrictors are key elements in improving the stiffness of EPG bearings. The pressure distribution in the bearing is determined by the type of inlet restrictors and the types of bearing gap shapes. A different type of the inlet restrictor determines a different boundary value of the inlet pressure, as well as the pressure gradient with respect to the working gap height, which determines inlet stiffness. The bearing gap shapes determine the pressure gradient with respect to the coordinate and with respect to working gap height, which means that the bearing gap shape determines the outlet stiffness.

The types of restrictors are illustrated in Fig. 2.6. The bearing gap shape controls the gas out-flow which can be seen as an outlet restrictor. From their functions, the restrictors can be divided into two types: one is the rigid restrictor and the other is the changeable restrictor which is applicable for both the inlet and the outlet restrictors. The rigid restrictor

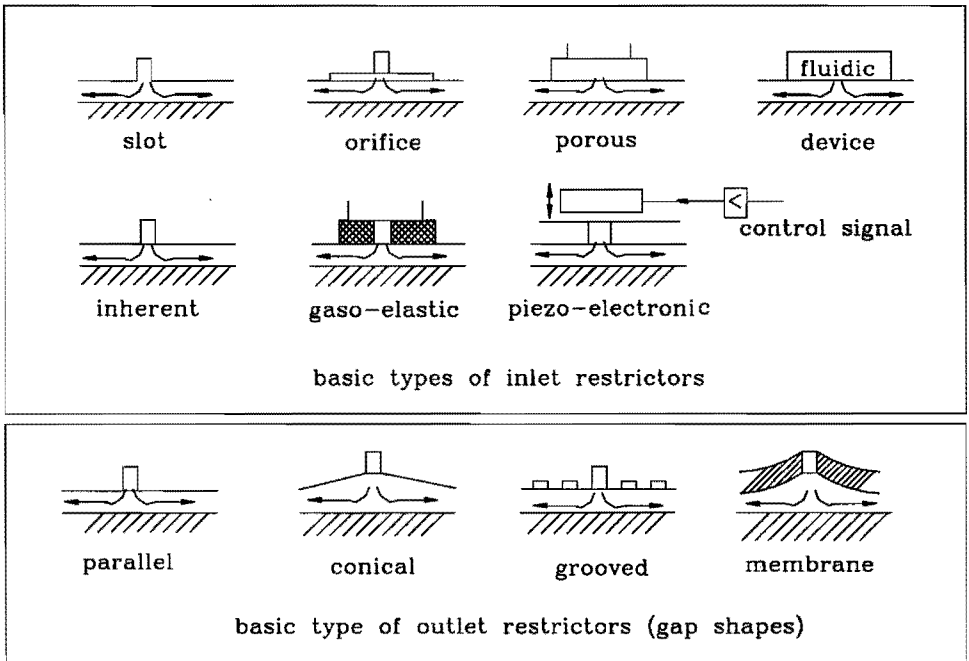


Fig. 2.6. Illustration of restrictor types

is named according to the geometry of restrictor shapes. The rigid restrictor can be further classified as hole, slot and device restrictors for the inlet restrictors and as simple (parallel) or modified gap shapes (such as conical and/or grooves) for outlet restrictor (bearing surfaces). The changeable restrictors are known by their auxiliary means, such as by the gaso-elastic properties of materials or by additional piezo-electric devices. The changeable restrictor can be used to design extremely high stiffness, as summarized in the references [Wang, 1988] [Wang, 1990].

2.4.4. Damping stiffness

The shape of the pressure profile is determined by the gap shape, the working gap height, and the boundary conditions of the pressure, the flow, the velocities and temperature in the ends of the gap outlet and the restrictor inlet. Therefore, both load capacity and stiffness depend on those parameters. When those parameters vary with time, the load capacity and stiffness become

complex variables and have two parts: in-phase and out of phase. The stiffness characteristics of EPG bearings can be expressed by a complex term which may be called complex stiffness. The imaginary part of the stiffness relates to the damping properties of the bearing. Therefore, the imaginary part of stiffness is defined as damping stiffness. The equivalent damping factor can be defined and will be treated in Chapter 4.

EPG bearings suffer self-excited vibration, termed pneumatic hammer, i.e. negative damping stiffness occurs. This is due to an unsuitable combination of operation and design parameters.

2.5. REFINEMENT OF RESTRICTOR FLOW MODEL

2.5.1. Principles of orifice/inherent restrictors

These are two types of restrictors which are commonly used, one is called an orifice restrictor and the other an inherent restrictor. The flow processes in those restrictors are traditionally modeled as adiabatic flow because of the very short flow length. The gas velocity under the conditions of non-viscous and incompressible flow is equal to the enthalpy change, [Yahya, 1982] i.e. :

$$u = [2c_p (T_0 - T)]^{1/2} \tag{2.48}$$

The mass flow rate can be calculated by :

$$\dot{m} = \rho u A \tag{2.49}$$

By using the adiabatic relationships :

$$T/T_0 = (p/p_0)^{(k-1)/k}, \rho/\rho_0 = (p/p_0)^{1/k} \tag{2.50}$$

the commonly used form can be derived :

$$m = c_d A P_0 [2 k/(k-1)/RT_0]^{1/2} \chi \tag{2.51}$$

where

$$\chi = \begin{cases} [(p_d/p_0)^{2/k} - (p_d/p_0)^{(k+1)/k}]^{1/2} & \text{when } p_d/p_0 > [2/(k+1)]^{k/(k-1)} \\ \{0.5 (k-1) [2/(k+1)]^{(k+1)/(k-1)}\}^{1/2} & \text{when } p_d/p_0 \leq [2/(k+1)]^{k/(k-1)} \end{cases}$$

c_d is known as the "discharge coefficient" and used to correct the errors due to the simplification of real flow.

In an inherent restrictor, gas flowing through the restrictor is proportionally controlled by the bearing working gap height and the restrictor area (A) which equals to the gap entrance area ($A = \pi d h_w$). In an orifice restrictor, a recess is introduced between the restrictor and the bearing gap, its restriction area is the hole area ($A = \pi d^2/4$). In applications, a realistic restriction area can be obtained by either an equivalent area [Holster and

Jacobs, 1986] or two restrictors connected in series [Gross et al, 1980]. The consideration on the entrance effect can be found in many references, such as luminary recovery [McCabe et al, 1969], geometrical effects [Bennett et al, 1976] [Wen et al, 1983] [Scharrer and Hibbs, 1990] and turbulent effect [Vorh, 1969] [Pan, 1980].

2.5.2. Refinement

From the earlier discussion of the derivation of the Reynolds equation for EPG lubrication, we noted that the restrictor flow was in the y-direction, which is beyond the limits of the two dimensional equation in the x-z plane (see Fig. 2.1). Therefore, an extra term was introduced to consider the restrictor flow, which directly results from the integral of the continuity equation. Note that the derivation of the mass flow introduces twice the uncertainty of a flow process, one by the temperature-pressure transformation and the other by the density-pressure transformation. The modified Reynolds equation derived in this chapter shows that the transform from density to pressure is not really necessary. The parameters evolved in the equation are the local pressure and the local velocity. By doing the density-pressure transform and using mass flow in the solution of the Reynolds equation, the local temperature appears again. The vague use of the environmental temperature instead of the local temperature, like that used in many references, already conflicts with the starting equation (2.48). The second problem in the traditional treatment of restrictors is to consider the turbulent effect. It is physically true that long before the turbulent occurs, the inertia effect can no longer be neglected. In practice, the bearing working gap height is below 20 μm , even below 10 μm in many applications so that the Reynolds number will be below the starting point for turbulent flow.

Those arguments define the present approach to look for a more realistic way to model the restrictor flow. From the discussion above, it is understood that only temperature-pressure relationship is important. From the basic theory of thermodynamics, we understand that devices like the inherent/orifice restrictor may show the Joule-Thomson effect [Zhang and Shi, 1978]. If the Joule-Thomson coefficient (μ) is added to the equation (2.48), the gas velocity becomes (the detailed derivation will be given in Appendix 3) :

$$u = [2c_p (T_0 - T_d) - \mu_j (P_0 - P_d)]^{1/2} \quad (2.53)$$

By comparison with the equation (2.48), the "discharge coefficient" for local velocity can be determined by :

$$c_d = [1 - \mu_j (P_0 - P_d)/(T_0 - T_d)]^{1/2} \tag{2.54}$$

From experience, it is known that the flow process through the restrictor is neither adiabatic nor isothermal, but somewhere in between. The Joule-Thomson coefficient is just a physical quantity to indicate the flow process. Fig. 2.7 presents the "discharge coefficient" with the pressure ratio calculated by the equation (2.54).

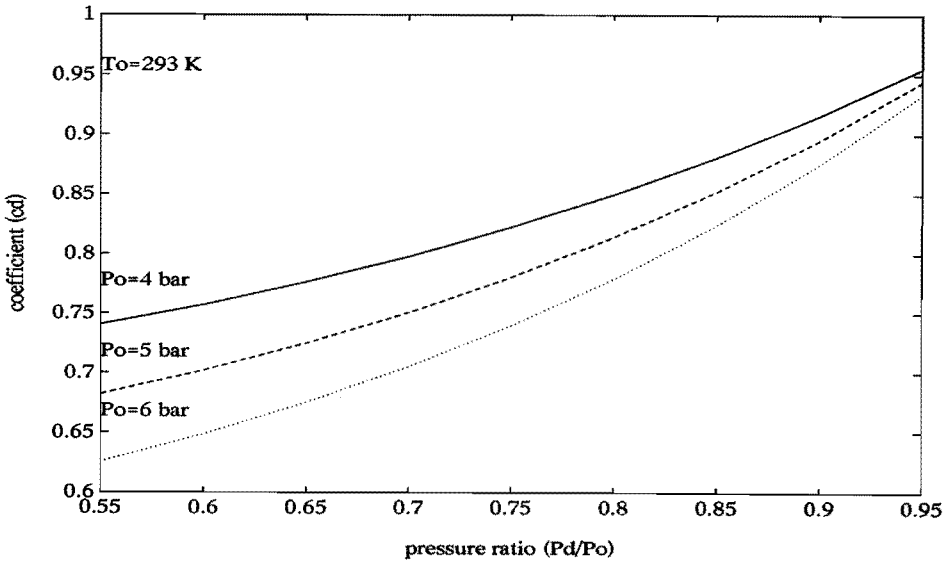


Fig. 2.7. "Discharge coefficient" of the flow through the restrictor calculated by the Joule-Thomson effect

CHAPTER 3.

NUMERICAL CALCULATIONS AND EXPERIMENTAL VERIFICATIONS

3.1. INTRODUCTION

This chapter deals with the practical aspects of designing an EPG bearing, including developments of the software and the experimental system. The Finite Element Method (FEM) was used to solve the Reynolds equation in order to calculate the overall characteristics of an EPG bearing. An experimental system was also developed to perform both static and dynamic tests of EPG bearings. Furthermore, the numerical and experimental results on both circular and rectangular pads are presented with particular attention to the effects of gap shape, bearing body tilt, surface imperfections, motion velocity and wall temperature.

3.2. NUMERICAL METHODS

With the ever increasing development and application of computer technology, it is convenient to use numerical methods to solve lubrication problems for achieving more accurate and more sophisticated results. In the late 60s, the numerical methods for gas bearing film analysis had already been given more attention [Castelli and Pirvics, 1968]. Recently, several new methods have also been developed for and applied to the gas lubrication problem, such as the Boundary Element Method [Lui et al, 1987], the Finite Difference Method [Tawfik and Stout, 1989], the local partial differential equation method [Li and Pan, 1987], and the inner collection method [Arerkere and Nelson, 1988]. Nevertheless, the Finite Element Method (FEM) seems more popular for EPG lubrications. Two dimensional FEM software was developed for the calculation of static properties of cylindrical and spherical journal bearing [Lui et al, 1983] and of conical and spherical journal bearings [Lin et al, 1990]. By using the standard FEM package, one dimensional FEM software was developed both for static and dynamic properties [Holster and Jacobs, 1989] and was later extended to combine the surface and permeability effects [Wang, 1990]. In this work, two dimensional FEM software was developed to calculate both static and dynamic characteristics with consideration of body tilt, surface imperfection and variable gap shape.

3.2.1. Linearization

The Reynolds equation given in Chapter 2. can be further separated into three equations by a harmonic perturbation around an equilibrium condition, $h = h_0 + \Delta h$ and $p = p_0 - \Delta p$. For a small change of periodic working gap height, say :

$$\Delta h = h' \sin(\omega t) \tag{3.1}$$

if the following change of the dynamic pressure distribution is chosen :

$$\Delta p = p^i \sin(\omega t) + p^u \cos(\omega t) \tag{3.2}$$

the time term can be eliminated from the Reynolds equation [Stiffler and Smith, 1975]. p^i is the dynamic pressure change in-phase with working gap height and p^u is the out of phase change with working gap height.

The part of the Reynolds equation for static operation reads :

$$\frac{\partial}{\partial x} \left(\frac{p_0 h_0^3}{12\mu} \frac{\partial p_0}{\partial x} \right) + \frac{\partial}{\partial z} \left(\frac{p_0^3 h_0}{12\mu} \frac{\partial p_0}{\partial z} \right) + \sum_{j=1}^n \delta f(p_j) = \frac{\partial p_0 h_0 U}{\partial x} + \frac{\partial p_0 h_0 W}{\partial z} \tag{3.3}$$

where $f(p_j) = p_j V_j$, the expression of V was given in Chapter 2.
 n: the number of restrictors

The part of the equation for dynamic operation with the term $\sin(\omega t)$ reads :

$$\begin{aligned} & \frac{\partial}{\partial x} \left(\frac{p_0 h_0^3}{12\mu} \frac{\partial p^i}{\partial x} \right) + \frac{\partial}{\partial z} \left(\frac{p_0 h_0^3}{12\mu} \frac{\partial p^i}{\partial z} \right) + \frac{\partial}{\partial x} \left(\frac{p^i h_0^3}{12\mu} \frac{\partial p_0}{\partial x} \right) + \frac{\partial}{\partial z} \left(\frac{p^i h_0^3}{12\mu} \frac{\partial p_0}{\partial z} \right) \\ & + 3p_0 h_0^2 h' \left(\frac{\partial p_0}{\partial x} + \frac{\partial p_0}{\partial z} \right) + \sum_{j=1}^n \delta p_j \frac{\partial f^0}{\partial p_j} + h' \frac{\partial f^0}{\partial h} \\ & = (\omega h_0 p^U) + \frac{1}{2} \left[\left(\frac{\partial p_0 h' U}{\partial x} + \frac{\partial p^i h_0 U}{\partial x} \right) + \left(\frac{\partial p_0 h' W}{\partial z} + \frac{\partial p^i h_0 W}{\partial z} \right) \right] \end{aligned} \tag{3.4}$$

The part of the equation for dynamic operation with the term of $\cos(\omega t)$ reads :

$$\begin{aligned} & \frac{\partial}{\partial x} \left(\frac{p_0 h_0^3}{12\mu} \frac{\partial p^u}{\partial x} \right) + \frac{\partial}{\partial z} \left(\frac{p_0 h_0^3}{12\mu} \frac{\partial p^u}{\partial z} \right) + \frac{\partial}{\partial x} \left(\frac{p^u h_0^3}{12\mu} \frac{\partial p_0}{\partial x} \right) + \frac{\partial}{\partial z} \left(\frac{p^u h_0^3}{12\mu} \frac{\partial p_0}{\partial z} \right) + \sum_{j=1}^n \delta p_j^u \frac{\partial f^0}{\partial p_j} = \\ & \omega(h_0 p^i + h' p_0) + \frac{1}{2} \left[\frac{\partial p^u h_0 U}{\partial x} + \frac{\partial p^u h_0 W}{\partial z} \right] \end{aligned} \tag{3.5}$$

The part of the equation for the static operation (3.3) can be further linearized by using the relation, $p_0 = p^0 - \Delta p_0$:

$$\begin{aligned} & \frac{\partial}{\partial x} \left[\frac{h_0^3}{12\mu} (p^0 \frac{\partial p_0}{\partial x} + p_0 \frac{\partial p^0}{\partial x}) \right] + \frac{\partial}{\partial z} \left[\frac{h_0^3}{12\mu} (p^0 \frac{\partial p_0}{\partial z} + p_0 \frac{\partial p^0}{\partial z}) \right] - \frac{\partial}{\partial x} \left(\frac{p^0 h_0^3}{12\mu} \frac{\partial p^0}{\partial x} \right) + \frac{\partial}{\partial z} \left(\frac{p^0 h_0^3}{12\mu} \frac{\partial p^0}{\partial z} \right) \\ & + \sum_{j=1}^n \delta (f^0(p_j) - p_j^0 \frac{\partial f^0}{\partial p_j} + p_0^0 \frac{\partial f^0}{\partial p_i}) = \frac{\partial p^0 h_0 U}{\partial x} + \frac{\partial p^0 h_0 W}{\partial z} \end{aligned} \tag{3.6}$$

3.2.2. FEM equations

The basis of FEM is to divide the total solution area into a finite number of sub-regions (so called sub-mesh). An example of the submesh plot for circular pads is given in Fig. 3.1. The triangular element is often used because it can be easily treated and has sufficient accuracy. The triangular element defines the interpolation function as a linear function which means that the pressure distribution over an element is a linear function of coordinates. At the edge of the bearing pad, the pressure is equal to the environmental pressure.

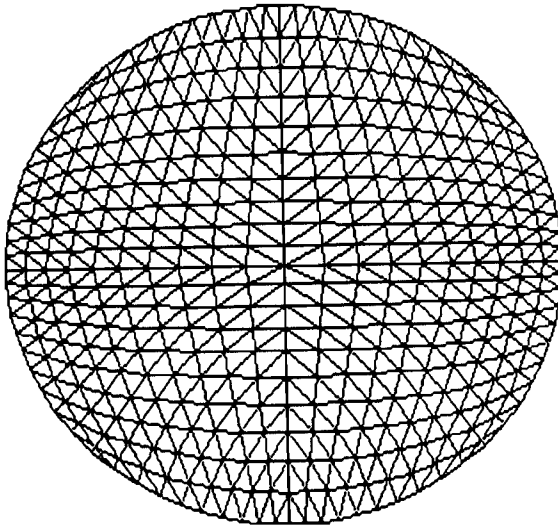


Fig. 3.1. Illustration of the FEM mesh of a circular EPG pad

FEM formulation can be performed with a combination of the Galerkin method, which can lead to a system of linear equations with nice numerical properties. The FEM formulation of the Reynolds equation can be derived by following the standard procedures [Cuvelier et al, 1986]. The resulting final system of linear algebraic equations for nodal pressure can be written in the matrix form :

$$\mathbf{K} \mathbf{P} = \mathbf{R} \quad (3.7)$$

where $\mathbf{P} = [P_1, P_2, \dots, P_N]^T$
 $\mathbf{R} = [R_1, R_2, \dots, R_N]^T$

From the FEM formulation, the components of the local coefficient matrix

K_{ij} and the components of the right-hand side vector, R_j in an element can be written as (the derivation will be given in Appendix 4) :

$$K_{kj} = \frac{h_e^3}{24\mu} \frac{|\Delta|}{\Delta^2} [(B_j \sum P_k B_k + C_j \sum P_k C_k)/3 + P_e^0 (B_j B_k + C_j C_k)] - \frac{h_e |\Delta|}{12 \Delta} (U^e B_k + W^e C_k) \tag{3.8a}$$

$$R_j = \frac{h_e^3}{24\mu} \frac{|\Delta|}{\Delta^2} p_e^0 (B_j \sum P_k B_k + C_j \sum P_k C_k) \tag{3.8b}$$

where

$$P_e = (P_1 + P_2 + P_3)/3 \text{ (due to the linear interpolation function)}$$

$$\int_{\Omega_e} d\Omega = |\Delta|/2, \quad \int_{\Omega} \psi_j d\Omega = |\Delta|/6$$

$$\frac{\partial p}{\partial \xi} = \sum_{j=1}^N P_j \frac{\partial \psi_j}{\partial \xi}$$

$$N = 3 \text{ for the triangular element and } \xi = x, z$$

$$\psi_j = (A_j + B_j x + C_j z)/\Delta$$

$$\frac{\partial \psi_j}{\partial x} = \frac{B_j}{\Delta} \quad \frac{\partial \psi_j}{\partial z} = \frac{C_j}{\Delta}$$

$$A_j = x_n z_{n+1} - x_{n+1} z_n, \quad B_j = z_n - z_{n+1}, \quad C_j = x_{n+1} - x_n$$

$$\text{with } n = \text{mod}[(j+1)/3], \text{ (mod is the operation to find remainder)}$$

Note that the restrictor area is so small that the restrictor region can be treated as a point element. The components in the coefficient matrix and the right-hand side vector read :

$$K_{mj} = -\frac{\partial f^0}{\partial p} A_d, \quad R_j = (f^0(p) - p \frac{\partial f^0}{\partial p}) A_d \tag{3.9}$$

The total matrix for the whole bearing area is arrived at by assembling all the local matrices and the right-hand side vectors.

Therefore, the pressure values in all the nodal points can be found by solving the set of linear equations, because the components in the coefficient matrix and the right hand side vector are all constants.

If the continuity equation is only used for the area which does not include the restrictor region, there will be no δ terms in the Reynolds equation. In this case, the restrictor flow is treated as the natural boundary, i.e. the flow or pressure gradient at the inlet is prescribed.

In the same way, the FEM formulation for the dynamic parts of the

Reynolds equation can be derived. In an element, the local matrix can be written as follows :

$$\mathbf{K} \mathbf{P} = 3 h_e P_e \mathbf{R} \quad (3.10)$$

where

$$\mathbf{P} = [P_1^i, P_1^u, P_2^i, P_2^u, P_3^i, P_3^u]^T \quad (3.11a)$$

$$\mathbf{K} = \begin{bmatrix} M_{11} & -2\omega N_{11} & M_{12} & -\omega N_{12} & M_{13} & -\omega N_{13} \\ 2\omega N_{11} & M_{12} & \omega N_{12} & M_{12} & \omega N_{13} & M_{13} \\ M_{21} & -\omega N_{21} & M_{22} & -2\omega N_{22} & M_{23} & -\omega N_{23} \\ \omega N_{21} & M_{21} & \omega N_{22} & M_{22} & 2\omega N_{23} & M_{23} \\ M_{31} & -\omega N_{31} & M_{32} & -\omega N_{32} & M_{33} & -2\omega N_{33} \\ \omega N_{31} & M_{31} & \omega N_{32} & M_{32} & 2\omega N_{33} & M_{33} \end{bmatrix} \quad (3.11b)$$

$$\mathbf{R} = [R_1^i, R_1^u, R_2^i, R_2^u, R_3^i, R_3^u]^T \quad (3.11c)$$

$$M_{kj} = \frac{h^3}{12\mu} \frac{|\Delta|}{\Delta} \left\{ (B_j \sum P_k B_k + C_j \sum P_k C_k)/6\Delta + P_e^0 (B_j B_k + C_j C_k)/2\Delta - (U^e B_k + W^e C_k) \right\} \quad (3.12a)$$

$$N_{kj} = h_d |\Delta| / 24 \quad (3.12b)$$

$$R_j^i = \frac{|\Delta|}{4\Delta} P_e^0 \left\{ \frac{h^2 h_d}{12\mu} (B_j \sum P_k B_k + C_j \sum P_k C_k) - (U^e B_k + W^e C_k) \right\} \quad (3.12c)$$

$$R_j^0 = h_d P_e^0 \omega |\Delta| / 8 \quad (3.12d)$$

In the point element, the components in the coefficient matrix and the right hand side vector read :

$$K_{ij}|_{i=j} = \frac{\partial f^0}{\partial p} A_d \quad R_j = \frac{\partial f^0}{\partial p} P_e^0 - \frac{\partial f^0}{\partial h} h_d \quad (3.13)$$

Therefore, the element subroutines for building the local matrix can be programmed by using the equations (3.8) ~ (3.13). The whole matrix is automatically assembled by the standard routines in the SEPRANTM package. The non-linear form of the static part of the Reynolds equation is solved by the Newton method. The use of the average value of the supply pressure and environmental pressure for a pad with distributed restrictor out of the centre (both a rectangular and circular pads) produces a good initial estimate of the static pressure P_0 . For the pad with a centre restrictor, the computation will converge more quickly to the desired accuracy by taking an initial estimate as

$$p(r) = [P_0 - (P_0 - P_e) r/R]^{1/2} \quad (3.14)$$

where

$$r = (x^2 + z^2)^{1/2} \text{ and } R \text{ is the radius of the bearing pads}$$

3.2.3. Bearing design software

A standard FEM package, SEPRANTM was installed in the PC computer, COMPAQ-386/20e, in the Laboratory of Precision Engineering, Eindhoven University of Technology, for solving problems of fluid flow or heat flow, and the problems coupled with mechanical structures. With the help of this package, a two dimensional, FEM, bearing design software was then developed in which effects of gap shape, bearing body tilt and surface imperfections were added. The software was written in FORTRAN supported by the FTN77/386TM compiler which was developed by the University of Salford, England. The software is capable of designing circular and rectangular EPG pads, as well as journal bearings. Both the static and dynamic properties can be calculated. For general purposes, the input parameters are divided into four groups:

- 1). operational parameters: supply and environmental pressures, frequency range, environmental temperature, working gap height and bearing motion velocity in the specified coordinate direction;
- 2). geometrical parameters: pad dimension(s) (e.g. diameter of circular pads), restrictor diameter, characteristic diameters (e.g. conical region diameter(s) and gap differences for conical gap shaped pads and groove parameters for both rectangular and circular pads;
- 3). gas properties: gas constant, viscosity, and specific heat ratio;
- 4). high order parameters: tilting ratios, surface wave lengths and their amplitudes, initial phases and orientation angles of waves.

The flow chart of the computer program is given in Fig. 3.2, which presents a global view of the program structure. The calculation starts with defining the input parameters and the desired outputs. The pressure distribution is then calculated under this specified condition. The load capacity is obtained by the integral of the pressure over the bearing area. The pressure distribution, load capacity, dynamic load changes, or stiffness and dynamic stiffness are separately stored in the ASCII files.

Some calculated pressure distributions are shown in Fig. 3.3, which demonstrate the capability of the software and show the inside view of the bearing characteristics.

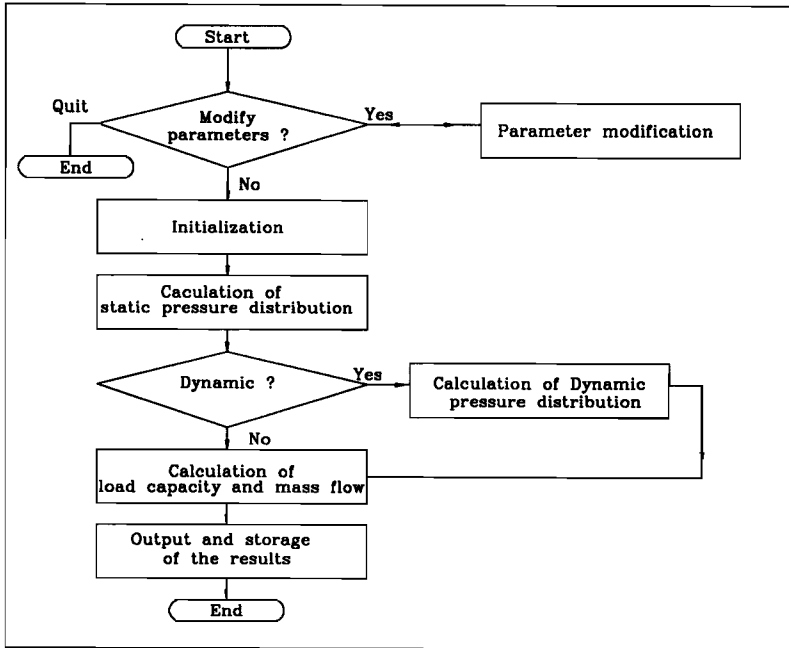


Fig. 3.2. The flow chart of the software for designing EPG bearings

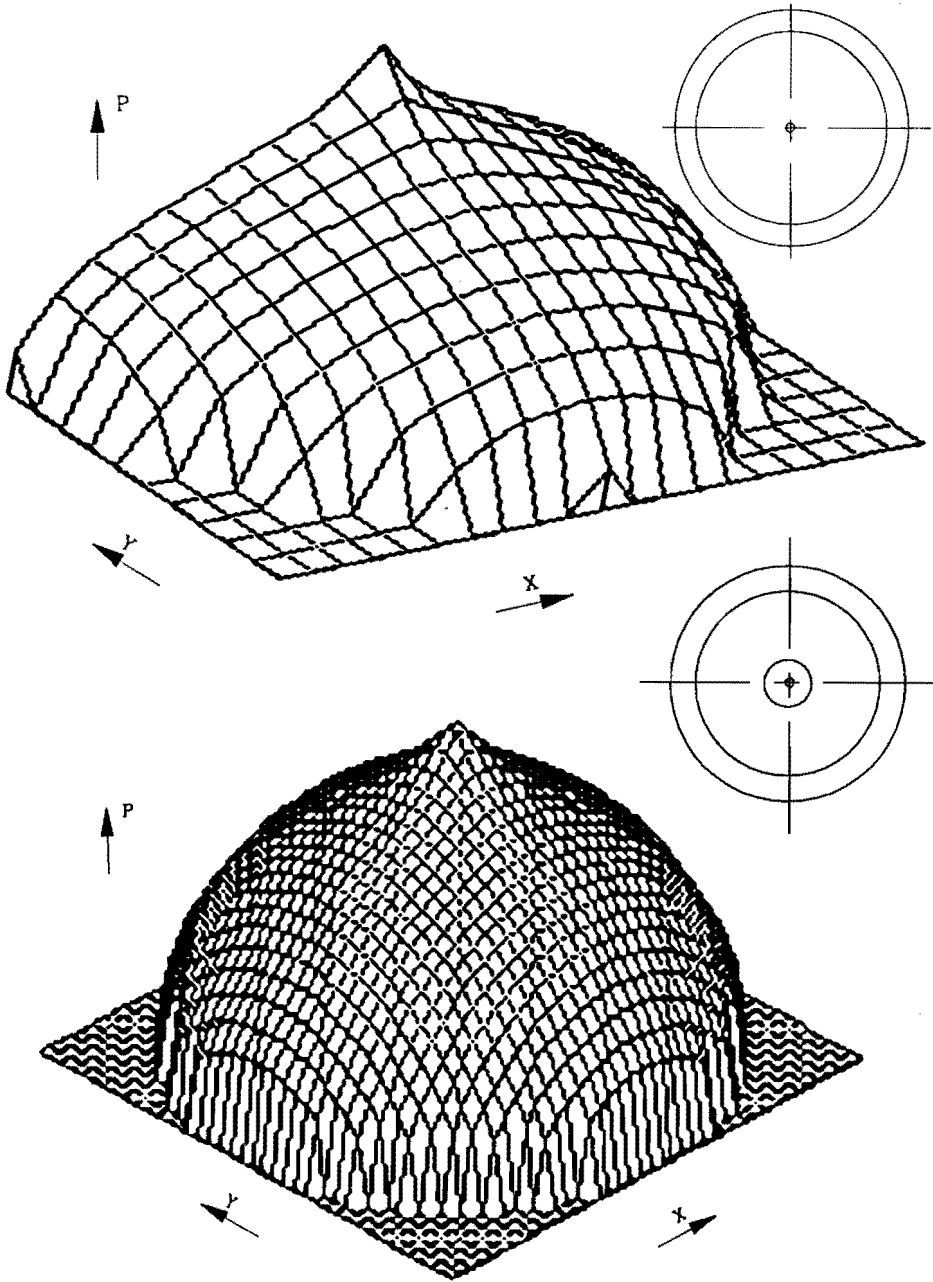
3.3. EXPERIMENTAL SYSTEMS

An experimental set-up was developed to perform both static and dynamic tests on bearing pads. Fig. 3.4 schematically illustrates the system. Through the air conditioning unit, the dust and oil in the inlet air are filtered out and the inlet air is also dried. The gas parameters, the pressure, temperature and flow rate of the inlet air are separately measured by the barometer, the built-in temperature sensor and the flow meter. The details will be explained in the following sections: 3.3.1. the mechanical structure and 3.3.2. the instrumentation.

3.3.1. The mechanical structure

The purpose of the mechanical structure is to support the elements for delivering the static and dynamic forces and to support the test bearings and pick-up sensors. The basic requirements are that:

- 1). its natural frequency should be out of the test frequency range;
- 2). it should be statically and dynamically stable during the test period;
- 3). there should be no interference between static and dynamic loading;



Conical gap shaped pads
Fig. 3.3a. Calculated pressure distributions (circular pads)

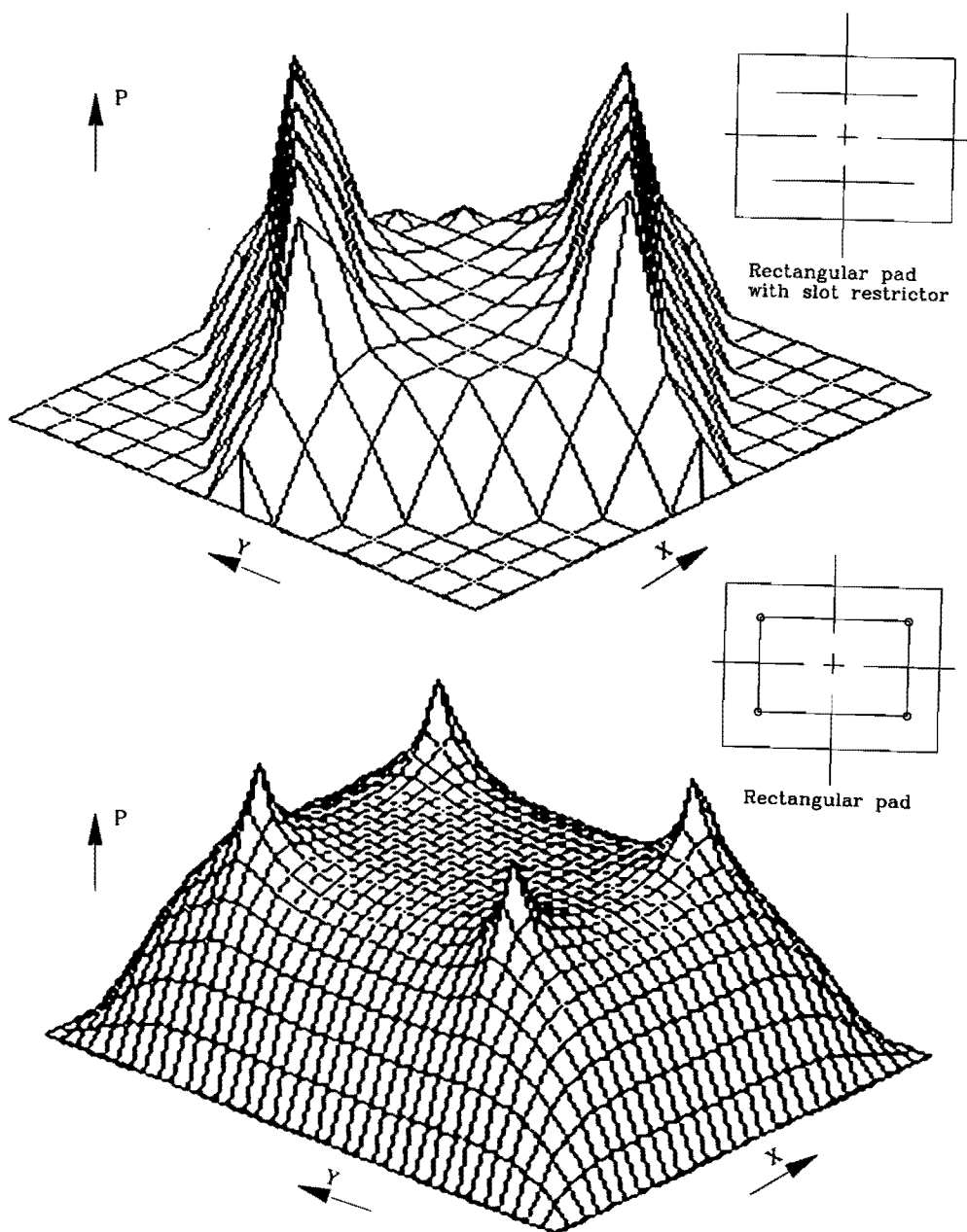


Fig. 3.3b. Calculated pressure distributions (rectangular pads)

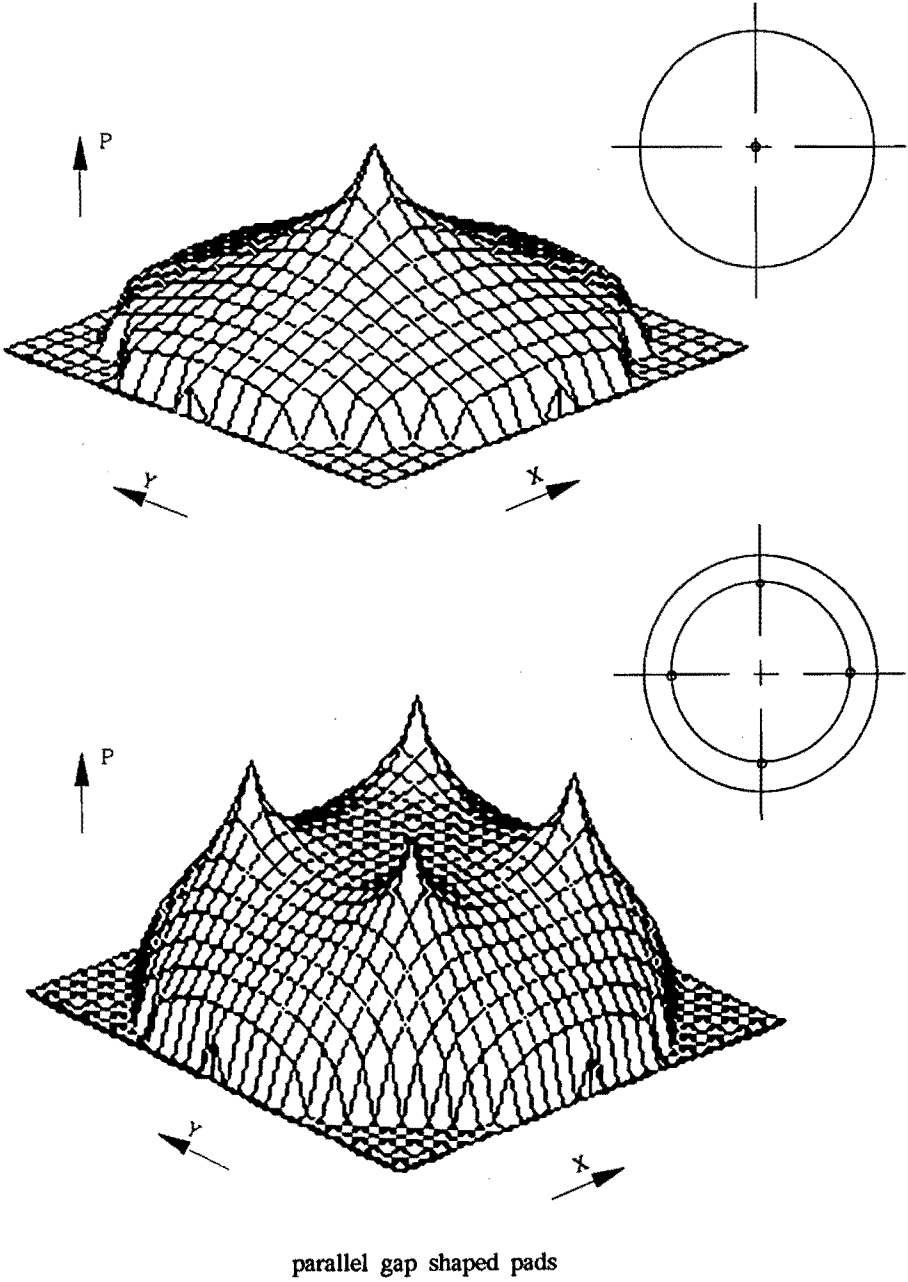


Fig. 3.3c. Calculated pressure distributions (circular pads)

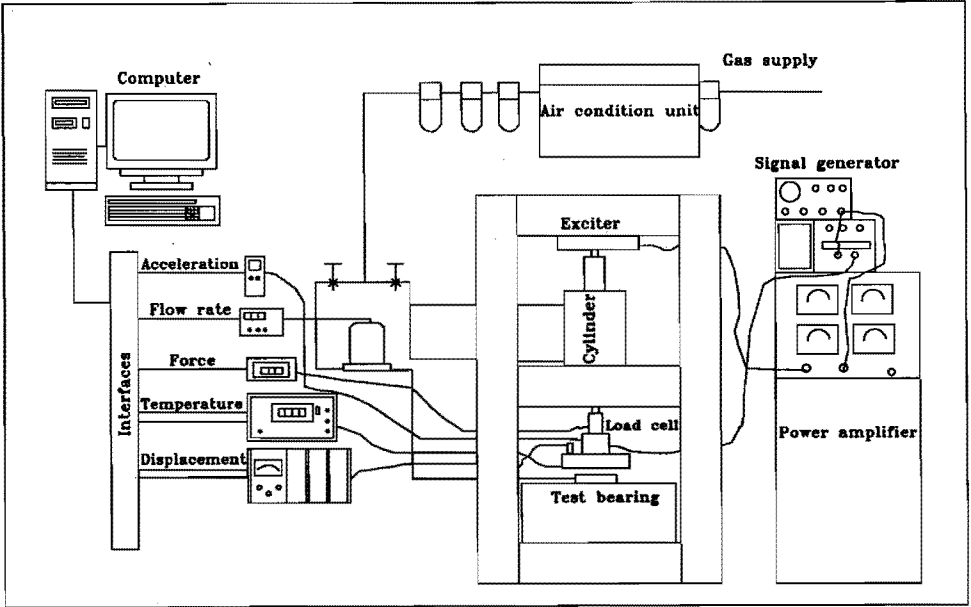


Fig. 3.4. Schematic illustration of experimental systems

4). there should be the following functions:

- 4a). to deliver the static and dynamic loads and to indicate them
- 4b). to indicate both static and dynamic displacements of the test bearing

Following these basic considerations, a mechanical structure was designed [Snip, 1991]. The dynamic load was applied by a magnetic shaker while static load was provided by a pneumatic cylinder which can also be used to produce low frequency dynamic load. The dynamic load was measured by the strain gauge. The displacement of a bearing body was measured by the conductive sensors. Three displacement sensors were mounted with the same radius. Two of them, which were arranged in one line through the geometrical centre, were used as the main sensors and the third one was put on a line perpendicular to the line determined by the first two sensors. The average value of two main sensor outputs is the true vertical displacement, provided that the influence of the pad eccentricity is small. The tilt of the bearing body can be calculated by the difference between the outputs of the sensors. The relationships of the true working gap height, h_w and the tilt angles, θ , η with the sensor outputs, h_1 , h_2 , h_3 , can be expressed in the following matrix :

$$\begin{bmatrix} \theta \\ \eta \\ h_w \end{bmatrix} = \frac{1}{2r} \begin{bmatrix} -1 & 2 & -1 \\ -1 & 0 & 1 \\ r-e_x-e_z & e_z & r+e_x-e_z \end{bmatrix} \begin{bmatrix} h_1 \\ h_2 \\ h_3 \end{bmatrix} \tag{3.14}$$

where

r : the radius determined by the three sensors

e_x, e_z : the eccentricities between the circle determined by the sensors

The displacements were measured by the inductive sensors and the force was measured by the strain gauge. The specifications of the sensors and the instruments are listed in Table 3.1.

Table 3.1. Specifications of the instruments

sensor/transducer	instruments	resolution	range	drift
W1/5 inductive sensor(HBM)	KWS 503A (0.02 μ m)	0.8 mV/V	0 -1000 Hz (-1db)	tem. 0.05 %
03-type load cell	K50 HBM		0-1000 Hz	tem. 0.05 %
4338 accelerometer (Brüel & Kjær)	5007 charge amplifier	98.7 pc/g		
5850 flow sensor (Brooks)	Model 5878	0.03 nl/min	0 - 30 nl/min.	
Pt-100 (Heraeus)	Home-made	0.01 $^{\circ}$ C		
V50 mk1 Vibrator	1 KW power amplifier		0 -120 N	
LabMaster D/A interface card,			8-bits digit I/O for temperature sensors 12 bits A/D converters for the others	

The dynamic properties of the mechanical structure were tested. A noise signal was fed to the shaker. The frequency response in the specified points was measured. The typical frequency response at measured points is shown in Fig. 3.5. It can be seen that the natural frequency of the loading loop is well above the 1 kHz, which meets the design requirements.

3.3.2. The instrumentation

The standard software, ASYSTANTTM is used to acquire and analyze dynamic test data. The necessary interfacing programs for temperature and static property measurement were also developed. The analog outputs from all instruments were converted into digital sets by the Labmaster interface card. The specifications of all the instruments are given in Table 3.1.

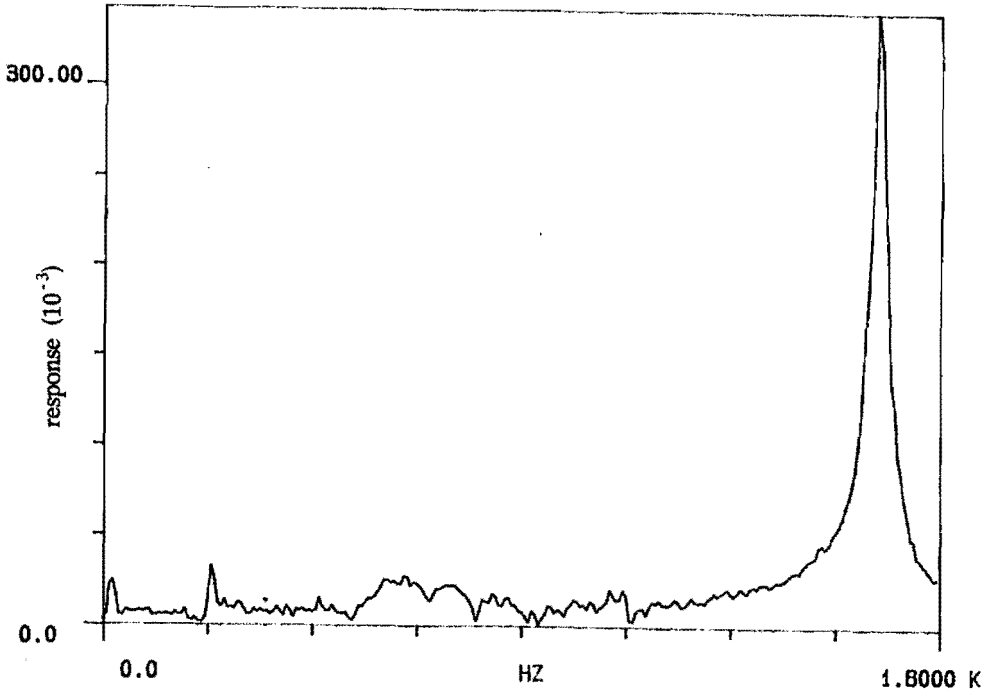


Fig. 3.5. *Vibration mode of loading loop of the experimental system*

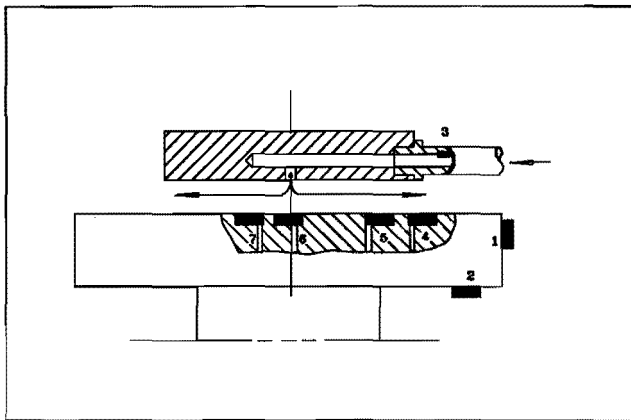


Fig. 3.6. *The test set-up for performing wall temperature experiments*

3.3.3. The test set-up for wall temperature

Fig. 3.6. shows the test set-up for performing experiments on the bearing wall temperature. Four flat Pt-100 temperature sensors (No. 4 ~7) are distributed in a radial direction of the standard block, one (No. 3) is put on the inside wall of the gas supply channel. Two other sensors (No. 1 and No. 2) are used to determine the local environmental temperature.

3.4. TRI-CONICAL GAP SHAPED EPG BEARINGS

The EPG pads with a centre inlet restrictor can avoid the problem of dust or other harmful matter trapping in the bearings. Also, they are easy to make and relatively cheap. That is why they are favorable in most applications. Furthermore, the research has shown that the load capacity and the stiffness can be much improved by designing a suitable gap shape [Wang, 1990]. It was found that tri-conical gap shaped pads have better overall characteristics than the other gap shaped pads. Under the same working conditions (working gap height, supply pressure etc.), the tri-conical pads provide high load capacity, high stiffness and high damping stiffness. The comparison of load capacity of different gap shaped EPG pads is given in Fig. 3.11, from which

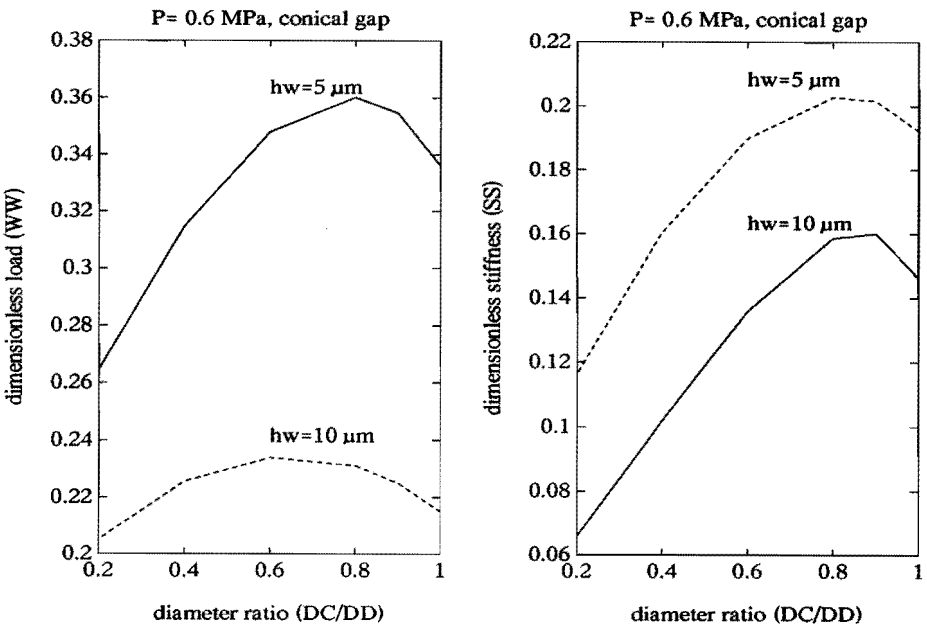


Fig. 3.7. The load and stiffness of bi-conical gap shaped EPG bearings in terms of diameter ratio (hw = 5 μm)

the advantage of tri-conical gap shaped pads can be seen easily. The tri-conical gap shaped pad was developed by the author based on the study of the relationship between the load/stiffness and the gap difference and between the load/stiffness and the diameter ratio of conical and bi-conical gap shaped pads [Wang and Schellekens 1991]. The dimensionless load is defined as the load capacity divided by the absolute value of the product of the supply pressure and the bearing area, i.e. $WW = W/(P_0 A)$. The dimensionless stiffness is defined as, $SS = S hw/(P_0 A)$.

Fig. 3.7 presents the load and stiffness changes with respect to diameter ratios. It can be seen that when the working gap height is less than 10 μm , the maximum load and maximum stiffness correspond to nearly the same diameter ratio ($DC/DD = 0.8 - 0.9$). It is also clear that the optimal diameter ratio is independent of the pad diameter and the supply pressure. Fig. 3.8 shows how load capacity and stiffness vary with gap difference. It can be seen that the load capacity increases with the gap difference [Wang, 1990]. However, the selection of the gap difference is limited by the occurrence of the "pneumatic hammer" (Fig. 3.9), a self-excitation due to the unsuitable combination of bearing parameters. It will be seen in Chapter 4 that the stability of gas system can be determined by the bearing film characteristics.

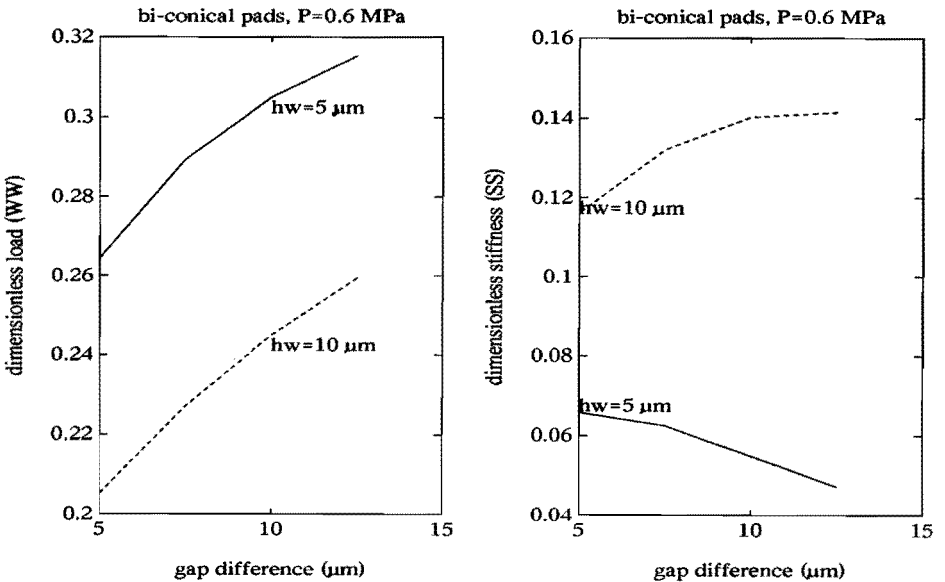


Fig. 3.8. The load capacity and the stiffness of conical pads in terms of gap difference

Fig. 3.9 gives the stability criterion in terms of diameter ratio, which reveals the gap shape limits for avoiding the self-excitation. From Fig. 3.8, one can see that to ensure the same stable operation there is still room for gap shape in the inner part to be modified, but not in the outer part. This implies that an additional conical part will increase load capacity and ensure the stability at the same time, which leads us to the concept of the tri-conical gap shaped EPG pads.

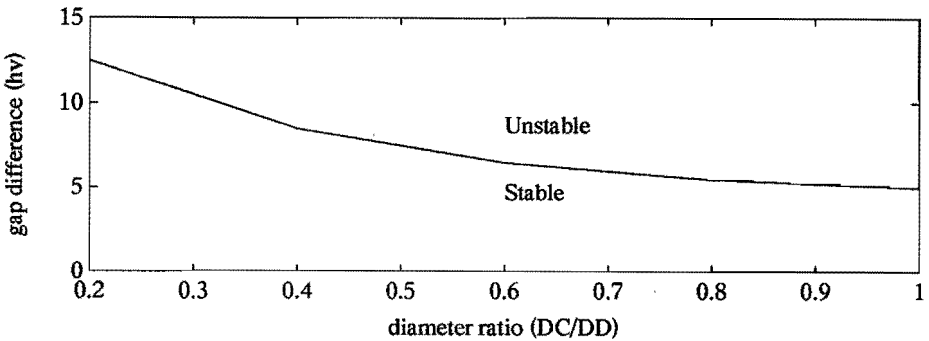


Fig. 3.9. The stability criterion of conical pads in terms of diameter ratio and gap difference

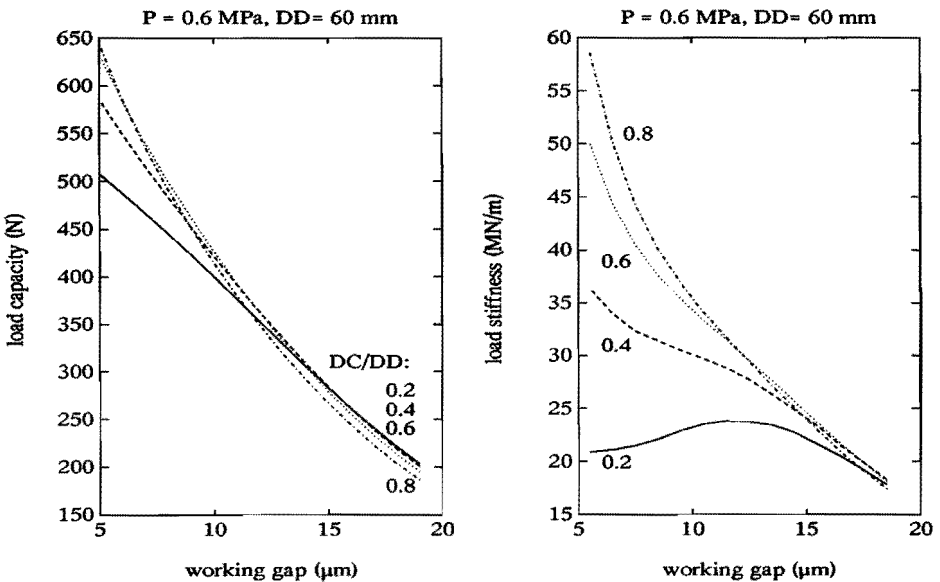


Fig. 3.10. The load and stiffness of tri-conical pads in terms of (outer) diameter ratio

Fig. 3.10 shows the effect of the outer diameter ratio of tri-conical gap shaped pads. It can be seen that the optimized outer diameter ratio ($DC2/DD$) has the same value as that for conical gap shaped pads.

Fig. 3.11 presents the comparison of the load capacity and stiffness among parallel shaped, simple, bi- and tri-conical shaped pads, which shows that tri-conical pads have the highest load capacity and the highest stiffness

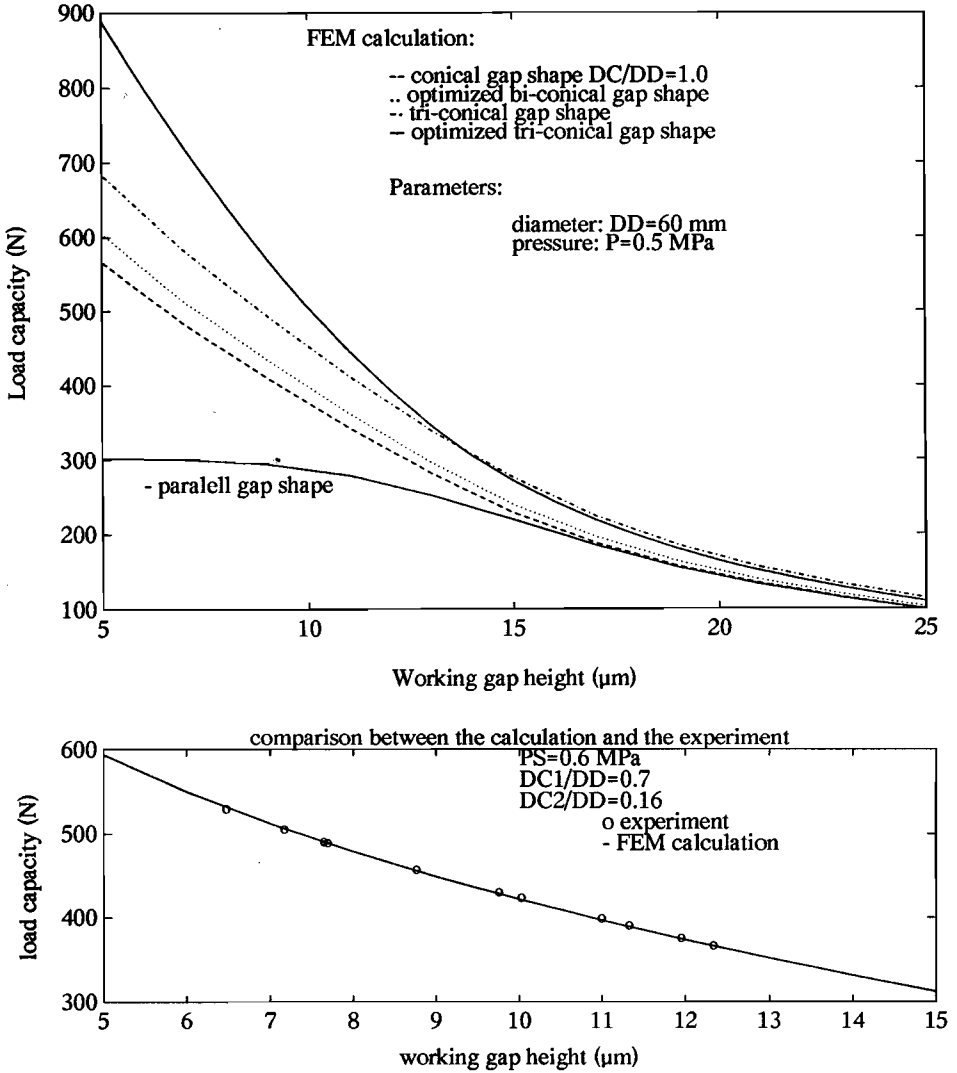


Fig. 3.11. The comparison of different gap shaped EPG pads

over the whole working gap range. The load capacity of the optimized tri-conical EPG pads at 5 μm working gap is 50 % higher than that of the bi-conical gap shaped EPG pads. The comparison of the experimental results with the FEM calculation for a tri-conical pad is given in a separate figure shown in the same figure. The uncertainty of load measurements is $\pm 1.2 \text{ N}$ and the uncertainty of displacement measurements is $\pm 0.05 \mu\text{m}$.

Fig. 3.12 shows the complex stiffness magnitude of those pads. The value at zero frequency is the static stiffness. In the range of higher frequencies, the stiffness magnitude approaches to a constant, i.e. the stiffness at infinite frequency (K_{∞}). This is because of the slow response of the gas

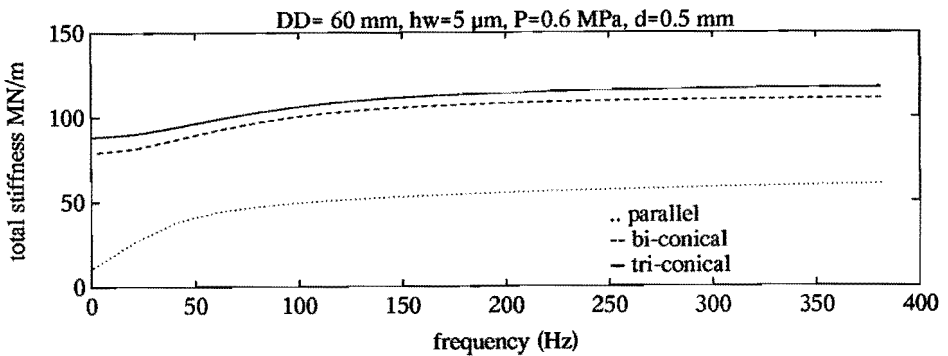


Fig. 3.12. The comparison of the magnitude of the complex stiffness

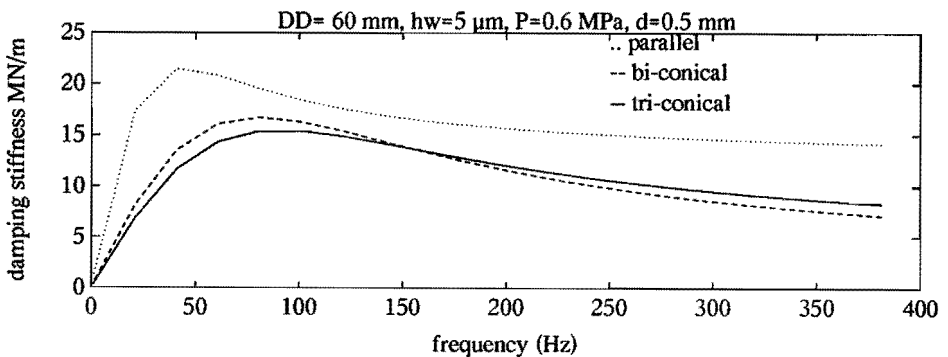


Fig. 3.13. The comparison of the magnitude of the damping stiffness

supply change, which implies that neither the restrictors nor the film squeeze effect are functioning in the high frequency range. From this figure, it can also be seen that K_{∞} increases from the parallel gap shaped pad to the

tri-conical gap shaped pad. In fact, K_{∞} is the average bulk stiffness of gas in the bearing. From Fig. 3.11, we understood that the load capacity at the same working gap height increases from the parallel gap shaped pad to the tri-conical gap shaped pad. Therefore, the average bulk stiffness should follow the same pattern.

Fig. 3.13 presents the frequency characteristics of the imaginary part of the stiffness which was defined as the damping stiffness [Wang, 1990]. This figure shows the frequency characteristics of damping stiffness. If a system can be so designed that its natural frequency is in the range between 50 to 150 Hz, the bearing damping property is optimally used. Therefore, the dynamic performance of the system can be enhanced.

3.5. THE EFFECT OF BEARING BODY TILT

In practical applications, the bearing body can be tilted for two reasons: 1). The presence of an unequal gap height contribution due to errors of manufacturing and assembly and/or distortion of the structure; 2). Imposed momentum resulting from unsymmetrical loading and/or thermal loading. In general, the tilt can change overall characteristics of bearings, such as load and stiffness; and positions of slide or rotor in bearing systems. In the structures with EPG pads, only the first aspect is important because each pad functions as a "point" to restrict the degree of freedom of a slide. In these situations, the design task is to discover an EPG pad with less sensitivity to tilt and less momentum to the structure.

Research [Wang and Schellekens, 1992] found that different types of EPG bearings may have different sensitivities to tilt. Therefore, it is necessary to consider the bearing body tilt in the design of EPG bearings in order to provide more reliable design data or to design a bearing with reduced or without effects from tilt. Pande [Pande, 1988] conducted a theoretical analysis of static performances of EPG pads under the conditions of tilt and rotation. He only reported the tilting effect of simple conical gap shaped pads with a small ratio of the pad diameter to the inlet hole diameter.

Because the order of the tilting angles η and θ is less than 10^{-3} rad., the effects on the reference coordinate system are of the same order and can be neglected. Furthermore, the typical parameters used in practice are chosen in the study, i.e.: the operational parameters were chosen as: 0.3 and 0.6 MPa supply pressures (absolute), 5 and 10 μm working gap heights and 60, 80 mm pad

diameters. The conicities of all the conical gap shaped pads were optimized for achieving better overall performance.

Fig. 3.14 schematically shows the configuration of a tri-conical gap shaped pad with a centre restrictor and a parallel gap shaped pad with four restrictors. In the text, the restrictor information will be omitted and EPG pads will be referred to tri-conical gap shaped and parallel gap shaped pads.

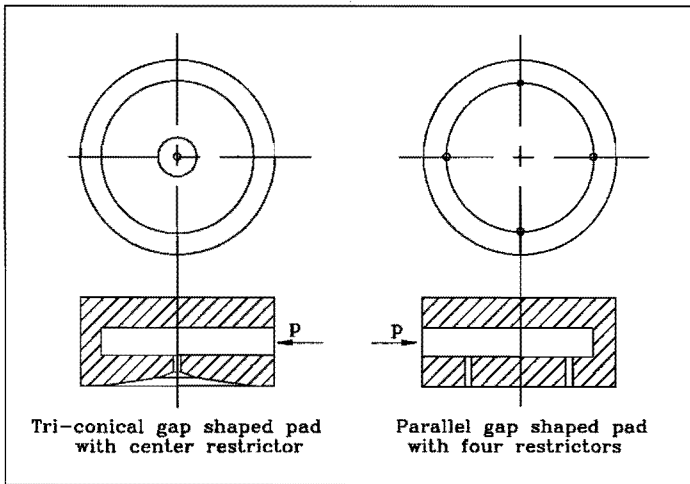


Fig. 3.14. Schematic illustration of EPG pad configurations

3.5.1 Higher supply pressure and lower working gap height

Fig. 3.15 shows the effects of bearing body tilt on the load capacity and stiffness of circular EPG pads at 0.6 MPa (absolute) supply pressure and 5 μm working gap height. The load capacity slightly increases with the tilt for all the pads. The parallel gap shaped pads have the higher magnitude of change. The influences on the stiffness are different, the stiffness of tri- and bi-conical gap shaped pads slightly decreases with tilt ratio while the stiffness of parallel gap shaped pads increase with tilt.

The improvement of the load capacity under tilt is due to the fact that the load enhancement due to decreasing the pressure gradient in one side is more than the load reduction due to increasing the pressure gradient on the other side. As a result, the bearing load capacity is enlarged. The pressure distribution of a tri-conical gap shaped pad is given in Fig. 3.16, from which one can get an idea what happens under tilt.

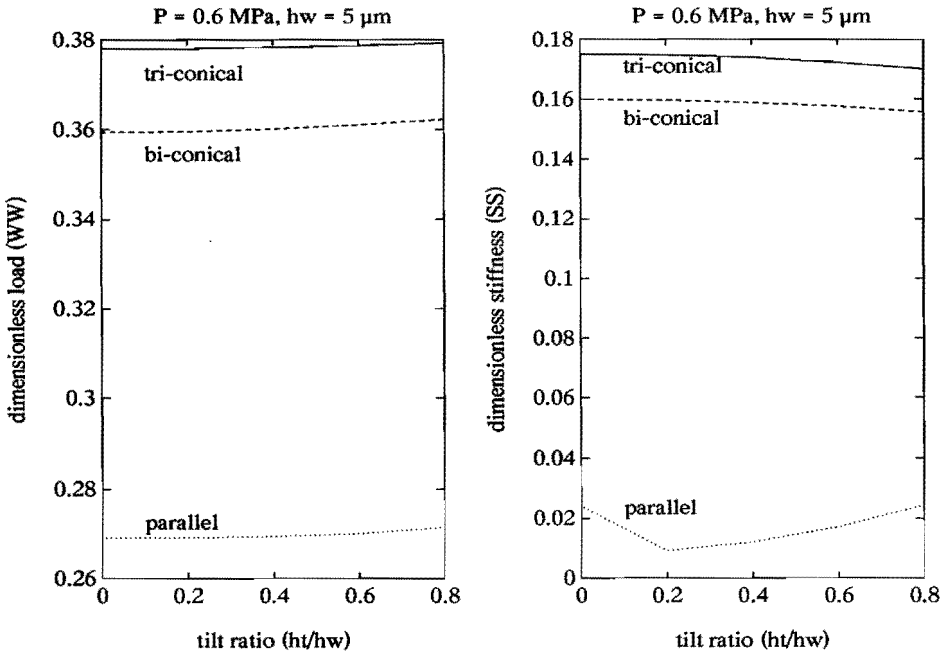


Fig. 3.15. Tilting effects on overall characteristics of circular EPG bearings with a center inlet restrictor ($p = 0.6$ MPa, $hw = 5$ μm)

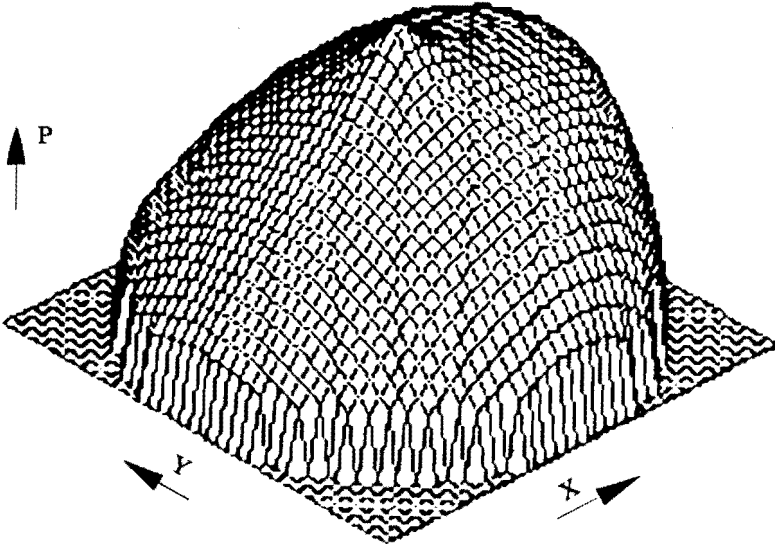


Fig. 3.16. Pressure distribution of circular EPG pads under tilt

3.5.2. Higher supply pressure and higher working gap height

Fig 3.17 presents the effects at 0.6 MPa supply pressure and 10 μm working gap height. The load capacity of the bearing pads with tri- and bi-conical gap shapes in these conditions rapidly increases with tilt, while the load capacity of the pads with parallel gap shape decreases rapidly with tilt. The stiffness of all the pads increases with tilt, but the stiffness of the pad with parallel gap shape changes very rapidly.

In comparison with Fig. 3.15, one may note that the performance becomes more complicated. From these two examples, one can see that there is nothing in common between the two different working gap heights. From the extensive study, it was found that the dimensionless overall characteristics of the supply and bearing dimension pressure show a similar trend.

A conclusion can be drawn that the normalized overall characteristics by the pressure or bearing dimension can be used in qualitative study only. However, the overall characteristics normalized in one working gap tell us nothing in the other.

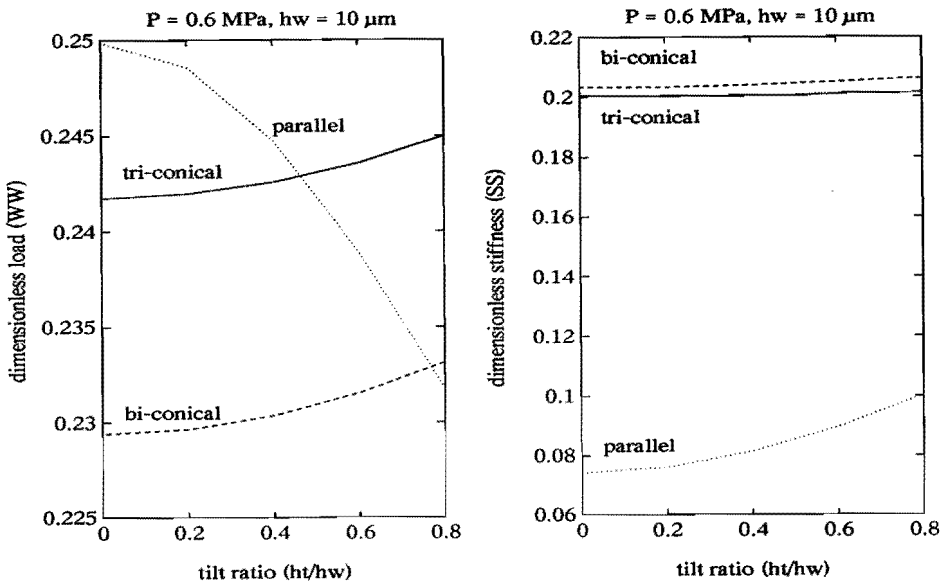


Fig. 3.17. Tilting effects on overall characteristics of circular EPG bearings with a center inlet restrictor ($p = 0.6 \text{ Pa}$, $hw = 10 \mu\text{m}$)

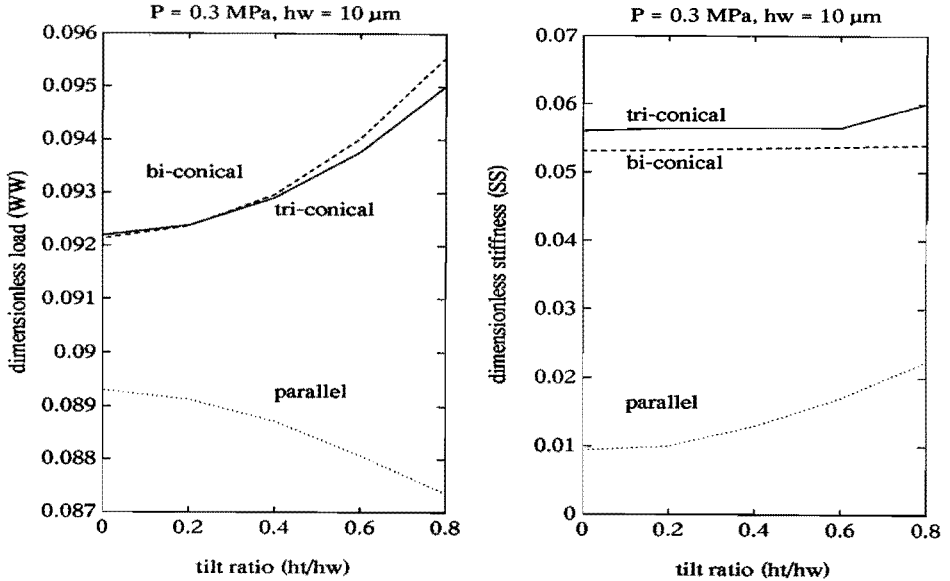


Fig. 3.18. Tilting effects on overall characteristics of circular EPG bearings with a center inlet restrictor ($p = 0.3 \text{ MPa}$, $h_w = 10 \text{ } \mu\text{m}$)

3.5.3. Lower supply pressure and higher working gap height

Fig 3.18 gives the results at 0.3 MPa supply pressure and 10 μm working gap height. The load capacity of all the EPG bearing pads varies considerably with the tilt. The load capacity of bi- and tri- conical gap shaped pads increases with tilt, while that of parallel gap shaped pads decreases with tilt. The stiffness of all the pads increases with tilt. On the contrary, the tri- and bi-conical gap shaped pads are much less influenced by tilt. The direction change of load capacity for different gap shaped pads further reminds us of the complexity of the performances.

3.5.4. Lower supply pressure and lower working gap height

The tilting effects under these conditions are depicted in Fig. 3.19. The results are similar to that at 0.6 MPa supply pressure and 5 μm gap height.

From these examples, one can conclude that bi- and tri- conical gap shaped EPG pads are much less influenced by the bearing body tilt.

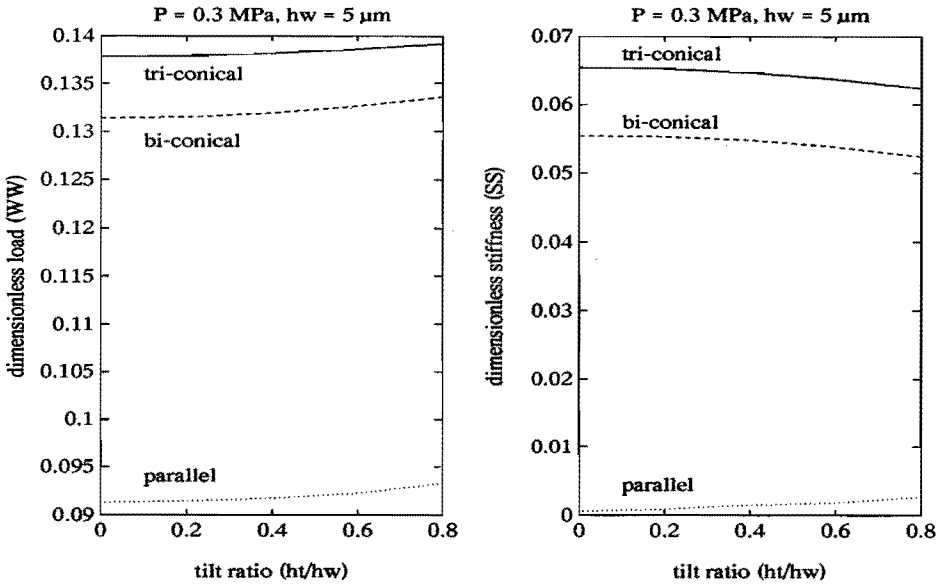


Fig. 3.19. Tilting effects on overall characteristics of circular EPG bearings with a center inlet restrictor ($p = 0.3 \text{ MPa}$, $hw = 5 \mu\text{m}$)

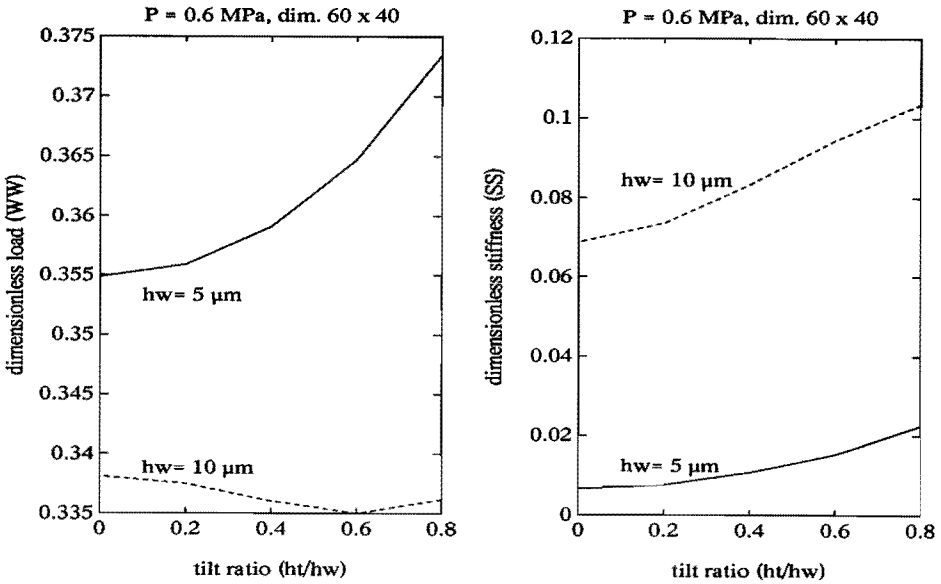


Fig. 3.20. Tilting effects on overall characteristics of rectangular EPG bearings with four inlet restrictors

3.5.5. Rectangular pads

Fig. 3.20 shows the tilting effects on rectangular pads, from which it can be seen that the effects on the load capacity and stiffness at higher working gap height are similar to those of the circular pads with parallel gap shape. However, at lower working gap height, the behaviour is different, both load capacity and stiffness increase.

3.5.6. Effects of dimensions

The dimensionless load and stiffness of two circular EPG pads with different diameters are shown in Fig. 3.21. The diameter ratio and the gap difference ratio (the gap difference over working gap height) are exactly the same in the two pads. From the graphs, it can be seen that there is not much difference between them. It suggests that the supply pressure and the pad area can be easily normalized because they have the simple relationships with the load capacity and stiffness.

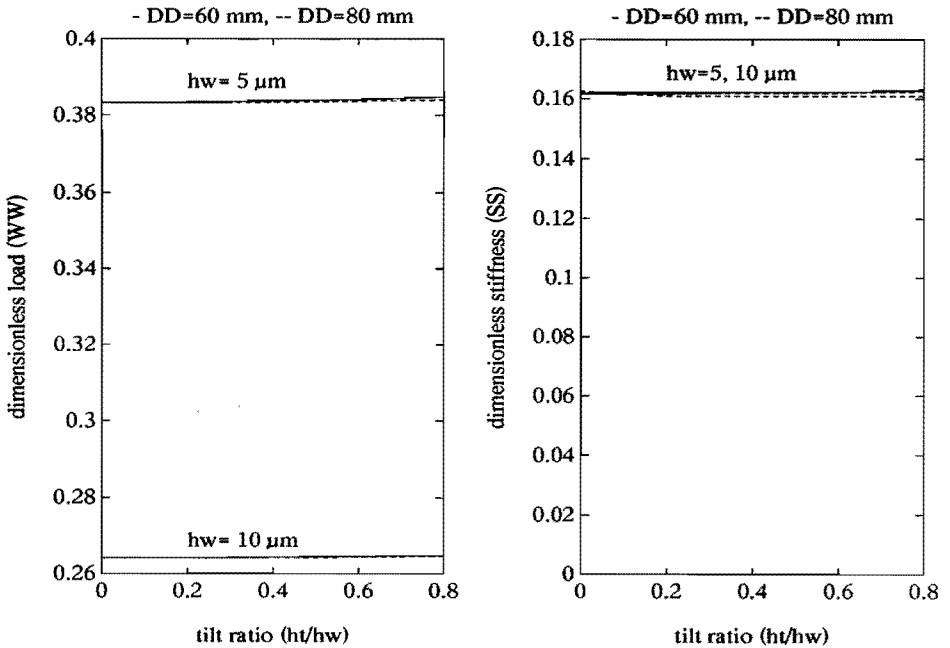


Fig. 3.21. The tilt effects on EPG pads with different dimensions

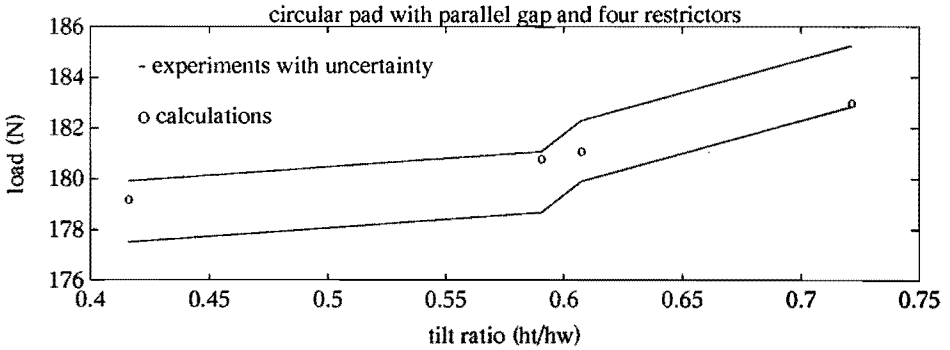


Fig. 3.22a. Experimental verification of tilt effects on parallel pads

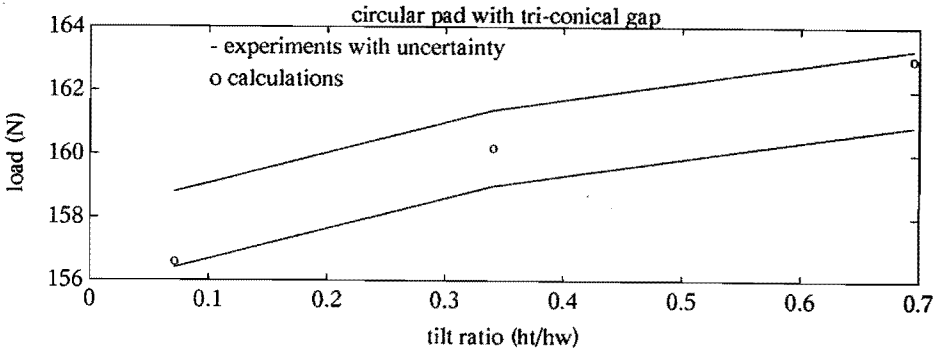


Fig. 3.22b. Experimental verification of tilt effects on tri-conical pads

3.5.7. Experimental verifications

Fig. 3.22 presents the comparison of load capacity between the calculation and the experiment on a tri-conical gap shaped pad and a parallel gap shaped pad at the supply pressure 0.3 MPa. It can be seen that the numerical and experimental results are agreed fairly well. This proves that the results of the numerical analysis are correct.

3.5.8. Tilt effects on the dynamic performance

Fig. 3.23 shows the tilt effects on the damping stiffness. The damping stiffness of bi-/tri-conical gap shaped pads increases under tilt. However, the damping stiffness of the parallel gap shaped pad decreases after about 40 Hz exciting frequency. The increasing rate of the damping stiffness of bi-conical gap shaped pad is from 37 % in high frequency to 62 % in lower frequency. The example was calculated at the tilt ratio 0.8, ht/hw. This

information further suggests that the bi-/tri-conical gap shaped pads are not sensitive to the tilt. Their overall characteristics under tilt are even improved.

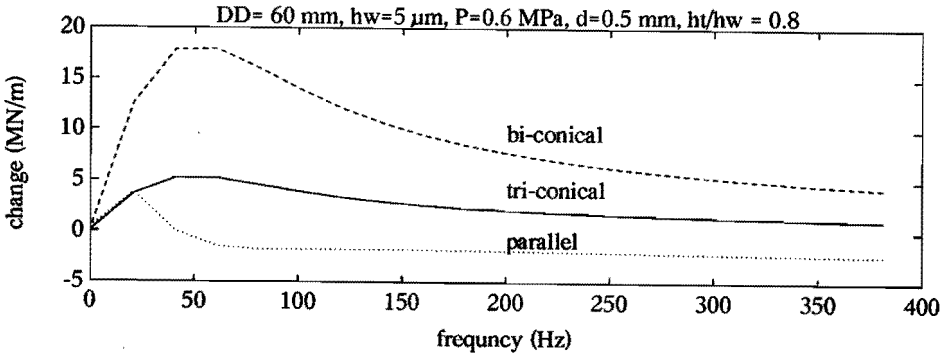


Fig. 3.23. Tilt effects on dynamic performance of EPG pads

3.6. EFFECTS OF SURFACE IMPERFECTIONS

Engineering surfaces are generally wavy and rough. In addition, a mechanical body may be distorted under load or temperature change. As a result, the surfaces form a non-ideal shape for the bearing gap. Fig. 3.24a shows waviness of a large granite beam, typically used in CMMs. It can be seen that waviness can have a big influence on the EPG pad behaviour. The most important point is that overall characteristics of the bearing on such a surface will change from place to place.

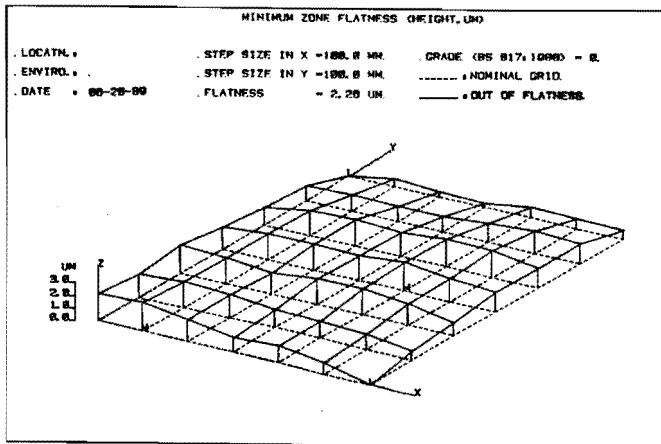


Fig. 3.24a. A measurement example of granite surface used in CMMs

Fig. 3.24b presents the micro view of typical granite surfaces. At first glance, it may be doubted that the permeability would play a significant role. Indeed, the experiments showed that the permeability of this kind of granite can be neglected, although the porosity may cause problems due to the local gas trapping.

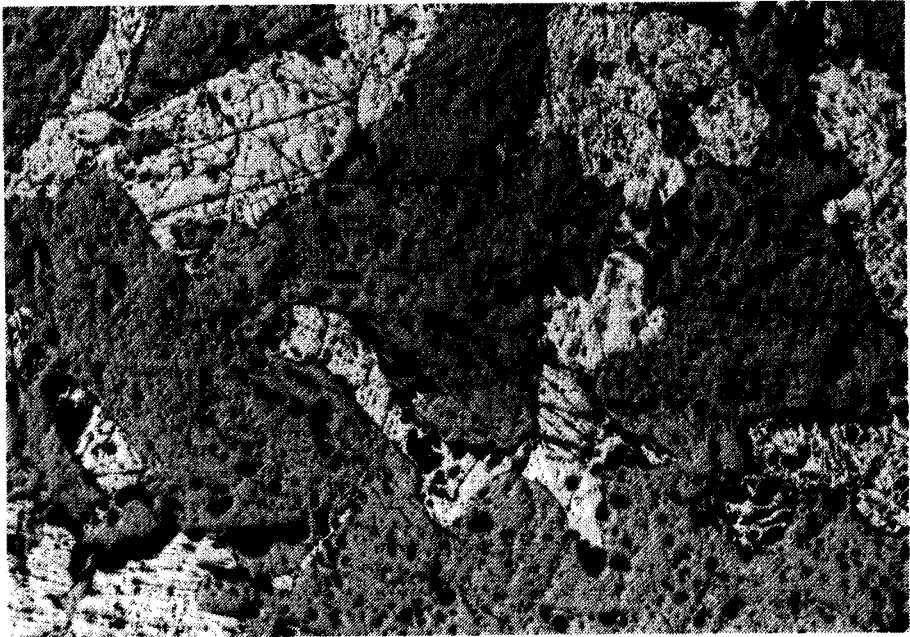


Fig. 3.24b. Micro view of typical granite surfaces (15 x)

3.6.1. Effects of waviness

As already noted [Wang, 1990], the bearing performance is more sensitive to the phase angle shift of the surface wave form. For practical purposes, this implies that the EPG bearing behaves differently in different positions. It is necessary to specify the surface wave shape when designing a gas bearing system with high accuracy. Fig. 3.25 shows the changes of load capacity and stiffness with the phase of a surface wave. It can be seen that in the worst case (amplitude is equal to $3 \mu\text{m}$), the change of load capacity is up 12 percent and stiffness up to 250 percent for the parallel gap shaped pad, while 10 percent in the load capacity and 13 percent in the stiffness for tri-conical gap shaped pad. The reason is due to the gap shape change with the pad position. When the phase in the negative 90 degrees, the bearing gap shape contributed from guide beam is concave, while when the phase in the positive

90 degrees, it is convex. Therefore, the load capacity and stiffness are much reduced in the later case.

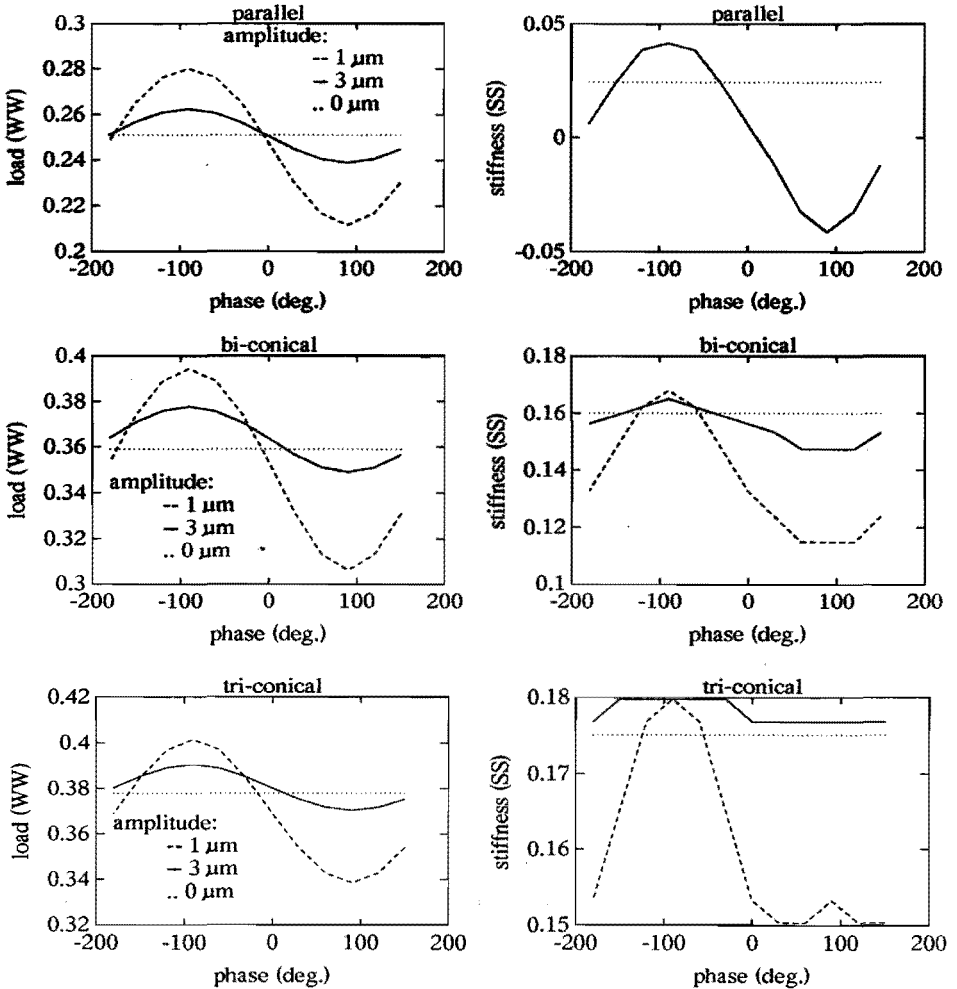


Fig. 3.25. The change of load capacity and stiffness of EPG bearings with phase of surfaces wave ($DD=60\text{ mm}$, $hw=5\text{ }\mu\text{m}$, $P=0.6\text{ MPa}$)

Fig. 3.26 shows the effects of the wavelength of the wave form. It can be seen that if the ratio of the half wave length over the pad diameter is greater than 1.5, the influence on the bi-/tri-conical pads is small, especially on the stiffness. On the other hand, the influences on the load and stiffness of parallel gap shaped pads increase with decreasing of wave length.

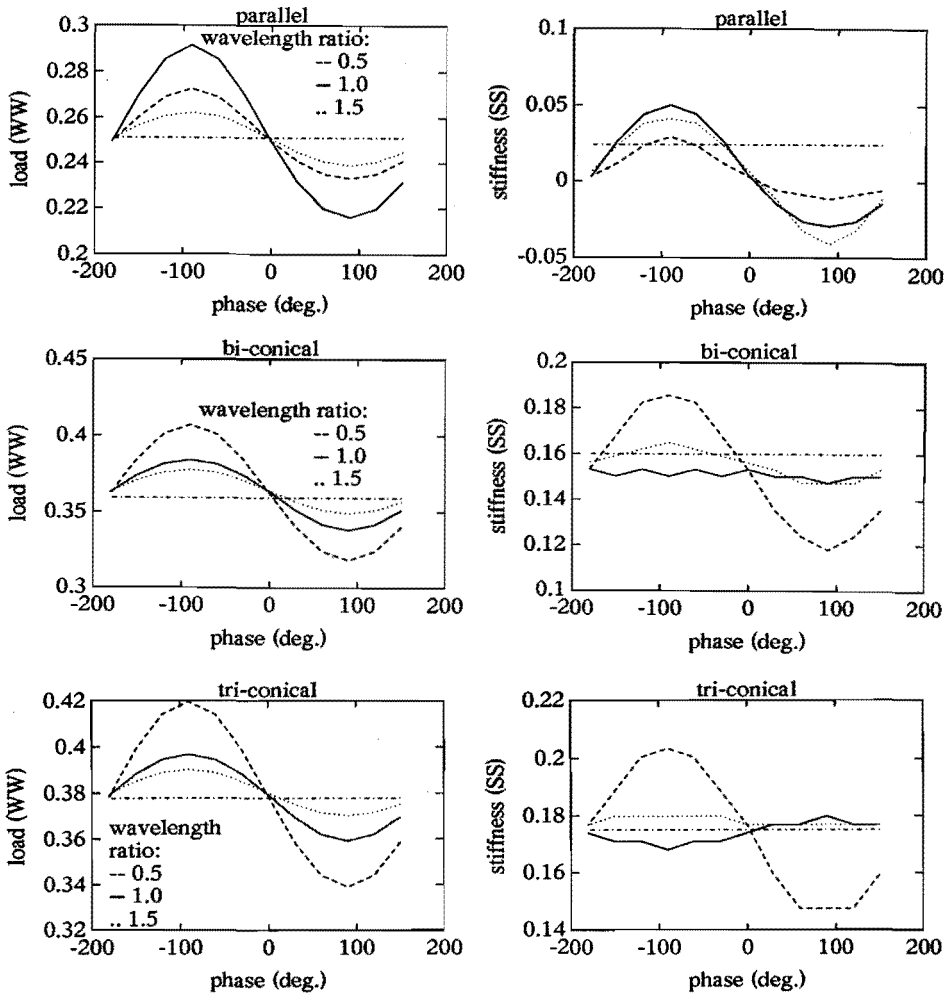


Fig. 3.26. The change of load capacity and stiffness of EPG bearings with wave-length of surfaces ($DD=60\text{ mm}$, $hw=5\text{ }\mu\text{m}$, $P=0.6\text{ MPa}$)

Fig. 3.27 shows the change of the damping stiffness in two extreme phase conditions ($+90^\circ$, top figure, and -90° , bottom figure) when the pads operate on the wavy surface. The figure only shows the change of the damping stiffness relative to the ideal condition. In the example, the single sine wave was used. The half wave length is taken the same as the pad diameter (60 mm) with $1\text{ }\mu\text{m}$ amplitude. It can be seen that the change is insignificant. The values of

the damping stiffness in this situation can be determined by adding the damping stiffness operating on smooth surfaces, given in Fig. 3.13.

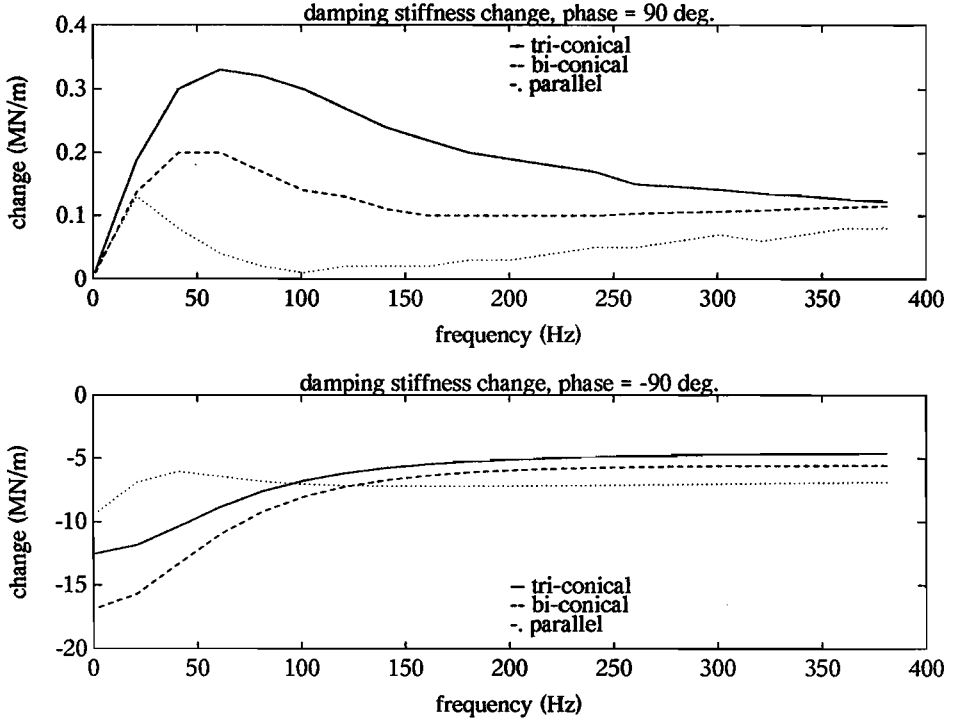


Fig. 3.27. The change of damping stiffness of EPG bearings with surface waves ($DD=60$ mm, $hw=5$ μ m, $P=0.6$ MPa)

3.6.2. Effects of roughness

The importance of the study of the effects of roughness is to select suitable roughness parameters. In lubrication problems, the exact meaning of roughness and waviness may be different from the definitions in the standard of the surface characterization. The flow average model was successfully used in the oil film lubrication [Patir and Cheng, 1984], but there is still disagreement in the application of gas lubrication [Raad and White, 1989] [Tøder, 1984]. In this study, we limit ourselves in the roughness (local waviness) in the condition that the Reynolds equation is still valid, i.e. so called "Reynolds roughness". This means that the local dimensional ratio, an amplitude of a wave over its half wave length, should have the same order as that we used in the derivation of the Reynolds equation. In this treatment, we

can simply use the geometrical average of gap height. The derivation of local gap height from the ideal surface is averaged in an element. An alternative flow averaged model was also proposed [Wang, 1990] to deal with more complicated surface profile.

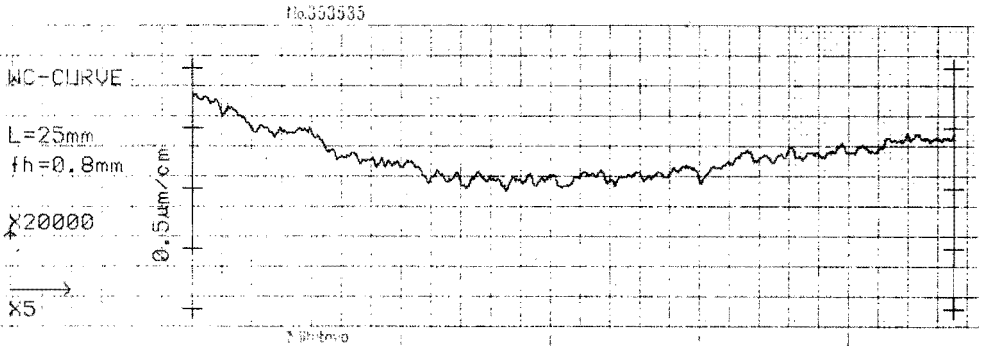


Fig. 3.28a. A surface profile of EPG pads

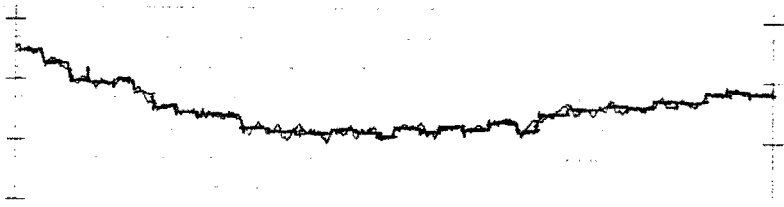


Fig. 3.28b. FEM averaged surface pattern of a typical surface

A grinding surface of an EPG pad is given in Fig. 3.28a. When the surface pattern is introduced to the FEM formulation, the surface profile is locally averaged in an element, shown in Fig. 3.28b. The derivations of load capacity and stiffness from the ideal conditions are shown in Fig. 3.29. It can be seen that both load capacity and stiffness show a significant change.

3.7. WALL TEMPERATURE

In general, the bearing wall temperature depends on the heat equilibrium in the bearing walls, or the heat exchange between the gas film and the walls and the heat exchange between the walls and the environment. The gas film in most applications acts as heat sink sources due to the cooling effects or a cooler gas supply, or both.

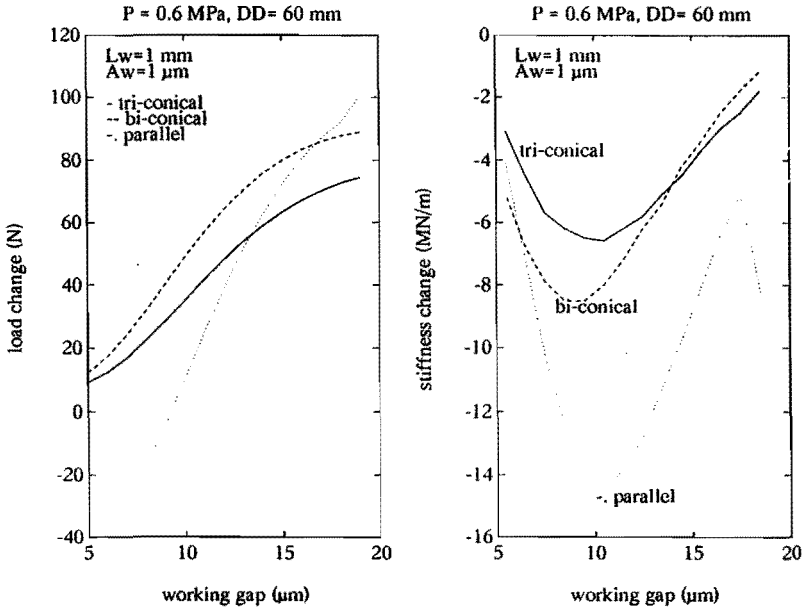


Fig. 3.29. Load capacity and stiffness change on a rough surface

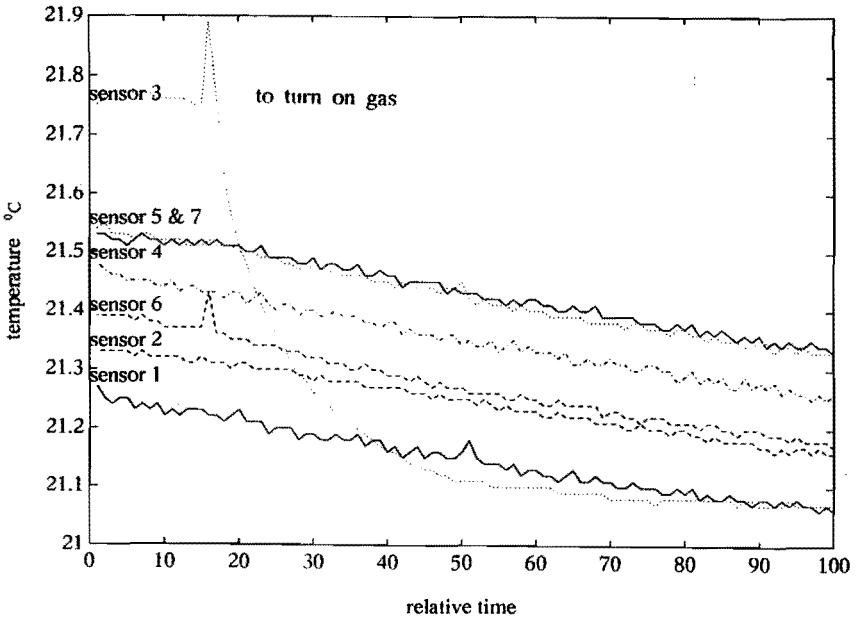


Fig. 3.30. The temperature of supply gas in the Metrology Laboratory, Eindhoven University of Technology

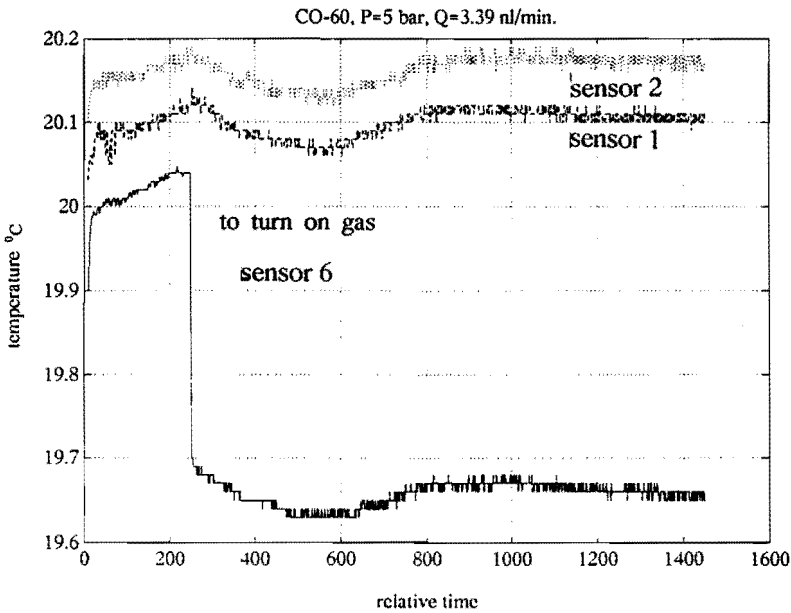
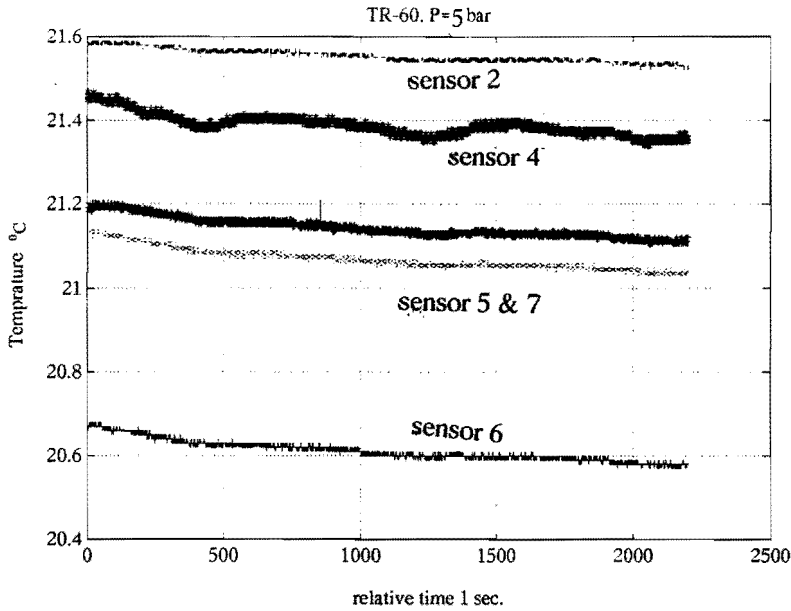


Fig. 3.31. The measured temperature drop in the steel plate in the opposite bearing pad

Fig. 3.30 shows the temperature measurement of the inlet air in the Metrology Laboratory, TUE. The experimental set-up was given in Fig. 3.6. It can be seen that the temperature of the supply gas (sensor 3) is lower than the room temperature. As a result, the cooler gas is introduced into the bearings, and also machine surface.

Additionally, the Joule-Thomson effect will occur in devices such as restrictors, which means that the gas will be further cooled down through a restrictor. Some experimental data on the three types of circular pads with two different type restrictors are given in Fig. 3.31 and 3.32. From these results, we can conclude that the gas temperature is indeed lowered through restrictor and a gas film acts as a heat sink source. The recessed pads (the bearing with orifice restrictor) cause a larger temperature drop. The bi- and tri-conical gap shaped pads cause a less temperature drop in the outlet restrictor because of the relatively fast gas speed in the region. Different

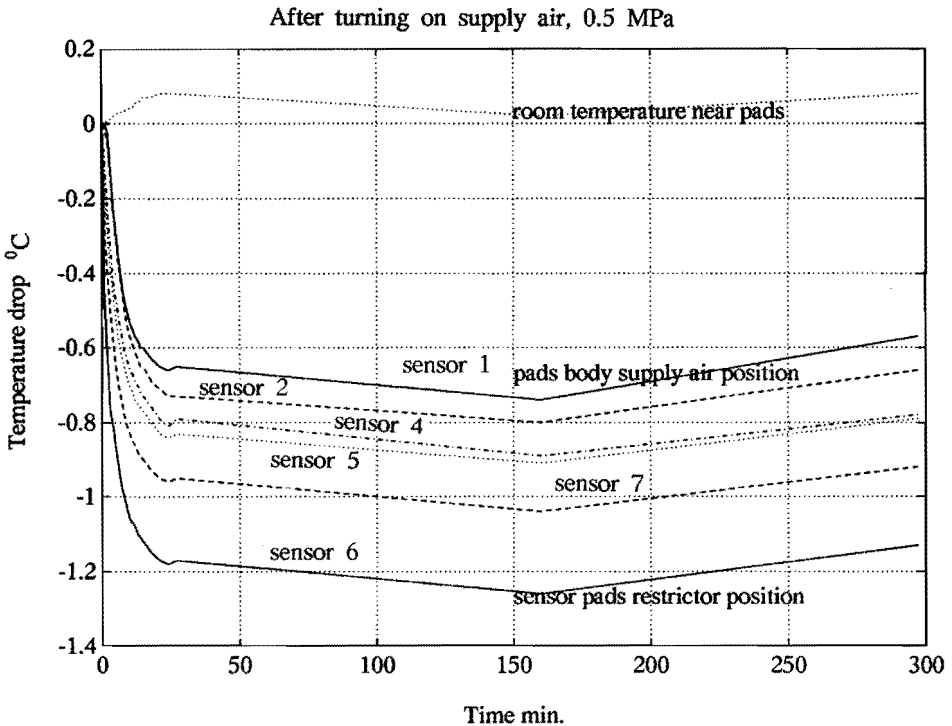


Fig. 3.32. The measured temperature drop in the aluminum plate opposite a recessed bearing pad

types of bearings (especially, restrictor types) will cause a different temperature drop.

3.8. EFFECTS OF BEARING MOTION VELOCITY

From the Reynolds equation, it can be seen that the motion velocity will influence the pressure distribution. The significance of this influence depends on the magnitude of the velocity. With increasing machine velocity, it is necessary to evaluate the effect of motion velocity. Until now, there is no such information available for EPG pads, particularly circular EPG pads, in the linear motion.

From the numerical analysis, it is understood that the motion velocity will not cause the problems for the machine with velocity less than one meter per second which is considered as the highest velocity in the current commercially available machines. Therefore, only a numerical study is presented. In principle, the motion velocity influences both static and

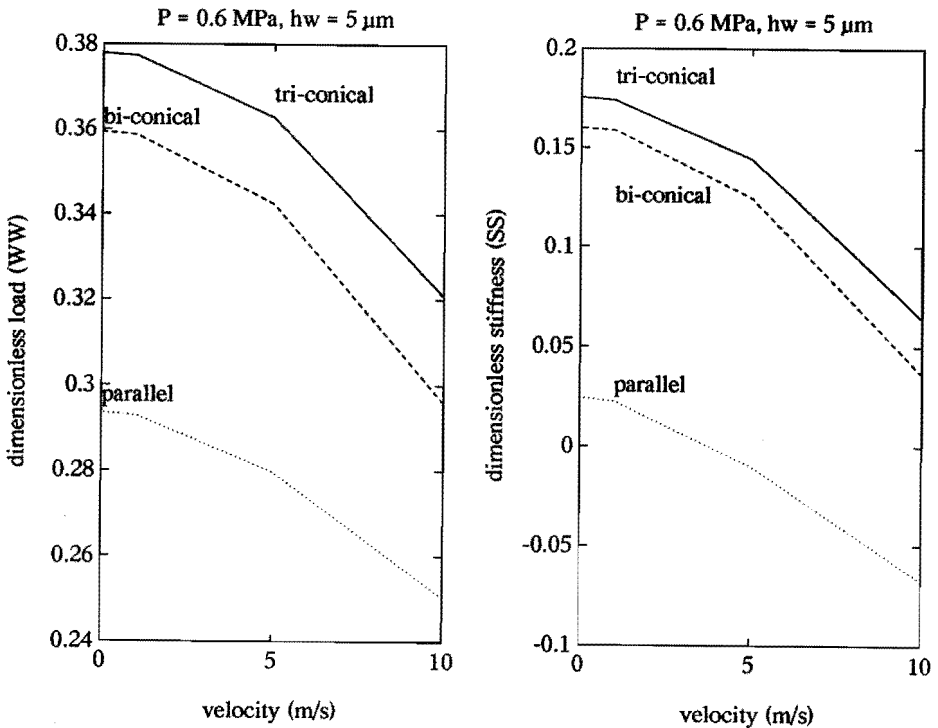


Fig. 3.33. Velocity effects on load capacity and stiffness of EPG pads

dynamic performance of an EPG bearing.

The velocity effects on load capacity and stiffness are shown in Fig. 3.33, from which one can find that the bi- and tri-conical EPG pads are relatively sensitive to velocity. The change is up to 15 % in load capacity and 63 % in stiffness at a velocity of 10 meter per second. Fortunately, the velocity range of currently used linear machines is less than 1 meter per second. From the graphs, it can be seen that in this velocity range, the influences are very small.

Note that the calculation is under the assumption that the bearing gap height does not change when the bearing moves. If a bearing pad is so designed that it can be fully self-aligned, i.e. gap height can freely change with velocity, the influences will be the same as the effect of tilt. In this situation, the bi- and tri-conical EPG pads will be less sensitive to the velocity than the parallel gap shaped pads.

The damping stiffness at 1 meter per second is shown in Fig. 3.34. The damping stiffness of bi-/tri-conical gap shaped pads greatly increases with velocity, up to 43 %.

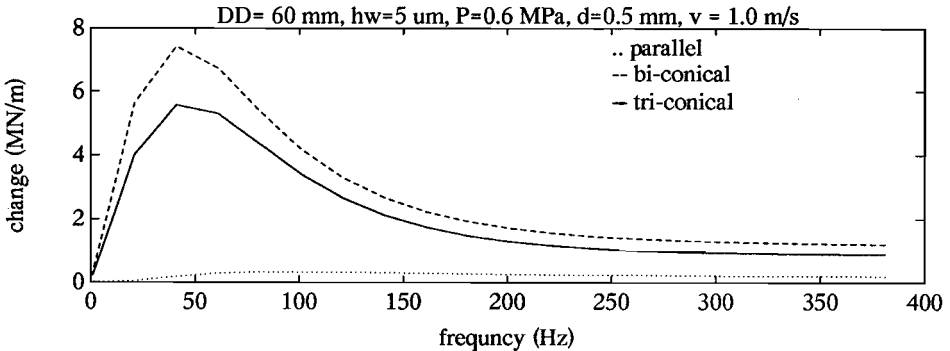


Fig. 3.34. Velocity effects on damping stiffness of EPG pads

3.9. CONCLUSIONS

The developed software and experimental system can be effectively used in the design, study and testing of the EPG bearings.

The numerical and experimental research further reveals that the EPG bearings with concave gap shapes provide higher load capacity and higher

stiffness. The tri-conical gap shaped pads are superior to the parallel and bi-conical gap shaped pads.

The bearing body tilt will greatly reduce the load capacity and stiffness of the parallel gap shaped bearing, maximum change of the stiffness is up to 60 % at the optimal working gap height. On the other hand, the tri-conical gap shaped pads are much less sensitive to tilt, e.g. the stiffness change is less than 1 % at the optimal working gap height.

The tri-/bi-conical gap shaped pads are also less influenced by surface imperfection, especially if the half wavelength is greater than 1.5 times pad reference dimension (e.g. diameter for circular pads). The worst case is that the half wave length is equal to the pad reference dimension.

In the velocity range of less than one meter per second, the load capacity and stiffness rarely change. However, the relatively high velocity will greatly reduce the bearing load capacity and stiffness.

The temperature of the gas supply is generally lower than the standard room temperature, 0.5 ~ 1 °C. The gas through a restrictor can be further cooled down by the Joule-Thomson effect. In very accurate applications, it may cause significant distortion of the structure.

From the study in this chapter, a general guideline to designing mechanical systems with EPG pads becomes clear. The bi/tri-conical EPG pads are preferable because they are less sensitive to tilt and surface imperfection.

PART TWO

DESIGN OF MECHANICAL SYSTEMS WITH EPG BEARING PADS

CHAPTER 4.

MODELLING OF LINEAR GUIDES WITH EPG BEARINGS

4.1. INTRODUCTION

Linear guides with EPG bearings are basic elements in CMMs (Coordinate Measuring Machines) and some other machine tools. The geometrical errors due to the finite stiffness of materials and thermal-elastic effects have been extensively studied, e.g. [Soons and Schellekens, 1991]. In this work, we concentrate on the role of EPG bearings in a linear guide. For clearness, both the guide beam and the slide are taken as the rigid body. In the previous chapters, we have already studied the overall characteristics of EPG pads, but the task still remains to investigate the influences of arrangements of EPG pads on system behaviour. Based on some typical linear guides, some important design concepts will be discussed, which include the loop stiffness, kinematical mounting and driving, symmetrical arrangement and preloading methods.

Furthermore, the appropriate models both for studying static and dynamic behaviour of linear guides are developed. The homogeneous transformation, the matrix form of coordinate transform, is used to describe the real gap height of an EPG bearing in a structure. Through this model, the slide behaviour, due to the change of bearing working gap height, can be determined, which can be used, for instance, to specify a guide surface quality for a desired accuracy. In general, the stiffness of the gas film is frequency and displacement dependent. For vibrations with a small amplitude (e.g. $0.5 \mu\text{m}$), constant stiffness at a specific frequency can be assumed. Therefore, the response of a gas bearing system can be obtained by the loci of the response of a continuous series of linear systems. At each frequency, the corresponding system is represented by a linear differential equation with constant coefficients. For a relatively high vibration amplitude, the response at a specific frequency can be determined by characterizing the film stiffness. It was found that the displacement dependence of bearing film stiffness can be characterized by a cubic function. The modal distribution at a specific space coordinate can be found by a transformation of the modal from the general coordinate system into the spatial coordinate system. The response in the time domain under the given excitation can be determined by using the same transformation.

4.2. LINEAR GUIDES

Some possible forms of linear guides are summarized in Fig. 4.1, some of which are the typical configurations in practice. Based on those we can reveal some general principles to achieve better mechanical systems. In general, the basic principles used to design precision structures were summarized in the ASPE tutorial [C. Teague and C. Evans, 1990]. Some of those principles can be directly applied in the design of structures with EPG bearings, while others require more attention, because the EPG bearings have lower stiffness than the solid contacts and a small working gap height. Those principles include kinematic mounting, loop stiffness, symmetry and kinematic driving. For EPG bearing systems, there is another important aspect - preloading.

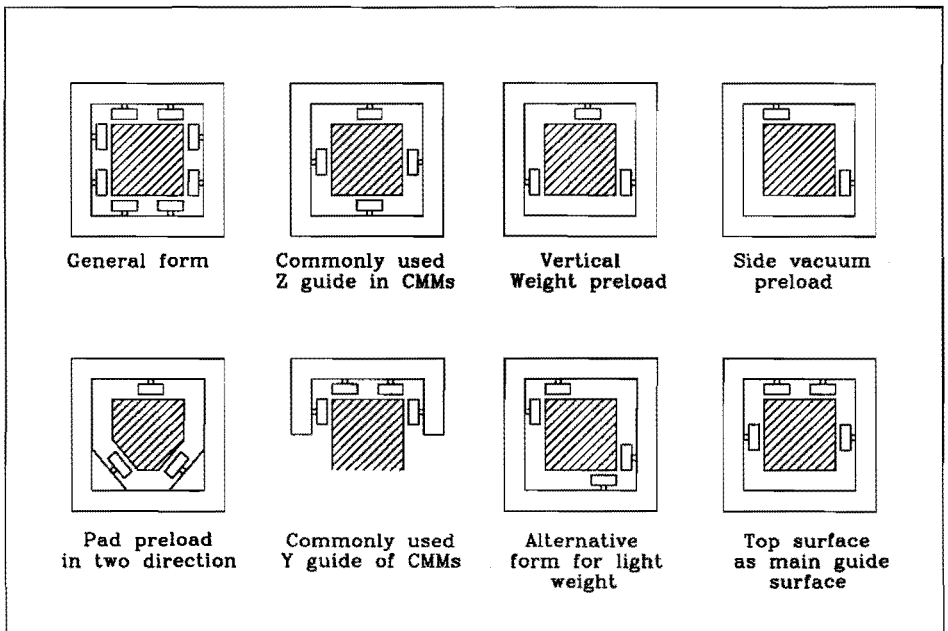


Fig. 4.1. Illustration of some typical configurations of linear guides with EPG bearings (section view)

4.2.1. Kinematical mounting

If a pad is rigidly mounted (no self-alignment), the maximum rotation angle (until touch down to the guide beam) is limited by the pad dimension (ξ) and its working gap height (h_w), i.e. :

$$\phi \leq hw/\xi \quad (4.1)$$

The ratio ϕ is approximately in the order 10^{-4} (≈ 20 arc. sec). In practice, the allowable rotation angle will be much smaller than this, which is actually defined by the allowable change of the bearing gap height, i.e. :

$$\phi \leq \Delta hw/\xi \quad (4.2)$$

Under normal working conditions, it is within a few arc seconds. If we consider this value is within the error range, one can say that one pad will be sufficient to restrain two rotations, particularly in the case of small structures. In most applications, an EPG pad has a self-alignment mechanism. If the self alignment mechanism does not work, the guide will be overpositioned. Strictly speaking, if any error in position of a pad is introduced in a bearing system, the system will be overpositioned. Furthermore, it should be noted that the rotation about the motion axis can be completely controlled by two pads mounted on two perpendicular surfaces. This implies that if one more pad in any surface is used, the slide will be overpositioned. In the suppression of a translational degree of freedom, a pad limits only one direction translation. In practice, preloading is necessary to restrain the degree of freedom in another direction.

Summarizing the above discussion, we can conclude that a purely kinematic mounting of a slide needs only two preloaded EPG pads (one with and one without self-alignment) mounted on the other side of two perpendicular surfaces. In practice, four preloaded EPG pads with effective self-alignments are preferable, especially in a large linear guide. Two pads mounted on the same side should be well-aligned to avoid overpositioning in the rotation about the motion axis.

Another important point in design of EPG pad systems is that with a small change of displacement it provides one **elastic restrain** in the direction of working gap height. This particular feature provides that there are less critical requirements on the kinematic mounting in the small change of slide position. If the number of pads used in a slide is more than the numbers for purely kinematic mounting and the tolerance is within $10 \mu\text{m}$, all pads can still work properly. On the other hand, the finite stiffness of EPG pads provides an imperfect restrain, which determines the existence of error motions of a slide. The bearing stiffness will be further reduced if the loop stiffness is not carefully designed.

4.2.2. Loop stiffness

This is one of the important conceptual patterns for precision structure design. It becomes more important in gas bearing systems because high film stiffness is easily lost by poor design of joints, which unfortunately occurs in applications, even in commercial products. In a linear guide system, all the elements involved in a chain from the gas film to the moving slide form a group of springs in series. In a linear guide, the loop elements include the gas film, the pad body, the pad mounting, the guide beam, the slide frame and the guide mounting. The stiffness loop is illustrated in Fig. 4.2. It is known that the overall stiffness of a linear guide equals the reciprocal of the reciprocal sum of all the element stiffness. In a mathematical form, it reads:

$$S_a = 1 / \sum (S_i^{-1}) \quad (4.3)$$

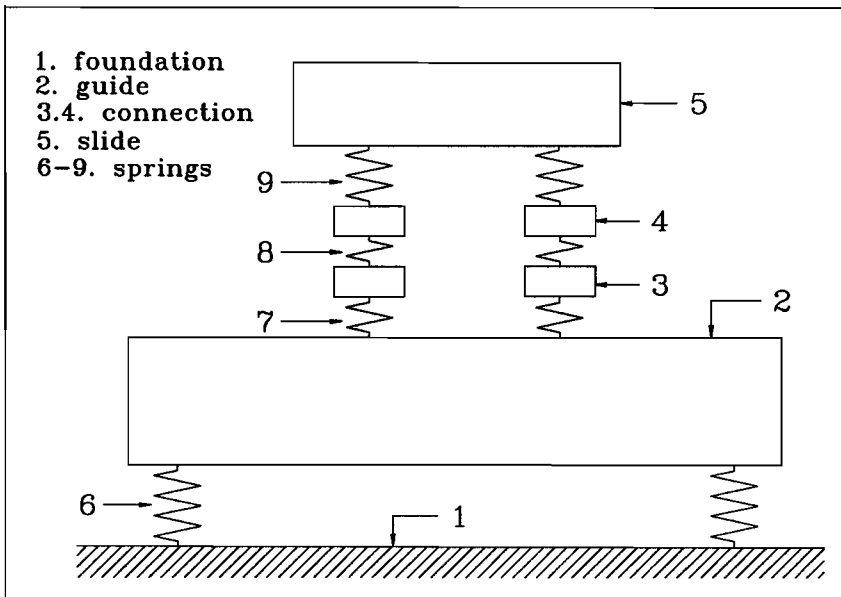


Fig. 4.2. Illustration of loop stiffness in a mechanical system with EPG bearing pads

In general, the gas film stiffness is more difficult to achieve than the stiffness of mechanical elements. Therefore, in the design, sufficient stiffness of all the mechanical elements should be ensured, a study on this subject was conducted to design a better mounting mechanism [Driessen, 1992] and some good examples will be illustrated in the next chapter.

4.2.3. Symmetrical arrangement

Symmetrical arrangements are very important for systems with gas bearings because gas bearings provide active forces to the support, for instance, the guide beam and the slide frame in Fig. 4.1. A fully symmetrical arrangement can provide the cancellation of distortions introduced by bearing forces. However, it will become more difficult to utilize a pair of opposite pads in large structures, like those in 3D CMMs. An ideal solution can be the preloading in the same side which can be realized by vacuum or magnet preloading. In order to eliminate the troubles introduced by EPG bearings, it is better to arrange all the bearings symmetrically whenever it is possible.

4.2.4. Kinematical driving

A kinematical driving system requires a purely driven force (or a pure moment for rotation systems) in the motion direction if possible. Driving stiffness should be as high as possible, because weak driving stiffness will shift the lowest vibration mode to the lower side of the frequency range. This lowest natural frequency will influence the vibration motion in the other coordinate directions, not only in the driving direction. Perforated hinge is one of suitable elements in such applications: it provides high stiffness in transverse direction and flexibility in other directions.

4.2.5. Preloading

Preloading can be used not only to restrain unwanted degrees of freedom completely but also to set the optimal working gap height of EPG pads. In general, preloading can be provided by an opposite EPG pad, a vacuum pad or a magnetic strip (force preloading) and structure weight (mass preloading).

Mass preloading is a simple way to provide preloading, but it can be only used in a vertical direction (or vertical direction and one rotation in the guide with eccentric mass), but the optimization of bearing characteristics is limited by mass value. This method is useful for relatively heavy structures. In a light structure extra mass may be necessary, which will lower the lowest natural frequency of the system.

The opposite EPG pad preloading requires the high accuracy, both in flatness and in parallelism of the two opposite surfaces of the guide beam, in the process of manufacturing and assembling of a structure. Due to technical limits, it may become impossible to build a highly accurate and large

structure by using this method. The benefit by doing so is the enhancement of the total stiffness of the system. In this situation, the total stiffness will be the sum of the stiffness in the two sides. It can also be used as an actuator for realizing sub-micron displacement in the stationary situation. It is very useful to realize small feeding in processing machines or small displacement in measuring machines. With one side elastic mounting, the critical requirements on assembling can be relaxed. But the total stiffness can only be about one side film stiffness.

Both magnet and vacuum preloading can be arranged in the same side as EPG pads. In this way, only one precise surface needs to be made, which leads to a cheaper manufacturing and assembling process. There are plenty of examples of light structures in which the magnet or vacuum is used as means of preloading. For large structures, they can also be the better means of setting optimal working gap height. The disadvantage of vacuum preloading is the additional vacuum device (or pump). The use of the Bernoulli effect [Wang, 1990] or supersonic effect in the form of EPG pads could be a best solution. The drawback of magnet preloading is the special requirement on materials.

The calculation of the attraction force due to vacuum can be performed by the similar procedure as that of EPG bearing force. The difference is that the flow direction in the vacuum pad flow goes inwards while in EPG pads it is outwards. The inward gas can be the outlet gas of EPG pads or using a separation grooves to avoid unfiltered gas going into the bearing working area. The calculation of the attraction force in a magnet can be performed by using the material specification of magnets.

4.3. MODEL TO DESCRIBE THE REAL BEARING GAP HEIGHT

The real gap height for each bearing mounted on a slide can be derived by using the homogeneous transformation. The homogeneous transformation has been used by many researchers to establish a generalized model to describe the geometrical errors of machines, e.g. [Teeuwesen et al 1990]. In order to derive the model to describe the real gap height of an EPG pad in a mechanical system, two coordinate systems can be defined: a reference coordinate system, $\mathcal{R}cs$ (X,Y,Z), connects to an unmovable guide beam and its centre is assigned in the mass centre of the guide beam; the other coordinate system, $\mathcal{G}cs$ (X',Y',Z'), is fixed on the slide. The coordinate systems are shown in Fig. 4.3. Because the bearing gap height is the distance between the bearing pad

and the guide beam, the change of working gap height will be the relative change of the coordinates \mathcal{C}_cs in the pad mounting position with respect to the reference coordinates \mathcal{R}_cs .

In this study, a rigid slide was used, which allows us to concentrate on studying the coordinates in the mass centre and the attitude angles of the slide. In a linear guide, the slide position is defined by all the EPG pads mounted on it. Therefore, the mass centre coordinates and the attitude angles of the slide can be described by all the bearing working gap heights. In practice, the working gap height will change due to the change of the effective load capacity, e.g. load capacity variation on a rough surface. By using the relationship between the working gap height and the slide behaviours, the slide motion errors can be determined. Moreover, for a desired level of accuracy, the manufacturing and assembling errors of a slide for a fixed type bearings can be defined.

In an arbitrary condition, the bearing position will be modified by the following matrix :

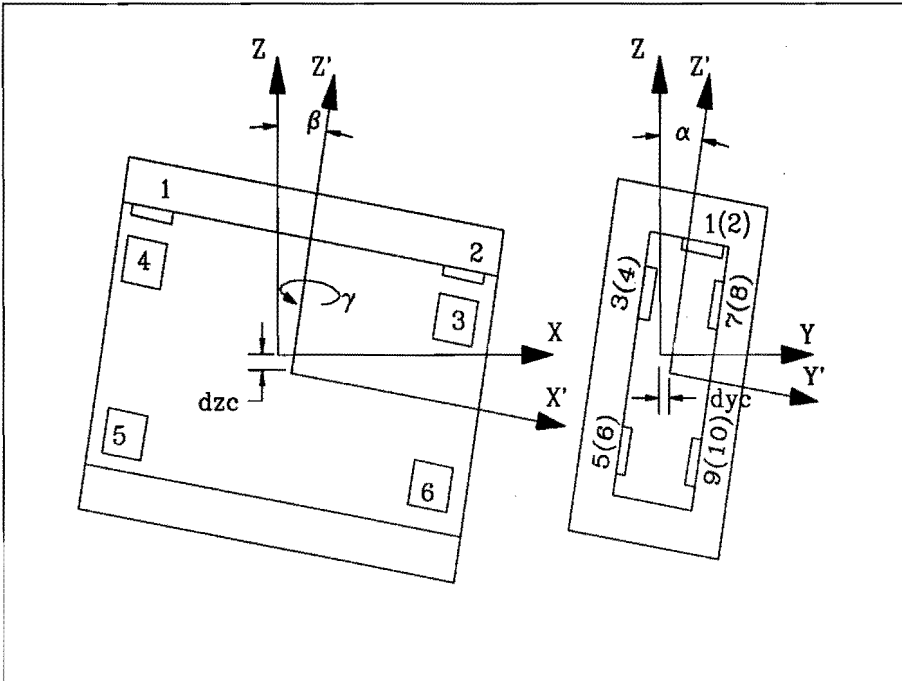


Fig. 4.3. An example of a linear guide with EPG bearings with the definition of coordinates and bearing gap height

$$\mathbf{\Sigma}_{hw} = \begin{bmatrix} 1 & -\gamma & \beta & 0 \\ \gamma & 1 & -\alpha & dy_c \\ -\beta & \alpha & 1 & dz_c \\ 0 & 0 & 0 & 1 \end{bmatrix} \quad (4.4)$$

where dy_c, dz_c : mass centre changes of the slides
 α, β, γ : the attitude angles of the slides

It should be noted that the translations parallel to a bearing surface and the rotations about the axis perpendicular to this bearing surface have no significance in describing this bearing working gap height. Furthermore, because there is no pad parallel to the Y-Z plane, the translational derivations in the X- direction do not contribute to the bearing working gap height. It should also be noted that the attitude angles of slides are very small, the trigonometrical function in the transformation matrix can be replaced by their radiant angles directly. The products of angles ($\alpha\beta, \alpha\gamma, \beta\gamma, \alpha\beta\gamma$) are far smaller than the angles themselves so that the terms with the angle products in the transformation matrix can also be ignored.

Using the transformation matrix, any coordinate on the slide coordinate system $\mathbf{6cs}$ can be transformed to the reference coordinate system \mathbf{Rcs} . Therefore, the real working gap height can be determined by the difference between two vectors in the bearing gap direction: the vector defining a pad position, $[a_{pi}, b_{pi}, c_{pi}, 1]$, and the reference vector on the guide $[a_{gi}, b_{gi}, c_{gi}, 1]$ defining the initial working gap height. Therefore, the working gap height can be calculated by the corresponding row in the transformation matrix (a transformation vector), for instance, the second row for the bearings mounted on the surface(s) perpendicular to the Y-axis and the third row for the bearings perpendicular to the Z-axis, i.e. :

$$hw_{yi} = [\gamma, 1, -\alpha, dy_c] [a_{pi}, b_{pi}, c_{pi}, 1]^T - b_{gi} \quad (4.5)$$

$$hw_{yi} = a_{pi} \gamma - c_{pi} \alpha + dy_c h^0_{wyi} \quad (4.5a)$$

$$hw_{zi} = [-\beta, \alpha, 1, dz_c] [a_{pi}, b_{pi}, c_{pi}, 1]^T - c_{gi} \quad (4.6)$$

$$hw_{zi} = -a_{pi} \beta + b_{pi} \alpha + dz_c + h^0_{wzi} \quad (4.6a)$$

where

a_i, b_i, c_i : the mounting position coordinates of pad i in X,Y,Z coordinate directions.

footnote :

p, g : pad, guide, i : i th pad, x, y : coordinates

superscript :

0 : initial gap heights, $h^0_{wzi} = c_{pi} - c_{gi}$ and $h^0_{wyi} = b_{pi} - b_{gi}$

If all the pads in a linear guide are arranged fully symmetrically with respect to the Y-Z plane, the change of the centre coordinates and the attitude angles of the slide can be expressed by the working gap height :

$$dy_c = (\Sigma h\hat{w}_{yi} - \Sigma hw_{yi})/n \quad (4.7)$$

$$dz_c = (\Sigma h\hat{w}_{zi} - \Sigma hw_{zi})/n \quad (4.8)$$

$$\gamma = (\Sigma \Delta hw_{yx}^+ - \Sigma \Delta hw_{yx}^-)/2a_y \quad (4.9)$$

$$\beta = (\Sigma \Delta hw_{zx}^+ - \Sigma \Delta hw_{zx}^-)/2a_z \quad (4.10)$$

$$\alpha = (\Sigma \Delta hw_{yz}^+ - \Sigma \Delta hw_{yz}^-)/2c_y = (\Sigma hw_{zy}^+ - \Sigma hw_{zy}^-)/2b_z \quad (4.11)$$

or
$$\alpha = [(\Sigma \Delta hw_{yz}^+ + \Sigma \Delta hw_{yz}^-) + (\Sigma \Delta hw_{zy}^+ + \Sigma \Delta hw_{zy}^-)]/(2c_z + 2c_y) \quad (4.11a)$$

where

$$\Delta hw_{yi} = h\hat{w}_{yi} - hw_{yi}, \text{ and } \Delta hw_{zi} = h\hat{w}_{zi} - hw_{zi}$$

superscript:

- + referring to the gap height corresponding to the pad in the positive coordinate direction
- referring to the gap height corresponding to the pad in the negative coordinate direction

footnote: x,y,z, coordinates, e.g.

Σhw_{yz}^+ stands for the sum of all the gap heights in the Y direction with the positive z coordinate

a_y implies the coordinate X for the bearing mounted in the surface perpendicular to Y axis

n : number of pads

In Chapter 3, it was established that the overall characteristics of EPG bearings vary with the phase shift of a surface wave. A gas bearing system has a constant weight, or constant force in general, so that the real working gap height will change to balance the slide weight (or forces acting on the slide). As a result, the changes of the pad working gap height directly contribute to the slide motion errors. It follows that the rotational motion error will be reduced if the distance between two pads is not equal to the half wave length of the surface wave. The use of those formulas to describe the motion errors of a linear guide will be demonstrated in the next chapter with specific examples.

4.4. IDEALIZATION OF GAS FILM STIFFNESS

Before going any further in modelling the dynamic behaviour of a slide, we need to idealize the gas film stiffness in order to couple EPG pads into

structures in the usual manner.

4.4.1. The description of displacement dependence

The stiffness of EPG bearing films, in general, is not constant. However, the vibration always starts from a small amplitude, this allows us to limit our study to a small change of the bearing displacement, e.g. $\pm 0.5 \mu\text{m}$, in which the bearing stiffness can be estimated to be a constant at an equilibrium gap height. For the pad studied in this thesis, the stiffness error due to non-linearity is less than 5 % and the error of the natural frequency for the single degree of freedom will be 2.2 %. If necessary, more accurate results can be obtained by introducing the stiffness function from the curve fitting into the equation of the motion of the bearing system. It was found that film stiffness can be accurately described by a cubic function of the bearing displacement, as illustrated in Fig. 4.4.

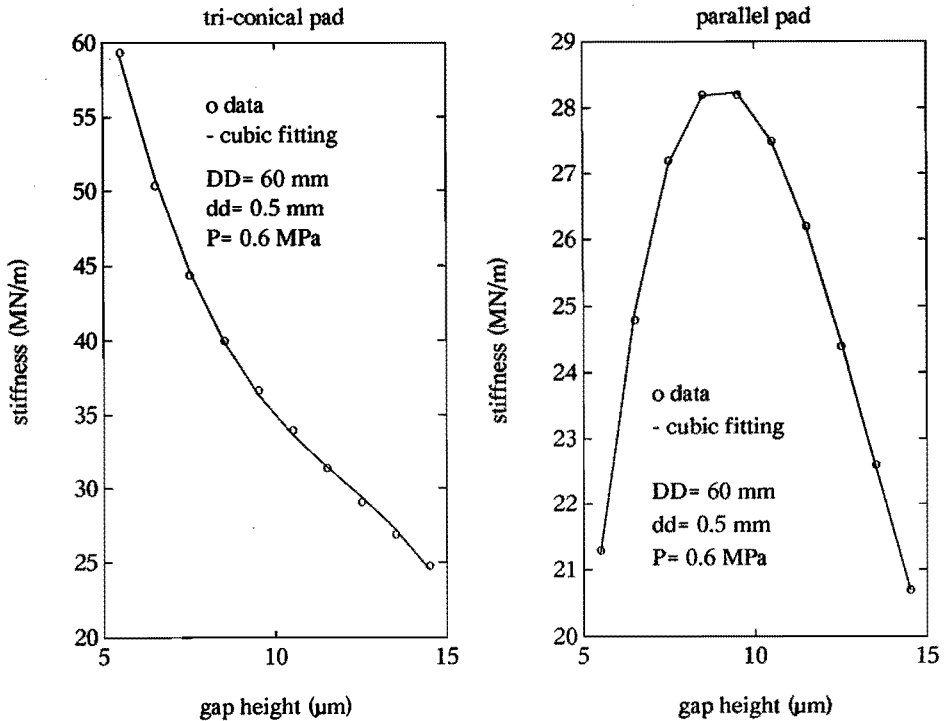


Fig. 4.4. Illustration of the bearing stiffness characteristics

4.4.2. The description of frequency dependence

From the solution of the Reynolds equation under dynamic operations, we often find the dynamic stiffness in the frequency domain. Therefore, it is convenient to use the concept of the damping (loss) factor (the structural damping factor) which was introduced to study the material damping, e.g. [Newland, 1989] rather than the damping coefficient used to investigate the viscous damping. The damping factor for the general resilient element is defined as the ratio of the imaginary modulus over the real modulus. Following this definition, we can define the (equivalent) damping factor for gas film. It is a ratio of the damping stiffness over the total stiffness which is the sum of the real part of the dynamic stiffness and the static stiffness (expression in page 86) :

$$\eta(\omega) = \text{Im}[K(\omega)]/\text{Re}[K(\omega)] \tag{4.12}$$

By using the damping factor, the total stiffness of an EPG pad reads :

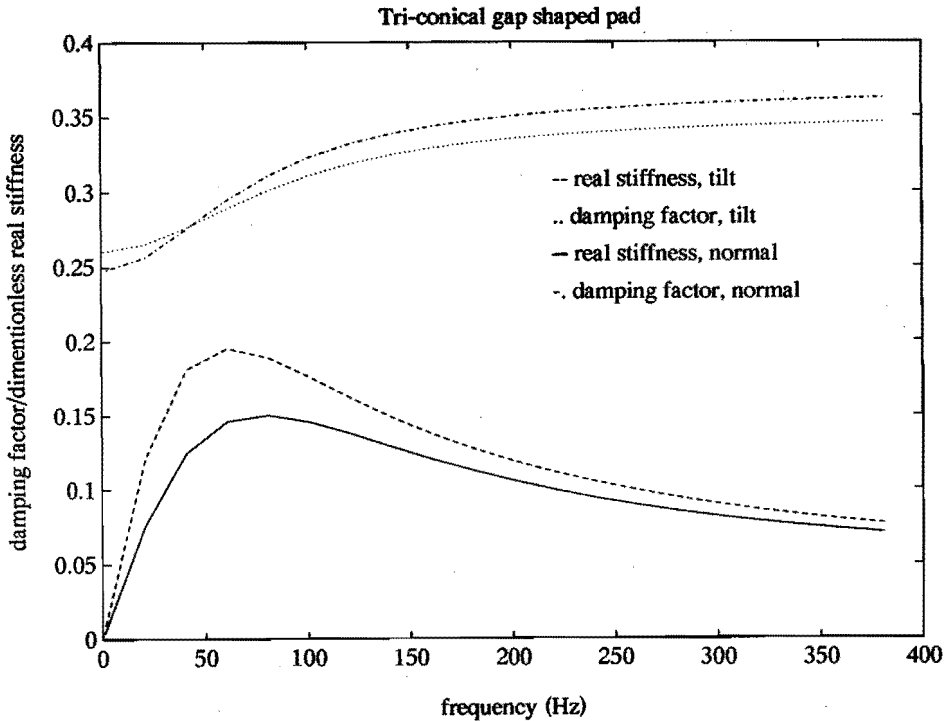


Fig. 4.5. The real stiffness and damping loss factor of tri-conical gap shaped EPG pads ($p = 0.6 \text{ MPa}$, $hw = 5 \text{ }\mu\text{m}$)

$$K(j\omega) = \text{Re}[K(\omega)][1 + j \eta(\omega)] \quad (4.13)$$

With the comparison of the damping coefficient, it can be seen that the damping factor at resonance is twice the damping coefficient in the viscous vibration model and the inverse of the quality factor.

Fig. 4.5 shows the distribution of the $\text{Re}[K(\omega)]$ and $\eta(\omega)$ for an EPG pad with tri-conical gap shape from which one can see that they are nonlinear functions of the frequency. Therefore, the response of a gas bearing system can only be obtained by the loci of the response of a continuous series of linear systems. We take this bearing as an example to illustrate the idea by assuming this bearing support a 60 kg mass. At a specific frequency, the damping factor and the total stiffness are constants. At this frequency, we solve the linear differential equations with constant coefficients. In this example, we solve 20 equations and the loci of frequency response is given in Fig. 4.6, from which it can be seen that the characteristics of tri-conical gap shaped pads are improved under tilt of pad body and the vibration amplitude decreases. This is due to the increase of the damping factor. The role of the damping factor in the control of the vibration amplitude will be discussed later by using the equation of the vibration motion.

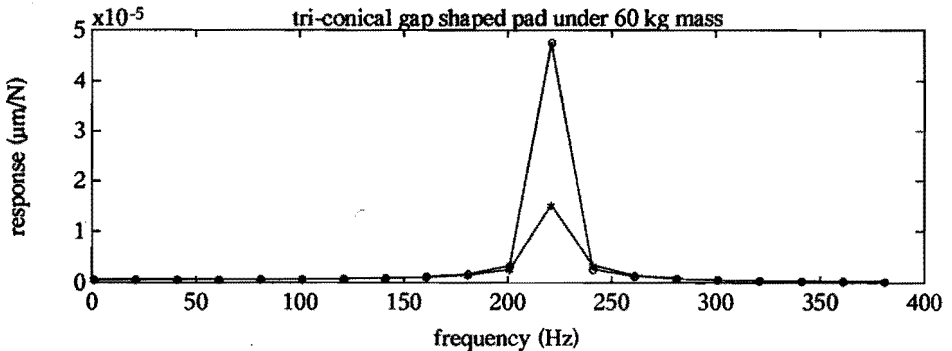


Fig 4.6. The frequency response of one degree of freedom system with an EPG bearing pad with tri-conical gap shape

In order to avoid the frequency-dependent term, the film stiffness can be approximated by a proper combination of certain numbers of constant springs and dashpots [Wang, 1990]. In general, five elements, three spring elements and two dashpots, are needed to model the overall characteristic of a gas

film. In the special case, e.g. for the absolutely stable or absolutely unstable bearings, three elements, two spring elements and one dashpot, are sufficient to describe the characteristic of the gas film. The physical meaning of the model can be described by the overall compressibility of gas film, the reciprocal of the mass content bulk modulus (K_∞) and the modulus associated with the change of mass content. It can be directly seen in the three-element model, the representations of the element models are given in Fig. 4.7.

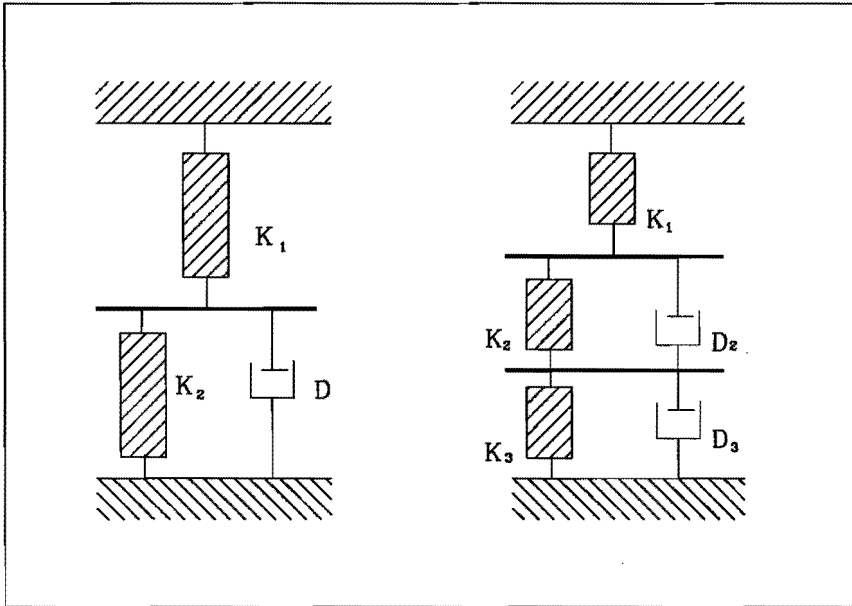


Fig. 4.7. Representation of bearing films stiffness in the combination of constant spring elements and constant damping elements

The constants of equivalent bearing stiffness and damping dashpots in an element model can be determined from the bearing characteristics, e.g. the constants in the three element model are :

$$K_1 = \text{Re}[K(\omega)] \Big|_{\omega \Rightarrow \infty} = K_\infty \tag{4.14}$$

$$\text{Re}[K(\omega)] \Big|_{\omega \Rightarrow 0} = K_1 / (1 + K_1 / K_2) = K_0 \tag{4.15}$$

$$K_2 = K_0 / (1 - K_0 / K_\infty) \tag{4.15}$$

$$D = K_2 \tau_1 \tag{4.16}$$

where τ_1 : time constant

From the structural analysis point of view, a three-element model can be

seen as a mechanical system with the zero mass and one spring in the top and one spring and one dashpot in the bottom. If this model is used in the equation of the vibration motion, one more degree of freedom for a bearing pad will be introduced. The benefit is that all stiffness in the system is constant.

4.5. DYNAMIC MODEL

4.5.1. The equation of motion

In general, the equation of motion for the mass centre of a bearing system reads :

$$\mathbf{M} \{\ddot{\mathbf{X}}\} = \{\mathbf{W}\} - \{\mathbf{F}_m\} - \{\mathbf{F}\} \quad (4.17)$$

where \mathbf{W} : vector of load capacity, both static and dynamic parts

$$\mathbf{W} = \mathbf{W}_0 + (\partial \mathbf{W} / \partial \mathbf{x}) \, d\mathbf{x} + (\partial \mathbf{W} / \partial t) \, (\partial t / \partial \mathbf{x}) \, d\mathbf{x} \quad (4.18)$$

in the frequency domain, it reads :

$$\mathbf{W} = \mathbf{W}_0 + (k_0 + \text{Re}[\mathbf{K}_d(j\omega)] + j \text{Im}[\mathbf{K}_d(j\omega)]) \, d\mathbf{x} \quad (4.19)$$

$$\mathbf{W} = \mathbf{W}_0 + (\text{Re}[\mathbf{K}(j\omega)] + j \text{Im}[\mathbf{K}(j\omega)]) \, d\mathbf{x}$$

\mathbf{W}_0 : vector of static load capacity

\mathbf{x} : static coordinate vector, \mathbf{X} : dynamic change coordinate vector,

$d\mathbf{x}$: in the equation of motion for dynamics, only the relative change with respect to the equilibrium point is involved, so that $d\mathbf{x} = \mathbf{X}$

\mathbf{M} : mass matrix; if we takes the mass centre as the reference, the mass matrix is always a diagonal matrix

\mathbf{K}_d : dynamic stiffness, \mathbf{K} : total stiffness, k_0 : static stiffness

$\ddot{\mathbf{X}}$: Acceleration vector, \mathbf{F}_m : mass force vector

\mathbf{F} : force vector, e.g. preloading force, excitation force etc.

By considering the initial balance between the static forces and the static moment, such as mass and/or other preloading forces and the bearing static load capacity, the equation of motion for an EPG bearing system becomes :

$$-\mathbf{M} \, \omega^2 \{\mathbf{X}\} = -(\text{Re}[\mathbf{K}(\omega)] + j \text{Im}[\mathbf{K}(\omega)]) \{\mathbf{X}\} + \{\mathbf{F}_d\} \quad (4.20)$$

where \mathbf{F}_d : dynamic force vector

By introducing the concept of the damping factor, the equation of motion

becomes :

$$- M \omega^2 \{X\} = - \operatorname{Re}[K(\omega)](1 + j \{\eta(\omega)\}) \{X\} + \{F_d\} \quad (4.21)$$

If we use the element approach to model the film stiffness, the equation of the motion for a gas bearing system can be written with constant coefficients and with increased degrees of freedom. In the three-element model, one additional degree of freedom will be introduced for a pad.

From the definition of the damping factor [Newland, 1979], it is understood that the natural frequency is not influenced by the damping factor. If we are interested in the (dynamic) natural frequency only, the equation of the motion can be further reduced to the following form :

$$- M \omega^2 \{X\} = - (\operatorname{Re}[K(\omega)]) \{X\} \quad (4.22)$$

The components in each matrix or vector depend on the specific design. The abstract forms of the equations of the vibration motion from (4.17) to (4.22) are valid for all kinds of preloading structures and they are also the same whether or not the structures are symmetrical. The detailed treatment will be illustrated with a specific example given in the next chapter.

4.5.2. The natural frequency

Before discussing the solution, it is necessary to devote some attention to the natural frequency. Due to the frequency dependence of bearing film stiffness, it is puzzling to select the stiffness value to determine the natural frequency, especially for the more complicated bearing systems. In order to use a single parameter to indicate the stability criteria, the dynamic natural frequency [Wang and Schellekens, 1990a] was introduced.

The dynamic natural frequency can be derived by considering an EPG bearing as a servomechanism. The servo model of EPG bearings was put forward by Wilcock [Wilcock, 1967] and used by many other researchers [Stowell, 1971] [Haycock, 1976] [Plessers, 1985]. In this way, the system characteristics can be expressed by means of the transfer function of load change to working gap change. The block diagram of the servo system for an EPG bearing system is shown in Fig. 4.8. The frequency response of the bearing supported mass is the main loop with transfer function of $M(j\omega) = - 1/M\omega^2$ and the response of the gas film is a feedback loop with a transfer function $K(j\omega)$ - the stiffness characteristic of the EPG bearings. The gain factor of the transfer function

for the feedback loop is the static stiffness, the real part of the transfer function is the dynamic stiffness and the imaginary part is the damping stiffness. The product of these two transfer functions reads :

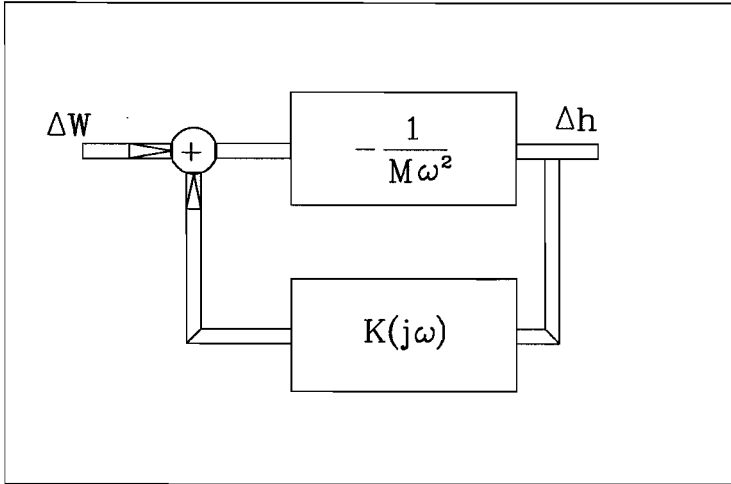


Fig. 4.8. The block diagram of an EPG bearing system

$$S(j\omega) = - \frac{1}{M\omega^2} \{ \text{Re}[K(j\omega)] + j \text{Im}[K(j\omega)] \} \tag{4.23}$$

According to the Nyquist stability criteria, the stability of a system with single degree of freedom requires that :

$$\text{Im}[S(j\omega)] < 0, \text{ if } \text{Re}[S(j\omega)] = -1 \tag{4.24}$$

In terms of bearing film stiffness and mass, it implies :

$$\text{Im}[K(j\omega_n)] > 0, \text{ if } |\text{Re}[K(j\omega_n)]| / M\omega_n^2 = 1 \tag{4.25}$$

This implies that a stable bearing system should have positive damping stiffness, which further illustrates the stability criteria used in Chapter 3. From this expression, it can also be seen that the natural frequency of a bearing system is determined by a specific value of the total stiffness which results from the frequency dependence of stiffness characteristics. For convenience, this value was defined as the dynamic natural stiffness. It is readily to see that this value is dependent of the mass. For a selected system

with a fixed mass value, the dynamic natural stiffness can be determined by the trial-and-error method through the equation $|\text{Re}[K(j\omega)]| = M\omega^2$. This equation can only be satisfied at a specific frequency value, which is the natural frequency.

If the transfer function of a bearing stiffness characteristics has the cross over frequency (the plot goes through the real axis), the stability can be expressed in an alternative way :

$$|\text{Re}[K(j\omega_c)]|/M\omega_c^2 \Big|_{\text{Im}^+ \Rightarrow \text{Im}^-} > 1 \text{ if } \text{Im}[K(j\omega_c)] = 0 \quad (4.26)$$

or $|\text{Re}[K(j\omega_c)]|/M\omega_c^2 \Big|_{\text{Im}^- \Rightarrow \text{Im}^+} < 1 \text{ if } \text{Im}[K(j\omega_c)] = 0$

For convenience, the term, $(\text{Re}[K(\omega)]/M)^{1/2}$ is defined as the dynamic natural frequency. Then, the stability criteria will be stated as follows: If the product plot goes through the real axis from the positive (negative) to the negative (positive) half plane of the imaginary part and the dynamic natural frequency is greater (less) than the resonant frequency, the system is stable. For a more complicated system, e.g. having more cross over frequencies, the dynamic natural frequency is that cross over frequency near the resonant frequency.

For a system with a single degree of freedom, it is easy to see that $M\omega^2$ is an increasing function of ω so that the cross-over frequency can only be produced by the transfer function of the bearing stiffness. In general, the transfer function of an EPG bearing can be expressed by a function with two poles and two zeros :

$$K(j\omega) = K_0 (1+j\omega\tau_3)(1+j\omega\tau_2)/(1+j\omega\tau_1)(1+j\omega\tau_4) \quad (4.27)$$

It can be verified that there exists one cross over frequency for the transfer function with two poles and two zeros.

The time constants, τ_1 , τ_2 , τ_3 and τ_4 can be determined from the bearing stiffness characteristics (as illustrated in Fig. 4.9). However, it should be noted that they are all working gap-dependent for a selected bearing under the same supply pressure. If all the bearings in a structure do not operate in the same working gap height, the total stiffness characteristics will become more complicated, more cross over frequencies may be introduced, particularly in the system with mixed bearing characteristics.

In special cases, i.e. absolutely stable ($\tau_1 > \tau_2$) or absolutely unstable,

$(\tau_1 < \tau_2)$, the transfer function is simplified as the function with one pole and one zero, i.e. :

$$K(j\omega) = K_0 (1+j\omega\tau_1)/(1+j\omega\tau_2) \tag{4.28}$$

or
$$K(j\omega) = K_0 [(1+\omega^2\tau_1\tau_2)+j\omega(\tau_1-\tau_2)]/[(1+(\tau_2\omega)^2)] \tag{4.29}$$

In this case, no cross over frequency is involved. The stable bearing system requires positive damping stiffness, i.e. $\tau_1 > \tau_2$ (see equation 4.29).

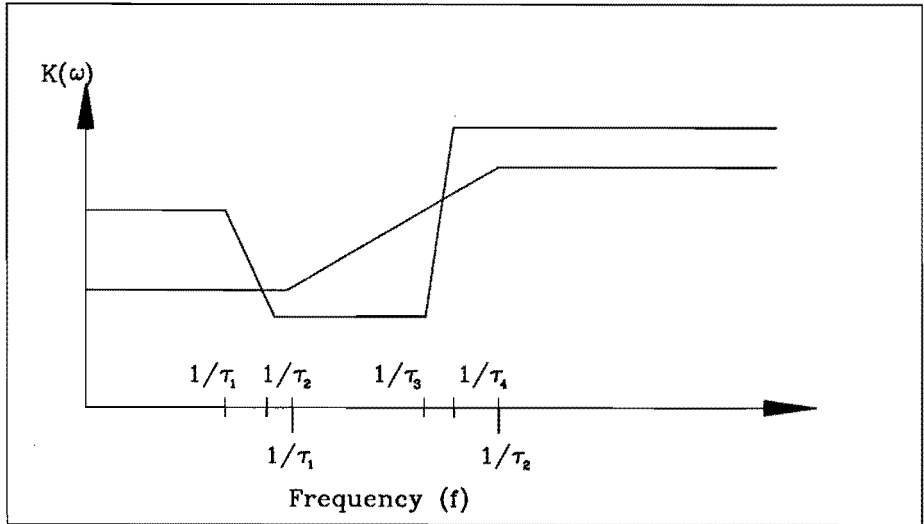


Fig. 4.9. Illustration of log-log plot of an EPG bearing stiffness

4.5.3. Solution methods

In a system with large degrees of freedom, it is very difficult to get a direct correlation between system parameters and natural frequencies of the system by using analytical formulas [Yang, 1989]. Since a lot of standard software is available to solve matrix problems, it is convenient to solve a system with the large degrees of freedom numerically.

If we are only interested in the natural frequency, we can disregard the damping stiffness of the EPG bearing. Therefore, the solution of the bearing system at a specific frequency becomes a normal eigenvalue problem, i.e. to solve the following equation :

$$\det\{[M]^{-1}[Re[K(\omega)]-\lambda[I]\} = 0 \tag{4.30}$$

In the three-element model, the mass matrix is singular due to the zero mass elements are introduced, e.g. for $M \times M$ mass matrix with N zero mass. The first thing to do is to reduce the mass matrix and reconstruct the damping and stiffness matrices in order to get the eigenvalues of the matrix, in other words, the natural frequency of the system. The new matrix M_r , $(M-N) \times (M-N)$, can be obtained by cutting off the rows and columns corresponding to the zeros mass. New stiffness matrix S_r , $(M-N) \times M$, can be built up simply by canceling the rows with respect to the zero mass. However, the rows and columns in the damping matrix corresponding to the zero mass in the damping matrix must be made to zero if they are not zero and the new damping matrix D_r becomes $(M-N) \times (M-N)$ matrix.

Thereafter, the problem becomes the normal vibration problem with damping, which can be solved by the reduced order method [Newland, 1989]. A new square matrix with dimension, $(2M-N) \times (2M-N)$ is then composed. In the OS matrix, the rows (iis) corresponding to the zero mass diagonals, $m(ii,ii)$, have the new coefficients which are the ratio of the elements in the original stiffness matrix, $S(m, n)$, over the element, $D(ii,ii)$, in the original damping

$$A = \left[\begin{array}{c|c} OS(19 \times 19) & ID(19 \times 9) \\ \hline M_r^{-1} K_r & M_r^{-1} D_r \\ (9 \times 19) & (9 \times 9) \end{array} \right] \tag{4.31}$$

matrix for all the columns. In the ID matrix, there is the similar treatment, except only the elements corresponding to the non-zero mass diagonal (ii) are taken into account :

$$\begin{aligned} OS(m,n) |_{m(ii,ii)=0} &= S(m,n)/D(ii,ii) \\ ID(m,j) |_{m(ii,ii)=0} &= D(m,j)/D(ii,ii) \end{aligned} \tag{4.32}$$

where

$$ii = 1,2, \dots, \text{number of zero mass}, j = 1,2, \dots, \text{number of non-zero mass}$$

The eigenvalues of the matrix A will contain the natural frequencies of the systems. Physically, only the eigenvalues related to the non-zero mass are significant, which represent the natural frequencies of the slide.

Solving this matrix is the normal eigenvalue problem which can be easily solved by using MATLABTM. The computer program based on the MATLAB was

developed to solve this kind of problem.

The natural frequency in the complex stiffness model is not influenced by damping factor. Therefore, the natural frequencies of the slide can be solved by only using the real part of the complex stiffness of the bearings. However, due to the frequency dependence, the solution of the system natural frequency can not be obtained in one time. In this treatment, the mass matrix and stiffness are all the $M \times M$ matrices. At one frequency, we have a constant stiffness matrix, K , and we can have the difference between the given frequencies and the eigenvalues of the matrix $M^{-1}K(\omega)$, i.e. :

$$DD = |\text{diag}(\lambda(\omega)\mathbf{I}) - \text{diag}(\text{eig}[M^{-1}K(\omega)])| \quad (4.33)$$

where

eig : operation to find eigenvalues of the matrix

diag: diagonal vector of a matrix

At a given frequency, DD will be a vector with length of M . Using the formula (4.33) in a frequency range, DD becomes a matrix with the dimension M by the number of frequencies. It is obvious that the minimum value of the matrix DD will be the natural frequencies of the system. This model gives the direct forward solution and smaller dimension of matrices, the mass is also regular. However, it needs more calculations to find the natural frequencies of the system.

4.5.4. Determination of vibration modes

In order to find eigenvalues of a matrix, the spatial variables $\{X\}$ are transformed into the general coordinate system, $\{y\}$, through the similarity transformation of the matrix :

$$\{y\} = U^{-1}\{X\} \quad (4.34)$$

The transformation matrix U can be automatically derived through the matrix diagonalization which is composed by the eigenvectors, i.e. :

$$U = [\{u_{s1}\}, \{u_{s2}\}, \dots, \{u_{sn}\}] \quad (4.35)$$

Because the length of the eigenvectors is arbitrary, the real use of the transformation matrix needs to normalize the eigenvectors. The vibration modes which we have found are uncoupled modes in the generalized coordinates $\{y\}$. In practice, we like to know the relationship between a mode and the system parameters. This suggests that we need to analyze the composition of each mode

in terms of the real spatial coordinates. From the relation (4.34), it is easily to find that this can be done by using the transformation matrix, i.e.:

$$\{X\} = U \{y\} \quad (4.36)$$

By doing so, we can determine the relationship between the vibration modes and the system parameters. By using the eigenvector matrix, the observable modes in a spatial coordinate can be determined. Using this information, the system can be improved by adjusting the suitable parameters.

The transformation matrix is also useful to determine the vibration displacement with time in a real coordinate system :

$$\{x(t)\} = U \{\text{diag } e^{\lambda_i t}\} \left[\int \{\text{diag } e^{\lambda_i t}\} U^{-1} B \{F_d(t)\} dt + C \right] \quad (4.37)$$

where λ : eigenvalue

In our problems, the mass matrix is always diagonal so that the matrix B equals the inverse of the mass matrix, i.e. $B = M^{-1}$.

4.6. EFFECTS OF NON-LINEARITY OF FILM STIFFNESS

The displacement dependence of gas bearing film stiffness can also be studied by the loci of the response. The difference from the previous case is that the bearing stiffness is no longer a constant, but a fourth order polynomial function of the displacement. At a specific frequency, the equation of the vibration reads :

$$M \{\ddot{X}\} + \{ \Sigma a_i X^i \} \{X\} = \{F_d\} \quad (4.38)$$

If a simple single harmonic input is used at a specific frequency, it was proved [Storer and Tomlinson, 1991] that the higher order transfer function can be constructed by Volterra series, which presents the diagonals of the higher order frequency response functions. Therefore, the first order transfer function under this single harmonic excitation will be described as following:

$$FT_1 = H_1(j\omega) + H_2(j\omega, j\omega) |F_d|^2/2 + \dots \quad (4.39)$$

By this technique, the non-linearity of bearing film stiffness can be studied. However, one should note that the dynamic displacement is no longer one harmonic wave. Therefore, the dynamic characteristics given in Chapter 3 are no longer true. This can be a significant subject in the further study.

4.7. CONCLUSIONS

This chapter presented the models to describe the real gap height, which are the inter-connection tools between EPG pads and machine structures. It can be used to define a requirement on the guide beam tolerance in terms of surface waviness and the parallelism in the opposite arrangement of EPG pads. It may be also used in software correction by coupling the overall characteristics of EPG bearing pads.

The stiffness of the gas film is generally a non-linear function of frequency and displacement. Nevertheless, in the study of the natural frequencies of a gas bearing system, the bearing stiffness can be taken as a specific constant value, i.e. the dynamic natural stiffness, to adapt the general methods to solve the time-invariant, linear systems. Under a specified excitation with a constant frequency, it is also reasonable to treat the gas film with constant characteristics: constant stiffness and constant damping. Thereafter, the method was developed to determine natural frequencies of a system, the observable modes in a spatial coordinate and the vibration displacement with time.

In the design of a gas bearing system, there are some more things to be carefully considered, such as loop stiffness, kinematically positioning and driving, symmetry and preloading.

CHAPTER 5.

EXPERIMENTS ON A LINEAR GUIDE WITH EPG BEARING PADS

5.1. INTRODUCTION

This chapter will present the detailed analysis and experiments for a large linear guide with EPG bearings, which can act as an important component in CMMs (Coordinate Measuring Machines) and some other machines with linear motion components. The linear guide used in this research was designed in a way similar to one slide in a CMM. The purpose of the study is to find out the role of the EPG bearings in the slide, especially referring to the natural frequencies of gas bearing systems and the design principles such as loop stiffness, symmetry, preloading, which were discussed in Chapter 4. In order to reach this goal, the slide frame was designed with high transmissive stiffness so that the slide can be considered as a rigid body. Therefore, the effect of the gas bearing on the slide behaviour can be easily studied. Such a slide can only be constructed by considering constructional details very carefully, not only the slide frame but also the connection of the EPG pads to the structure, the detailed design considerations were reported earlier [Driessen, 1992]. The transmissive stiffness of 10^3 N/ μ m was realized on the frame at bearing mounting positions and on the bearing connection in which elastic hinges were used. The soft plate spring was selected as a preloading mechanism due to its compact size and other special features: to guarantee the parallel movement of a pad and to realize the self-alignment in the same mechanism. The hinge-soft spring pair reduces the influence of non-parallelism of the guide beam on the bearing behaviour.

Furthermore, this chapter will present detailed treatments of the models to determine the natural frequencies of the linear guide and their experimental verifications. The slide was studied in three different configurations both theoretically and experimentally. The purposes are :

- 1). to verify the models;
- 2). to emphasize some essential concepts in the design of a gas bearing system. These concepts include:
 - 1). fully symmetrical arrangement will decouple vibration modes;

- 2). eccentric mass will lower the lowest natural frequency;
- 3). any additional weak element will introduce lower natural frequencies than the lowest natural frequency determined by the gas bearings alone.

5.2. DESIGN OF THE LINEAR GUIDE

5.2.1. Mechanical structure

Fig. 5.1 shows the schematic diagram of the slide structure, Fig. 5.1a shows the frame with the pad mounting positions and Fig. 5.1b presents the whole slide : the frame with pads is supported by the granite beam. The overview of the realized guide is shown in Fig. 5.5. The granite guide beam was chosen because it is often used as the guide of X-slide in CMMs. The tri-conical gap shaped pads were used in the guide due to the fact that they provide the best overall characteristics as pointed out in chapter 3. Two pads of 80 mm diameter were mounted on the top of the slide in order to test possible situations with a heavier load. Pads of 60 mm diameter were used on the two sides of the slide. The frame structure of the slide is optimized in the sense that the slide can provide very high transmissive stiffness in the bearing mounting points and the weight of the moving part of the guide is comparable with that of CMMs. In order to study the effect of the bearing arrangement, pads can be mounted in 14 positions. Three basic arrangements were used in the experiments in order to compare the slide behaviour, i.e.

- I). fully symmetrical arrangement of all the pads, ten pads were used (positions 1 to 10 in Fig. 5.1a);
- II). not-fully-symmetrical arrangement, eight pads were used (there are no pads in the positions 3 and 7);
- III). eccentric loading, the arrangement is similar to the configuration II but without balancing load.

In the configuration I, four of the eight bearing pads were rigidly mounted on one side of the slide through elastic hinges (Fig. 5.2c) and the other four were mounted on the other side of the slide through plate springs (Fig. 5.3). The four bearings connected through plate springs function as the preloading mechanism. The plate spring mounting enables the slide to reduce the requirement for manufacturing and assembling accuracy. In configuration II three pads were mounted on each side and all the connections were the same as in configuration I. In these two configurations, an additional mass was used

to adjust the mass center in the vertical plane which goes through the line determined by two top bearings. In configuration III, the balancing mass was taken away and the weight of the slide structure acts as an eccentric loading as it is the case in many CMMs.

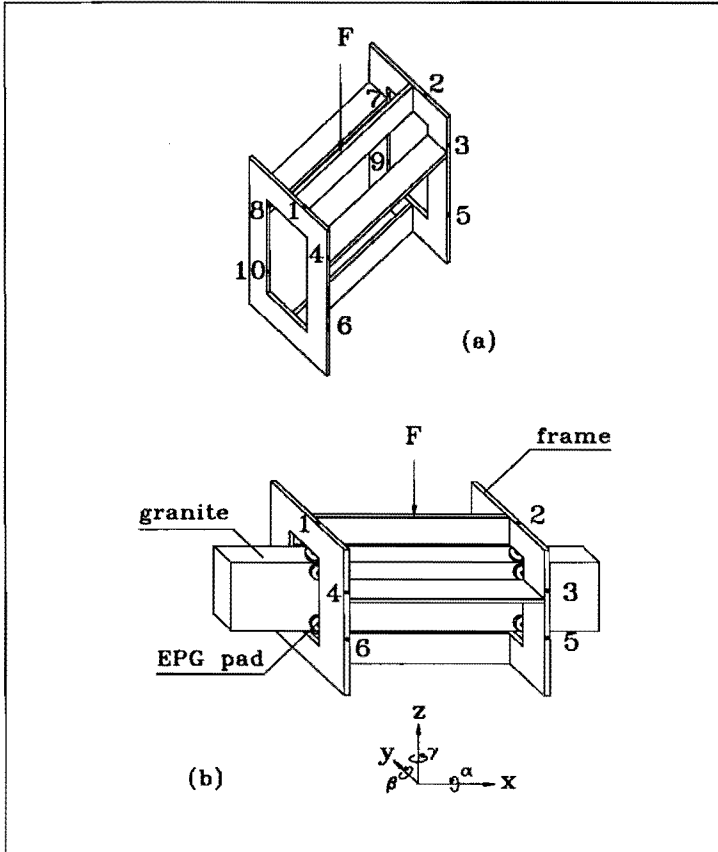


Fig. 5.1. Schematic illustration of the linear guide

Fig. 5.2 shows the configuration of the elastic hinge and two other possible elements to mount an EPG pad on the slide. The elastic hinge is a kind of ideal element to construct a precision mechanism, particularly for this kind of application. The hinge connection provides high transmissive stiffness to ensure loop stiffness which is a weak point in traditional designs. At the same time, it functions as a self-alignment mechanism which is extremely important to ensure the bearings work properly with less strict

requirements on manufacturing and assembly accuracy. In the hinge, the transmissive stiffness is guaranteed by the proper selection of the hinge parameters and in the same element self-alignment is ensured by the material elasticity.

In the pair of ball and conical surface (or other surfaces, e.g. a spherical surface) (Fig. 5.2a), the contact stiffness is often too low in normal working conditions for typical dimensions used in practice. The stiffness can be estimated by the formula used for line contacts in roller bearings. For high transmissive stiffness, e.g. for experiments with our slide, it is not practical to select such elements. The reason is that we do not want a large space between the slide and the guide beam, which will obviously weaken the structure. (The detailed analysis will be given in Appendix 5)

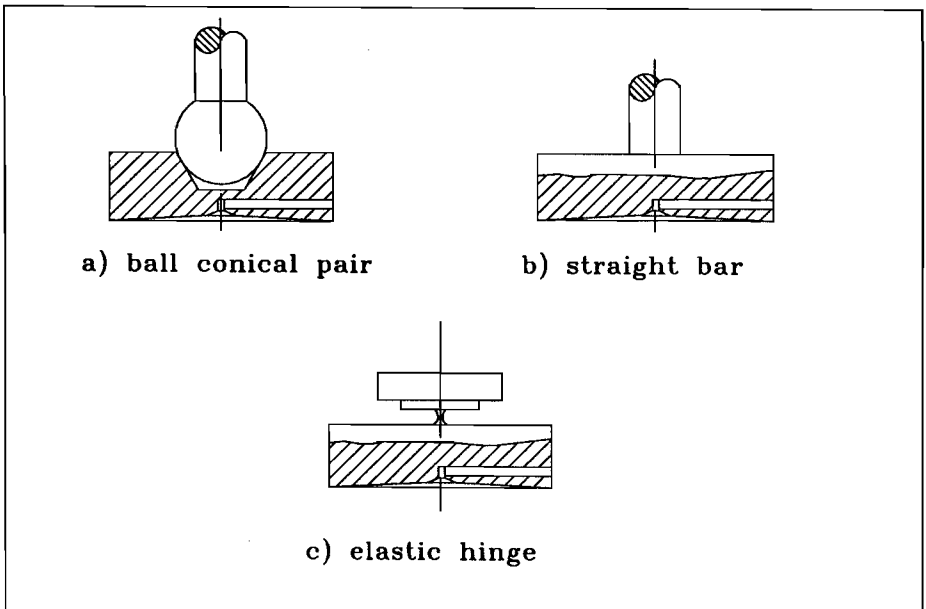


Fig. 5.2. Mechanisms to mount EPG pads on the slide

An additional important problem in the ball-cone pair is the the friction behaviour in the contact. This friction behaviour is unpredictable due to a lot of causes, e.g. the friction coefficient is not a constant and the line

contact situation may vary with the appearance of corrosion, dust and lubricants, etc. The self-alignment results from the balance between the friction moment and bearing moment. If we think one step further, we would doubt what really happens if one wants such a pair making a very small rotation (10^{-4} rad.)! The straight bar connection (Fig. 5.2b) really gets rid of the line contact but the connection with high transmissive stiffness and the efficient self-alignment can not be realized through the same bar.

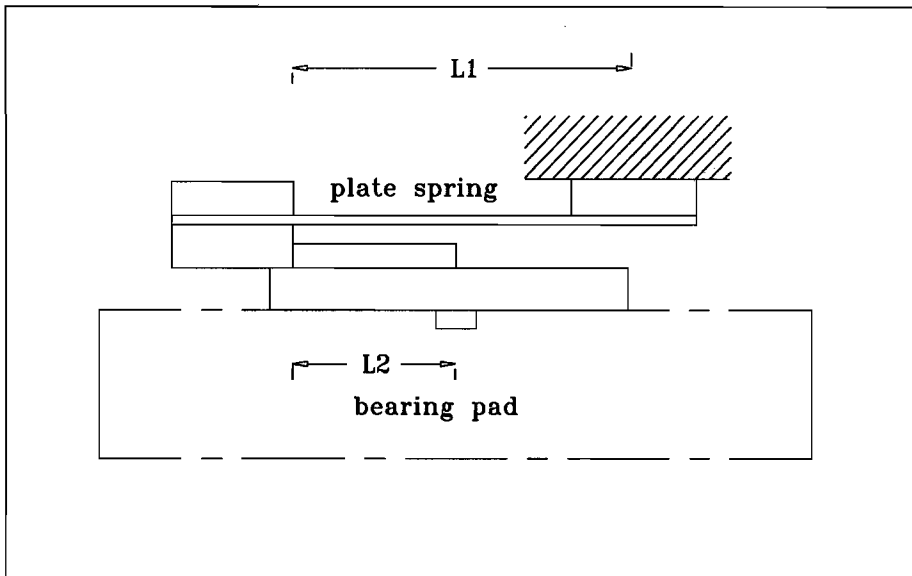


Fig. 5.3. Plate spring mechanisms to mount EPG pads on the slide

Furthermore, in the opposite EPG pad configuration, it is necessary to introduce a kind of soft connection (its stiffness is much lower than the bearing film stiffness) in the preloading side. The soft connection functions as the absorber of the displacement in the bearing gap height direction. If there is any change, e.g. due to non-parallelism of the two opposite surfaces of the granite beam, this change will dominantly go to the soft connections because its stiffness is much lower than that of the gas film (the detailed analysis is given in Appendix 6). By analysis and comparison, a plate spring shown in Fig. 5.3 was chosen in the slide. The plate spring is favorable in mounting a preloading pad because it can be designed with the desired stiffness in less space. At the same time, it can also be designed to

guarantee the parallel movement of a bearing pad by proper selection of the length of two arm lengths, i.e. $L_1 = 2 L_2$, shown in Fig. 5.3. In addition, due to lower bending stiffness and torsion stiffness, it can also act as a self-alignment mechanism. The experience in the developed slide shows that the plate spring works properly and is indeed a suitable element in such an application. Fig 5.4 shows the detailed view of a pair of pads : one is mounted through the elastic hinge and the other through the plate spring.

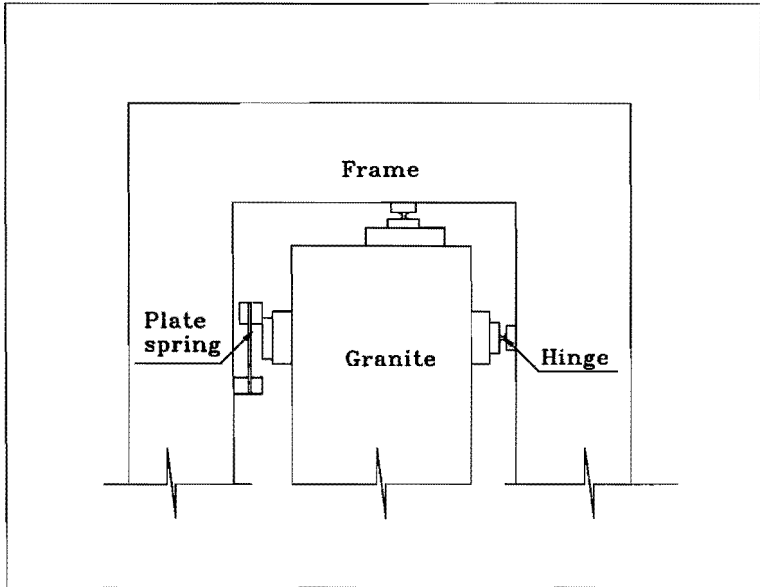


Fig. 5.4. Illustration of the hinge-plate spring mounting pair

The stiffness of the finally realized guide in the bearing mounting position is higher than 10^9 N/m, about 10 times the bearing film stiffness. The stiffness in the transmissive direction of the hinge is also higher than 10^9 N/m. These stiffness values ensure an acceptable loop stiffness. Therefore, the slide can be considered as a rigid body. Furthermore, the lowest natural frequency of the slide frame is about 900 Hz which is far out of the frequency range for testing the slide. Fig. 5.5. illustrates the realized linear guide.

5.2.2. Analysis

Before discussing the experimental verification, we first repeat the aim

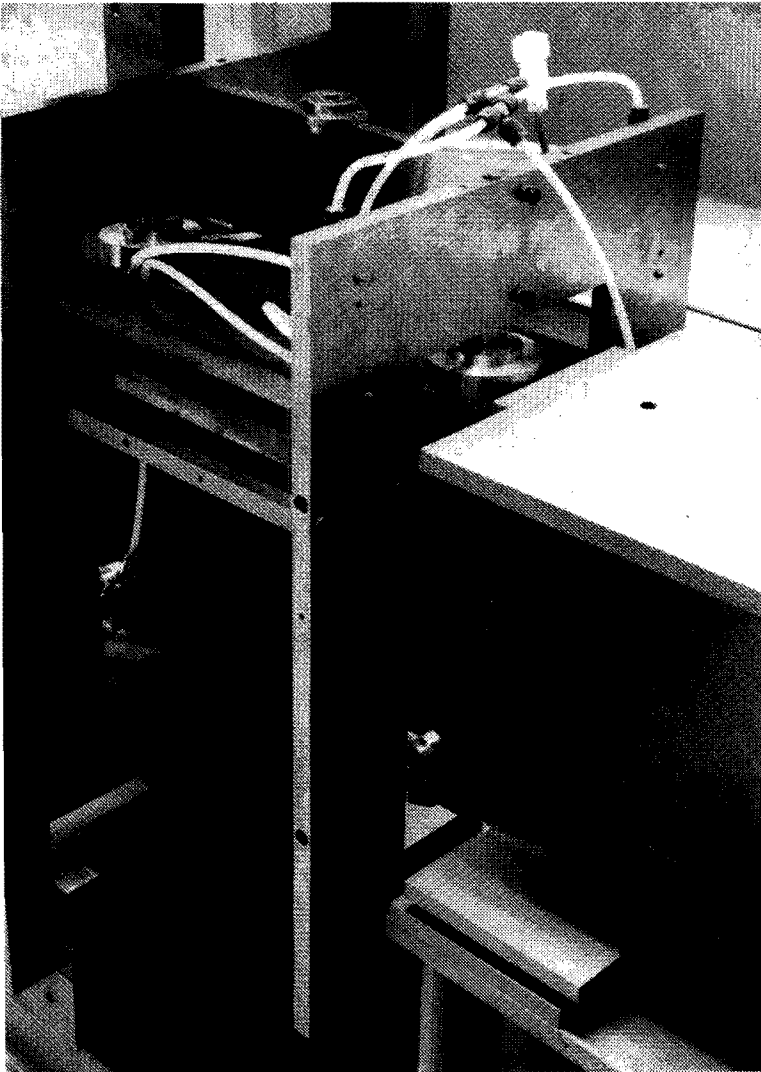


Fig. 5.5. Illustration of the realized slide

of the research on the slide and explain the techniques used in the solution.

Until now, the dynamics of complex, large machines, like CMMs, are rarely investigated, particularly the machines with EPG bearings. With further increasing requirements on machine accuracy and reliability, the dynamic behaviour of the machine becomes the most important factor for designers. The EPG bearing is a basic element in those machines and a key factor influencing

the dynamic behaviour of these machines. Therefore, there is an urgent need to develop appropriate models to study the machine's dynamic behaviour in relation to EPG bearings. In Chapter 4, two models were developed: 1). the three element model in which the gas film characteristics are represented by three constants: two springs and a dashpot; 2). the damping factor model (the complex stiffness model) in which the complex stiffness of a gas film is used. For clarity, the coordinates used in the models are shown in Fig. 5.6.

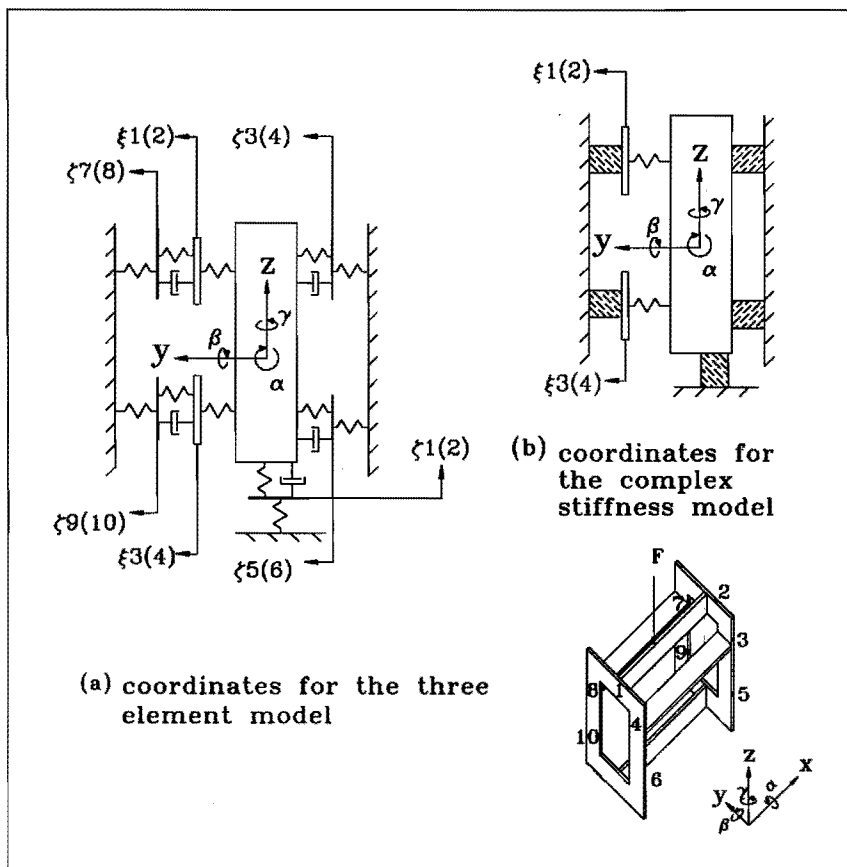


Fig. 5.6. Illustration of the coordinates used in the models

If we use the three element model, the generalized coordinate vector reads :

$$S=[Y, Z, \alpha, \beta, \gamma, \xi_1, \xi_2, \xi_3, \xi_4, \zeta_1, \zeta_2, \zeta_3, \zeta_4, \zeta_5, \zeta_6, \zeta_7, \zeta_8, \zeta_9, \zeta_{10}] \quad (5.1a)$$

for the configuration I (as described in 5.2.1.) and :

$$S = [Y, Z, \alpha, \beta, \gamma, \xi_1, \xi_2, \xi_3, \zeta_1, \zeta_2, \zeta_3, \zeta_4, \zeta_5, \zeta_6, \zeta_7, \zeta_8] \quad (5.1b)$$

for the configuration II, (also described in 5.2.1.).

The first five coordinates describe the slide motions, i.e. Y, Z, α , β , γ , ξ 's are the motions of the bearing body attached to the plate spring, and ζ 's are the motions of bearing zero mass elements.

The main diagonal element vectors of the mass matrices read as :

$$\{M\} = [ms, ms, jx, jy, jz, mb, mb, mb, mb, 0, 0, 0, 0, 0, 0, 0, 0, 0] \quad (5.2a)$$

$$\{M\} = [ms, ms, jx, jy, jz, mb, mb, mb, 0, 0, 0, 0, 0, 0, 0] \quad (5.2b)$$

where ms : the mass of the slide, mb : the mass of a pad,
 jx, jy, jz : moments of inertia of the slide about X, Y, and Z.

In the damping factor model, the coordinate vectors become :

$$S = [Y, Z, \alpha, \beta, \gamma, \xi_1, \xi_2, \xi_3, \xi_4] \quad (5.3a)$$

for the configuration I and :

$$S = [Y, Z, \alpha, \beta, \gamma, \xi_1, \xi_2, \xi_3] \quad (5.3b)$$

for the configuration II. Due to the constructional feature of the slide and the selection of the coordinate system, the mass matrix is the main diagonal matrix. The element vectors in the diagonal read respectively :

$$\{M\} = [ms, ms, jx, jy, jz, mb, mb, mb, mb] \quad (5.4a)$$

$$\{M\} = [ms, ms, jx, jy, jz, mb, mb, mb] \quad (5.4b)$$

It is clear that one more degree of freedom for one bearing is introduced in the three element model. In addition, the mass matrix is singular. Nevertheless, there exists a special technique to deal with it, as introduced in Chapter 4. The damping matrix and stiffness matrix can be filled according to the equations of vibration motion of the slide, which are the symmetrical matrices. All the elements in the stiffness matrix are constants so that the problem becomes an eigenvalue problem. In the complex stiffness model, the total degrees of freedom are less and the mass matrix is regular. However, the elements in the stiffness matrix are the dynamic stiffness of gas film which is frequency-dependent. The final solution can only be determined by the loci of a series of solutions, as explained in Chapter 4. For a given bearing, either the constants in the three element model or the dynamic stiffness distribution in the damping factor model can be obtained by using the bearing design software mentioned in Chapter 3.

By using the techniques described in Chapter 4, the spectrum of natural frequencies of the slide can be calculated. Fig. 5.7 shows nine of them

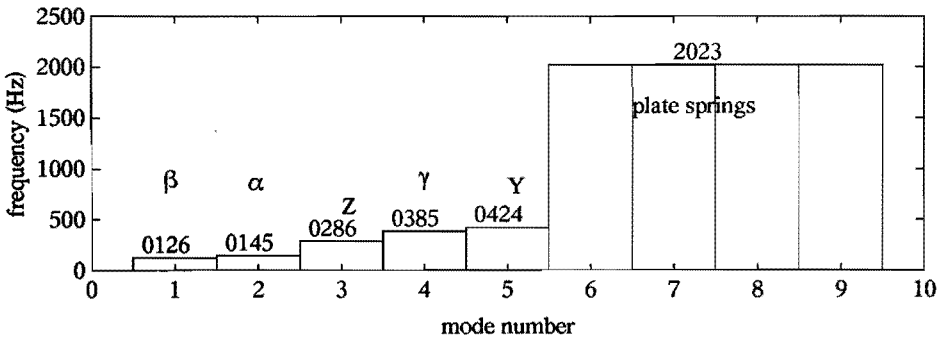


Fig. 5.7. The calculated spectrum of the natural frequencies

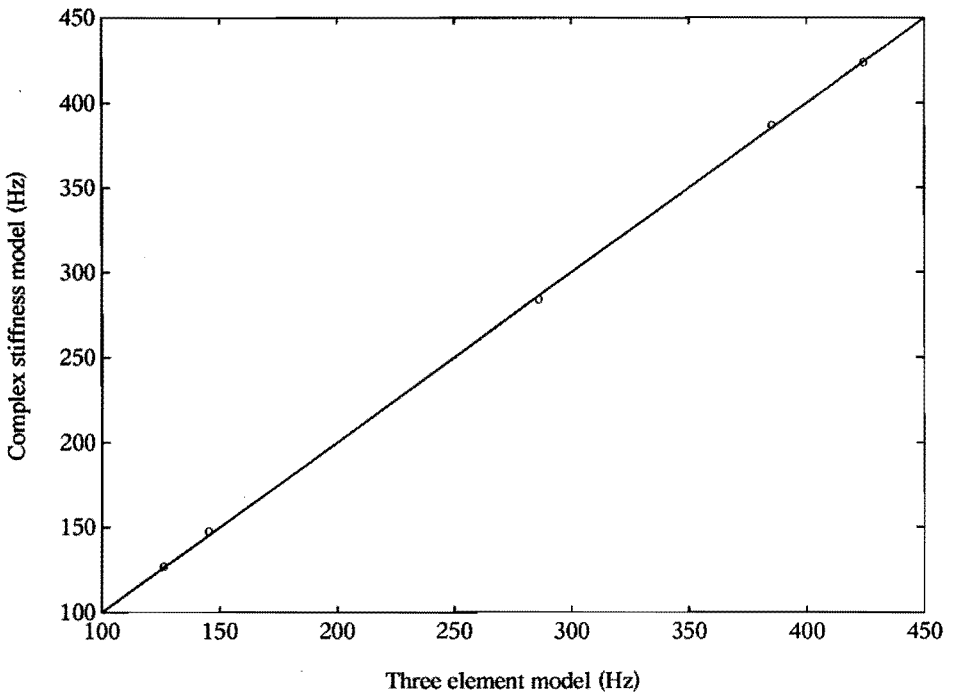


Fig. 5.8. The comparison of the calculated natural frequencies between the three element model and the complex stiffness model (configuration 1) (the test results will be given in Appendix 8)

corresponding to the non-zero masses, calculated by the three element model for the configuration I. Note that the eigenvalues are obtained by diagonalization of the matrix A which implies the coordinate transformation from the spatial coordinate system into a generalized coordinate system. The observable natural frequencies in a spatial coordinate can be determined by the eigenvector which can be used to transform the vibration modes from the generalized coordinate system back to the spatial coordinate system. In other words, the eigenvector indicates the movement of all the masses in the system along the corresponding spatial coordinate direction at the natural frequencies. With the help of the eigenvector, one can identify the mode shape of a vibration mode in the spatial coordinate(s), as indicated on the top of the frequency bars. Fig. 5.8 presents the comparison of the natural frequencies of the system between the complex stiffness model and the three element model. The straight line in the figure represents the perfect agreement between these two results and the symbols 'o' represent the natural frequencies calculated by the models. It can be seen that there is no conflict between these two models. Due to the fully symmetrical arrangement of all the pads, the vibration modes are not coupled.

5.3. EXPERIMENTS

5.3.1. Experimental set-up

Experiments were performed on the guide to verify the theory derived in this thesis. The experimental set-up for testing single pads (Fig. 2.5) was modified to perform the experiment on the guide, schematically shown in Fig. 5.9. The overview of the whole test system is given in Fig. 5.10. In order to eliminate the influence of the test set-up in the dynamic test of the slide, measurements on the structure were also performed, including the structure for supporting the shaker and the structure for supporting the guide beam. From the model, we deal with the slide frame vibration relative to the guide granite beam. Therefore, it is necessary to measure the vibration at reference points on the slide. The most accurate reference will be the point nearest to the test point on the frame.

The dynamic behaviour of the frame itself was also checked by a modal analyzer. The excitation was delivered by a hammer and the acceleration was measured. It confirms that the slide can be considered as a rigid body in the range for testing the slide, the test results are given in Appendix 8.

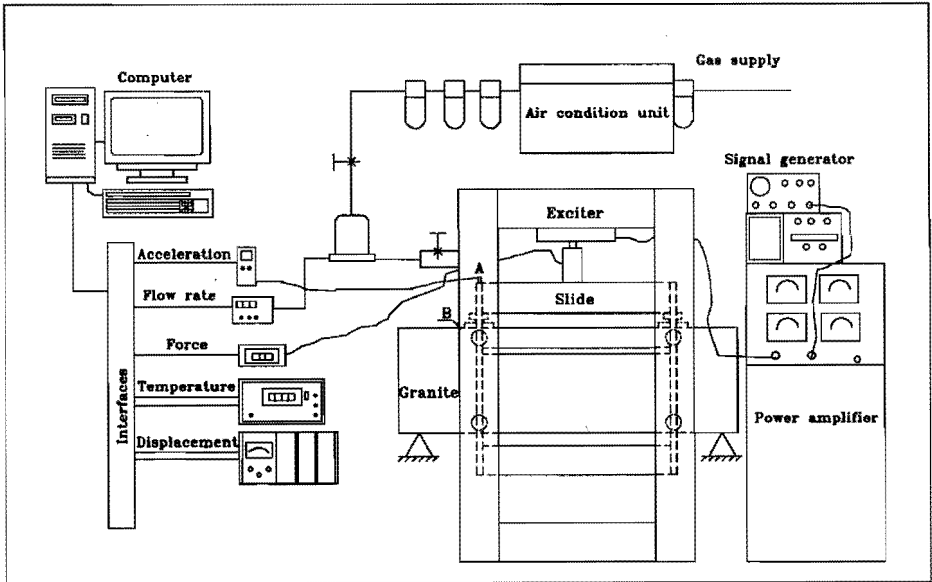


Fig. 5.9. Illustration of the test set-up for the dynamic test of a slide

5.3.2. The identification of vibration modes

The electro-magnetic exciter was used to generate the dynamic force and the force transducer was mounted between the exciter and the slide to measure the dynamic force in the random and step sine testing. The accelerometer or/and displacement sensor can be mounted on the slide to measure the response of the slide. In the detailed experiment, the stepwise sine testing signal was chosen in order to concentrate the energy on the measuring frequency. The dynamic force was delivered in the vertical direction at the center top of the slide, as indicated in Fig. 5.1. In this loading situation, it provides two excitation forces : the force in Z-direction and the moment about X-axis. This is because the top pads were designed at the off-center along the negative direction of the Y-axis, see Fig. 5.1. The accelerometer was mounted on the slide through a permanent magnet and on the granite through wax, which can provide sufficient accuracy in the specified frequency range. In the identification of the vibration in Y-direction and the rotations about the Z and about the Y axes, the hammer excitation was used. The hammer was also used to check the natural frequencies of the frame and the support. In this type of test, the sensitive excitation point was chosen for determining a desired natural frequency. Appendix 8 presents a typical test result.

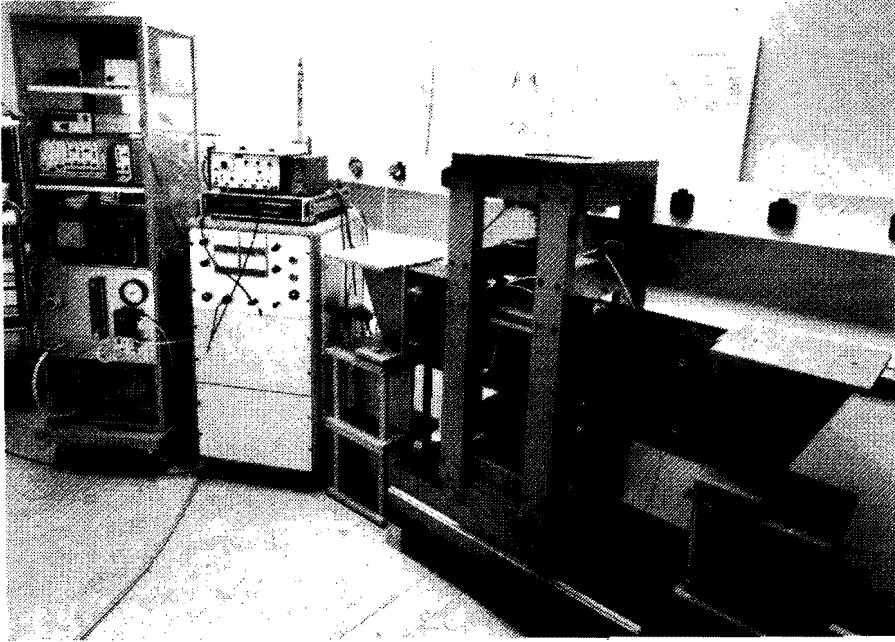


Fig. 5.10. Overview of the test set-up for the dynamic test of a slide

5.3.2.1. Fully symmetrical configuration (I)

The arrangement with 10 pads, two on the top and eight on two sides, was the first configuration in which the pads were fully symmetrically positioned on the slide referring to the mass center. Therefore, if each pair of symmetrically arranged pads has the same stiffness there will not be any cross-coupling between the vibration modes. After experimentally determining the real working parameters of the top bearings, the experimental results should correlate well with the theoretical predictions.

The analysis by using the three-element model indicated that the natural frequencies of the slide which can be observed in Z-direction are 145 Hz and the natural frequencies which can be observed in the rotation about the X-axis and the Y-axis are 286 Hz and 126 Hz (Fig. 5.7). By placing the accelerometer

in different positions, the natural frequencies corresponding to different spatial coordinates can be distinguished through comparing the results. As mentioned earlier, the dynamic loading on the slide from the shaker was delivered in the Z-direction and the rotation about X-axis, the moment generation was due to the eccentric loading (Fig. 5.1). Therefore, the really observable natural frequencies are only those in the Z-direction and the rotation about X-axis, i.e. 145 Hz and 286 Hz. Fig. 5.11 shows the comparison between the experimental results and the theoretical predictions. The straight line indicates the ideal conditions under which the experiments coincide with the theoretical predictions. If the line determined by the comparison points, 'o's, perfectly matches the straight line, it shows good agreement between the experiments and the predictions. If there is a systematic dispersion, it means that there is an unsuitable modeling of film stiffness or a wrong estimation of mass/moment of inertia. If a random dispersion appears, it may indicate deficiency in the experiments. At a natural frequency, the upward (downward) deviation of a comparative point from the straight line implies the under-(over-) estimation of that natural frequency by the model.

From Fig. 5.11, it can be seen that the experiments have very close correlations to the theoretical predictions. The two 'o's in one natural frequency are the calculated results from two models. This is a very encouraging result. Thereafter, more experiments were performed and compared with both the three-element model and the damping factor model. They all show very good agreement with the theoretical predictions.

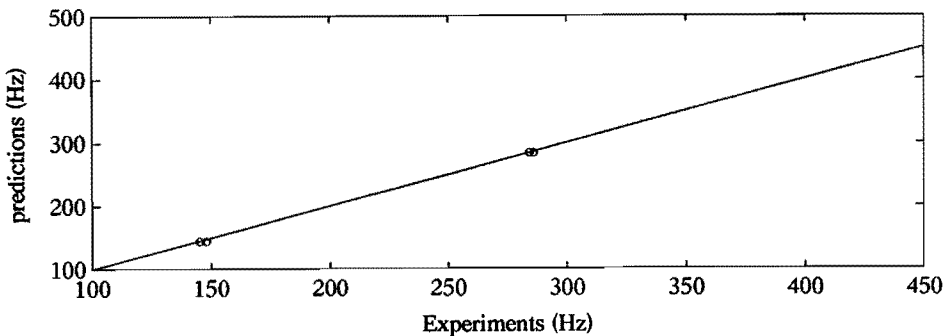


Fig. 5.11. The comparison of the natural frequencies of the slide between the experiments and theoretical predictions (configuration .1)

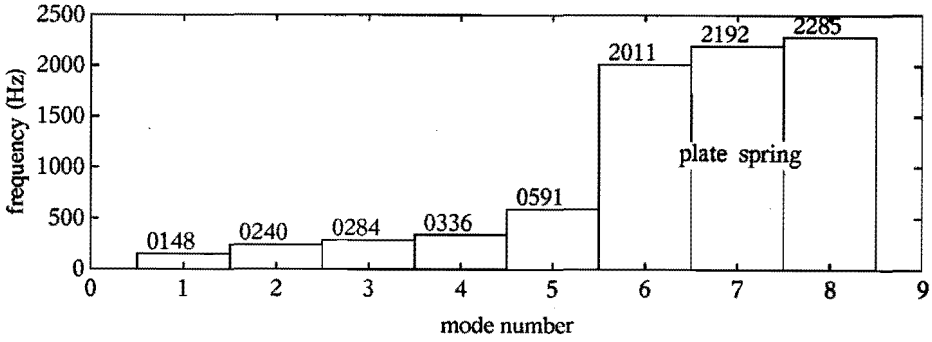


Fig. 5.12. The spectrum of natural frequencies (configuration II)

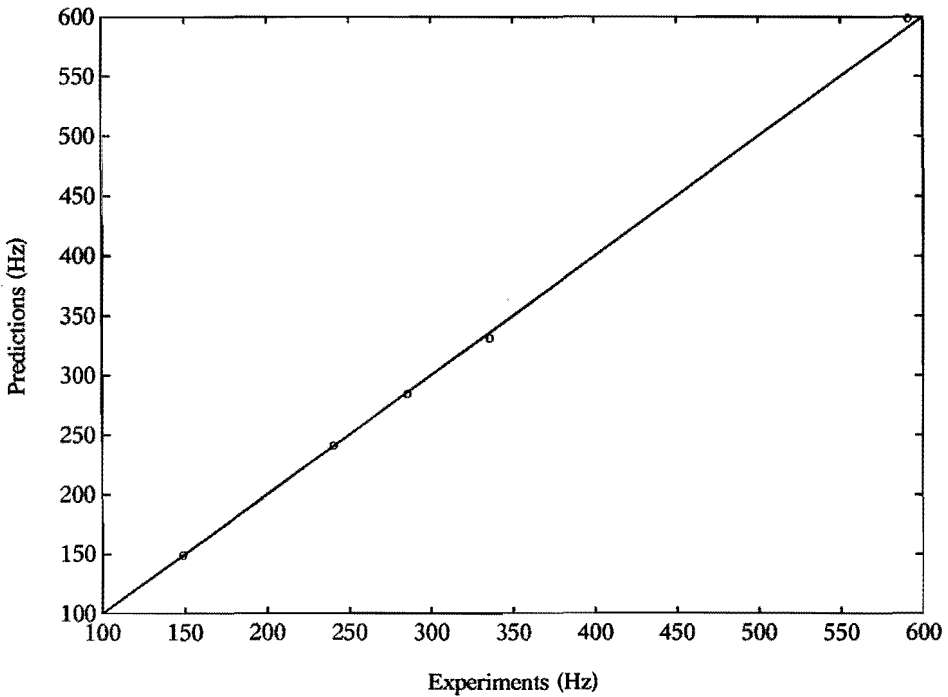


Fig. 5.13. Comparison between the theoretical predictions and experimental verifications in the configuration II

5.3.2.2. Partially symmetrical configuration (II)

The three pads on one side are rigidly mounted and the other three are mounted on the slide through plate springs. In this configuration, the working parameters of all the pads on the sides can be determined. Therefore, a more detailed and more accurate comparison can be performed. Fig. 5.12 shows the spectrum of the natural frequencies of the slide under the configuration II. Fig. 5.13 presents the comparison between the experiments and theoretical predictions. This result once more shows a good correlation between the model predictions and the experiments.

Because the pads in the configuration II are not fully symmetrically arranged in the side, the responses in Z , Y , α , and γ show strong cross coupling between the vibration modes. As one example, Fig. 5.14 presents the predictions on the mode shapes in Y -direction and α -rotation. The vertical axis represents the relative amplitude of each mode appeared in this coordinate. One can expect that if a weak driving mechanism is introduced in the system one lower natural frequency than those given in the figure will

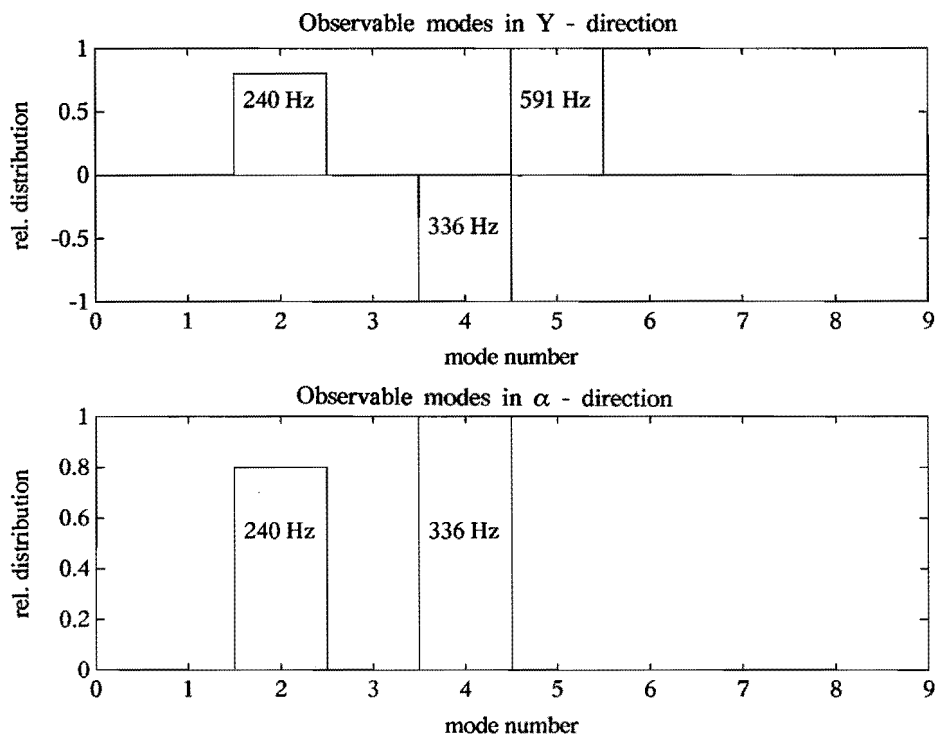


Fig. 5.14. Mode shapes in Z -direction and α -rotation (configuration II)

appear in these two coordinates. This is because the driving mechanism can not be mounted through the mass center.

5.3.2.3. Influences of eccentric mass

In practice, most machines work under eccentric loading, which is a typical situation in CMMs. The model to determine system natural frequencies is based on the mass center coordinates. A slide with eccentric mass, generally speaking, refers to the condition in which the mass center of the slide is different from the center determined by all the pads, which implies the change of mass and the moments of inertia and the change of the bearing position related to the mass center used in the model. If the model is used to study the machine with eccentric mass, we only need to change the constants related to the bearing positions and the moments of inertia of the slide. Obviously, one will expect the lowest natural frequency of the system will be decreased due to the increase of mass and moment of inertia. In most CMMs, the moment of inertia is much higher than that of our test slide, especially that about the X-axis and the stiffness is lower than that we used. Therefore, the CMMs will have lower lowest natural frequencies than the slide which we used in this study. Fig. 5.15 presents a test result on the slide with eccentric mass, configuration III (the configuration II without the balancing mass, see Fig. 5.1). The mass center has a distance 30 mm from the line determined by the two top pads. The calculated natural frequencies in the Z- and α -directions are 165 Hz and 256 Hz. Comparing these results with those shown in Fig. 5.15, one can see that it once more shows a very good agreement between the experiments and the model predictions.

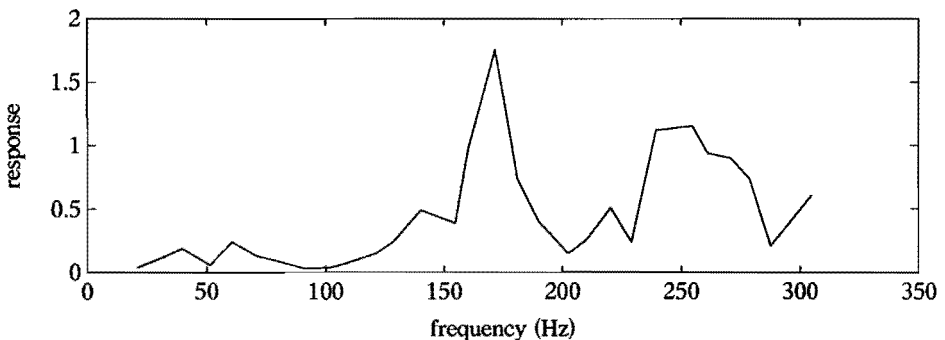


Fig. 5.15. A test result on the slide under eccentric loading

5.4. DISCUSSION

5.4.1. Symmetry

A fully symmetrical arrangement of all the pads will eliminate the cross-coupling among vibration modes, which is illustrated in Fig. 5.14, in which the calculation was based on the assumption that all the pads have the same characteristics. However, in practice it is almost impossible to ensure fully symmetrical configuration due to the difficulties in the control of the working parameters. As a result, weak cross-coupling, at least, will be observed in most machines. If we calculate the slide with real bearing parameters, the cross coupling can be predicted. For the slide with variable loading like those used in the Y-slide of CMMs, the pads work under different gap heights, which means that in general the pads operate with different stiffness and damping.

There is another point which is interesting to be mentioned, i.e. the driving mechanism. In most machines, the acting point of driving force is not through the mass center, which means that the vibration mode related to the driving system will be cross-coupled to all the coordinate directions. If driving stiffness is very low, it will introduce a much lower natural frequency than those determined by the bearings.

In practice, a machine slide may be heavier than the slide used in the study and the machine size may also be larger than that of the slide. Therefore, one will expect the appearance of lower natural frequencies than those determined in the study.

5.4.2. Influence of the support of the guide beam

The influence of the support can be studied by expanding the model to include the degree of freedom of the support. With similar extension, one can study the whole machine. With the extended model, it is possible to optimize the structural mass and bearing dynamic stiffness of X-slide and Y-slide in a machine, e.g. a CMM, to obtain better overall dynamic behaviour. In principle, the interaction of vibration modes in two bodies can be used to obtain minimal amplitude in the desired position, e.g. the tool holding position. The generalized theory of vibration isolation and vibration absorption can be the guide to perform the research. This strategy refers to the "hardware" correction of machine errors. With the help of the model, the effective algorithm for software correction of the machine error due to vibrations can

be developed. These topics are beyond the current scope of research and will not be treated in detail.

5.5. CONCLUSIONS

This chapter explained the theory and the solution techniques, as well as the experimental system for designing and analyzing a gas bearing slide. The experimental identification of the natural frequencies of the slide proves the correctness of the developed models. Therefore, the model developed in this work can be used in design and analysis of gas bearing slides, even for more complicated structures.

In the design and test of the slide, constructional details were emphasized, particularly the connection mechanisms were discussed in detail. It shows the importance of taking care with these details.

The method and model developed in this thesis were proved by experiments on the slide in three configurations. The model is not limited by the machine dimension and bearing working condition. Under a given condition, the parameters in the models remain constants. Therefore, the model can be directly used to design new slides and to analyze existing slides. It can also be extended to analyze complete multi-axis machines.

CHAPTER 6.

CONCLUSIONS AND RECOMMENDATION

6.1. CONCLUSIONS

The research in this project shows that the developed software and the experimental system can be effectively used in the design, study and testing of both single EPG bearings and EPG bearing systems.

From the research on the characteristics of bearings and bearing systems, one can draw the following conclusions:

1). The numerical and experimental research reveal that the EPG bearings with concave gap shapes provides higher load capacity and higher stiffness. The tri-conical gap shaped pads are superior to the parallel and bi-conical gap shaped pads. Under the same stable conditions, the tri-conical gap shaped pads provide higher load capacity and higher stiffness than those provided by the other two.

2). The bearing body tilt will greatly reduce the load capacity and stiffness of the parallel gap shaped bearing: maximum change of the stiffness is up to 60 % at the optimal working gap height. On the contrary, the tri-conical gap shaped pads are much less sensitive to tilt, the stiffness change is less than 1 % at the optimal working gap height.

3). The tri-/bi-conical gap shaped pads are also less influenced by surface imperfection, especially when half a wavelength is greater than 1.5 times the pad reference dimension (e.g. diameter for circular pads). The worst case is when half a wavelength is equal to the pad reference dimension. The overall characteristics follow the change of the surface profile, particularly load capacity. Under constant load, this means that the change of the working gap height follows the surface pattern.

4). In the velocity range of less than one meter per second, which is the current status of CMMs, the load capacity and stiffness are rarely changed. However, relatively high velocity will greatly reduce the bearing load capacity and stiffness.

5). The temperature of the gas supply is generally lower than the standard room temperature, 0.5 ~ 1 °C. The gas through a restrictor can be

further cooled down. In very accurate applications, it may cause significant distortion of the structure. From the study, a general guideline was established for designing mechanical systems with EPG pads. The bi/tri-conical EPG pads are preferable because they are less sensitive to bearing body tilt and surface imperfections.

6). In dealing with gas bearing systems, this thesis presents the model describing the real working gap height in a system, two models describing the bearing film stiffness and the method for applying the models to the gas bearing systems for the purposes of design and analysis.

7). The models describing the real gap height can be used to define a requirement on the guide beam tolerance in terms of surface waviness and the parallelism in the opposite arrangement of EPG pads.

8). The stiffness of the gas film is generally a non-linear function of frequency and displacement. Nevertheless, in the study of the natural frequencies of a gas bearing system, the bearing stiffness can be represented by springs and dashpots, as in the three-element model: one dashpot and two springs. The purpose of the treatment is to adapt the general methods to solve the time-invariant, linear systems. Under a specified excitation at a constant frequency, it is also reasonable to take the dynamic stiffness of gas film at that frequency into the vibration equation. The final solution can be derived from loci of a series of linear systems with constant stiffness and constant damping. Based on these, two models were developed to predict the natural frequencies of a gas bearing system. These two models all work well and can be conveniently used in designing and analyzing the gas bearing systems.

9). Theoretical analysis and the experiments on the three different configurations of a large linear guide showed the validity of these models. The experimental results correlate well with the predictions of the models. Furthermore, from the study, some essential concepts were revealed. It can be concluded that the models can be used to analyze the machines with EPG bearings, e.g. CMMs. In the design of a gas bearing system, there are some more constructional details to be carefully considered, such as loop stiffness, kinematical positioning and driving, symmetry and preloading. This thesis also provides some discussions and solutions for those aspects. In the system design, weak elements (or components) should be paid more attention because of the cross-coupling of vibration modes.

6.2. RECOMMENDATIONS

As a result of this research, we may also derive some areas for future studies. First of all, it may be concluded that the various investigations in this thesis could be extended to study the journal gas bearings, including modification of gap shape, effect of rotor tilt and surface imperfections. The method of determining the system's natural frequencies may also be used in the spindle system.

Secondly, the non-linear model for gas film stiffness is important for the large dynamic change of working gap height, as the case of Y-slide in a CMM.

Thirdly, on the question of developing the EPG bearings, it is worthwhile spending time and effort developing cheap, reliable, integrated, preloading mechanisms, such as the supersonic-pressurization combination or the Bernoulli-pressurization combination, for pad type bearings used in both linear motion and rotation systems.

Fourthly, in relation to the development of close-loop controlled EPG bearings, we would suggest stopping any attempt to control the supply pressure, including the control of the restrictor.

Finally, in the design of gas bearing systems, if one would like to design a close-loop controlled system, the ideal position to mount the actuator is at the connection between the bearing pad and the structure, which is also true for the tilting pad bearings used in spindles. For high speed spindles, this kind of controlled system could best be left to the active magnetic bearings.

APPENDIX 1.

THE SIMPLIFICATION OF THE EQUATION OF MOTION

The equation of motion can be derived by characterizing the dynamic equilibrium between the inertia forces, the mass forces and the stresses in the fluid and can be expressed in a compact form [Constantinuscu, 1969] :

$$\rho \frac{DV}{Dt} = f - \frac{\text{pressure force}}{\text{mass forces}} + \frac{2 \text{ div}(\mu D) - \frac{2}{3} \text{ grad}(\mu \text{ div } V)}{\text{viscosity force}} \quad (\text{A1.1})$$

pressure force
viscosity force
s stresses
mass forces
inertia forces

where V : velocity vector, t : time, ρ : density, μ : viscosity
 D : strain-rate tensor

$$D = \begin{vmatrix} \frac{\partial u}{\partial x} & (\frac{\partial u}{\partial y} + \frac{\partial v}{\partial x})/2 & (\frac{\partial u}{\partial z} + \frac{\partial w}{\partial x})/2 \\ (\frac{\partial u}{\partial y} + \frac{\partial v}{\partial x})/2 & \frac{\partial v}{\partial y} & (\frac{\partial v}{\partial z} + \frac{\partial w}{\partial y})/2 \\ (\frac{\partial u}{\partial z} + \frac{\partial w}{\partial x})/2 & (\frac{\partial v}{\partial z} + \frac{\partial w}{\partial y})/2 & \frac{\partial w}{\partial z} \end{vmatrix} \quad (\text{A1.2})$$

The expansions of the equation of motion in the rectangular coordinates read :

$$\begin{aligned} \rho \frac{Du}{Dt} &= - \frac{\partial p}{\partial x} + 2 \frac{\partial}{\partial x} \left(\mu \frac{\partial u}{\partial x} \right) + \frac{\partial}{\partial y} \left[\mu \left(\frac{\partial u}{\partial y} + \frac{\partial v}{\partial x} \right) \right] + \frac{\partial}{\partial z} \left[\mu \left(\frac{\partial u}{\partial z} + \frac{\partial w}{\partial x} \right) \right] - \frac{2\sigma}{3\partial x} (\mu \text{ div } V) \\ \rho \frac{Dv}{Dt} &= - \frac{\partial p}{\partial y} + 2 \frac{\partial}{\partial y} \left(\mu \frac{\partial v}{\partial y} \right) + \frac{\partial}{\partial x} \left[\mu \left(\frac{\partial u}{\partial y} + \frac{\partial v}{\partial x} \right) \right] + \frac{\partial}{\partial z} \left[\mu \left(\frac{\partial v}{\partial z} + \frac{\partial w}{\partial y} \right) \right] - \frac{2\sigma}{3\partial y} (\mu \text{ div } V) \\ \rho \frac{Dw}{Dt} &= - \frac{\partial p}{\partial z} + 2 \frac{\partial}{\partial z} \left(\mu \frac{\partial w}{\partial z} \right) + \frac{\partial}{\partial x} \left[\mu \left(\frac{\partial u}{\partial z} + \frac{\partial w}{\partial x} \right) \right] + \frac{\partial}{\partial y} \left[\mu \left(\frac{\partial v}{\partial z} + \frac{\partial w}{\partial y} \right) \right] - \frac{2\sigma}{3\partial z} (\mu \text{ div } V) \end{aligned} \quad (\text{A1.3})$$

where

$$\frac{D}{Dt} = \left(\frac{\partial}{\partial t} + u \frac{\partial}{\partial x} + v \frac{\partial}{\partial y} + w \frac{\partial}{\partial z} \right) \quad (\text{A1.4})$$

The dimensionless form of the equation of motion can be written in the following form if the dimensionless parameters are introduced :

$$\begin{aligned} x &= l_0 \bar{x}, \quad y = h_0 \bar{y} = l_0 (h_0/l_0) \bar{y}, \quad z = b_0 \bar{z} = l_0 \lambda \bar{z}, \quad \lambda = b_0/l_0 \\ u &= U_0 \bar{u}, \quad v = U_0 (h_0/l_0) \bar{v}, \quad w = U_0 \lambda \bar{w}, \quad p = p_0 \bar{p}, \quad \rho = \rho_0 \bar{\rho}, \\ \mu &= \mu_0 \bar{\mu}, \quad u = U_0 \bar{u}, \quad t = (l_0/U_0) \bar{t}, \\ M_a &= U_0^2 / (kRT_0), \quad \rho_0 = p_0 / (RT_0) \end{aligned}$$

$$\begin{aligned}
 kM_a^2 \bar{\rho} \frac{D\bar{u}}{Dt} &= -\frac{\partial \bar{p}}{\partial \bar{x}} + N\mu \left\{ 2 \left(\frac{h_0}{l_0}\right)^2 \frac{\partial}{\partial \bar{x}} \left(\bar{\mu} \frac{\partial \bar{u}}{\partial \bar{x}}\right) + \frac{\partial}{\partial \bar{y}} \left[\bar{\mu} \left(\frac{\partial \bar{u}}{\partial \bar{y}} + \left(\frac{h_0}{l_0}\right)^2 \frac{\partial \bar{v}}{\partial \bar{x}}\right)\right] \right. \\
 &+ \left. \left(\frac{h_0}{\lambda l_0}\right)^2 \frac{\partial}{\partial \bar{z}} \left[\bar{\mu} \left(\frac{\partial u}{\partial \bar{z}} + \frac{\partial u}{\partial \bar{x}}\right)\right] - \frac{2}{3} \left(\frac{h_0}{l_0}\right)^2 \frac{\partial}{\partial \bar{x}} (\bar{\mu} \operatorname{div} \bar{V}) \right\} \\
 kM_a^2 \left(\frac{h_0}{l_0}\right)^2 \bar{\rho} \frac{D\bar{v}}{Dt} &= -\frac{\partial \bar{p}}{\partial \bar{y}} + N\mu \left\{ 2 \left(\frac{h_0}{l_0}\right)^2 \frac{\partial}{\partial \bar{y}} \left(\bar{\mu} \frac{\partial \bar{v}}{\partial \bar{y}}\right) + \left(\frac{h_0}{l_0}\right)^2 \frac{\partial}{\partial \bar{x}} \left[\bar{\mu} \left(\frac{\partial \bar{u}}{\partial \bar{y}} + \left(\frac{h_0}{l_0}\right)^2 \frac{\partial \bar{v}}{\partial \bar{x}}\right)\right] \right. \\
 &+ \left. \left(\frac{h_0}{\lambda l_0}\right)^2 \frac{\partial}{\partial \bar{z}} \left[\bar{\mu} \left(\frac{\partial \bar{w}}{\partial \bar{z}} + \left(\frac{h_0}{l_0}\right)^2 \frac{\partial \bar{v}}{\partial \bar{z}}\right)\right] - \frac{2}{3} \left(\frac{h_0}{l_0}\right)^2 \frac{\partial}{\partial \bar{y}} (\bar{\mu} \operatorname{div} \bar{V}) \right\} \\
 k(\lambda M_a)^2 \bar{\rho} \frac{D\bar{w}}{Dt} &= -\frac{\partial \bar{p}}{\partial \bar{z}} + N\mu \left\{ \frac{2}{\lambda} \left(\frac{h_0}{l_0}\right)^2 \frac{\partial}{\partial \bar{z}} \left(\bar{\mu} \frac{\partial \bar{w}}{\partial \bar{z}}\right) + \frac{\partial}{\partial \bar{y}} \left[\bar{\mu} \left(\frac{\partial \bar{w}}{\partial \bar{y}} + \left(\frac{h_0}{l_0}\right)^2 \frac{\partial \bar{v}}{\partial \bar{z}}\right)\right] \right. \\
 &+ \left. \left(\frac{h_0}{l_0}\right)^2 \frac{\partial}{\partial \bar{z}} \left[\bar{\mu} \left(\frac{\partial \bar{w}}{\partial \bar{z}} + \frac{\partial \bar{w}}{\partial \bar{x}}\right)\right] - \frac{2}{3} \left(\frac{h_0}{l_0}\right)^2 \frac{\partial}{\partial \bar{z}} (\bar{\mu} \operatorname{div} \bar{V}) \right\}
 \end{aligned}
 \tag{A1.5}$$

Therefore, the relative order of the velocity derivatives can be listed in Table A1 :

TABLE A1 The Relative Order of Magnitude of the Derivatives in the Equation of Motion

Derivatives	Relative order
$\frac{\partial p}{\partial x}, \frac{\partial p}{\partial z}, \frac{\partial p}{\partial y}$	1
$\frac{Du}{Dt}, \frac{Dw}{Dt}, \frac{\partial^2 u}{\partial y^2}, \frac{\partial^2 w}{\partial y^2},$	$N\mu, kM_a^2, \lambda kM_a^2$
$\frac{Dv}{Dt}, \frac{\partial^2 u}{\partial x^2}, \frac{\partial^2 u}{\partial z^2}, \frac{\partial^2 w}{\partial x^2}, \frac{\partial^2 w}{\partial z^2}, \frac{\partial^2 v}{\partial y^2}, \frac{\partial^2 v}{\partial y \partial z}, \frac{\partial^2 v}{\partial x \partial y}, \frac{\partial^2 w}{\partial z \partial x}, \frac{\partial^2 u}{\partial x \partial z}$ grad(divV)	$kM_a^2 (h/L)^2$ $N\mu (h/L)^2$
$\frac{\partial^2 v}{\partial x^2}, \frac{\partial^2 v}{\partial z^2}$	$(h/L)^4$

Note that the working gap height (h) of EPG bearings is very small in comparison to bearing dimensions (L), $h/L \approx 10^{-3} - 10^{-4}$, in the restrictor region $10^{-1} - 10^{-2}$. Therefore, the terms of the derivative of velocity belonging to the third and fourth rows can be omitted. Hence, the equation of

motion reduces to the following form :

$$\begin{aligned}
 kM_a^2 \frac{D\bar{u}}{D\bar{t}} &= -\frac{\partial\bar{p}}{\partial\bar{x}} + N\mu \frac{\partial}{\partial\bar{y}} \left(\bar{\mu} \frac{\partial\bar{u}}{\partial\bar{y}} \right) \\
 0 &= -\frac{\partial\bar{p}}{\partial\bar{y}} \\
 k(\lambda M_a)^2 \frac{D\bar{w}}{D\bar{t}} &= -\frac{\partial\bar{p}}{\partial\bar{z}} + N\mu \frac{\partial}{\partial\bar{y}} \left(\bar{\mu} \frac{\partial\bar{w}}{\partial\bar{y}} \right)
 \end{aligned} \tag{A1.6}$$

or the dimensional form :

$$\begin{aligned}
 \rho \frac{Du}{Dt} &= -\frac{\partial p}{\partial x} + \frac{\partial}{\partial y} \left(\mu \frac{\partial u}{\partial y} \right) \\
 0 &= -\frac{\partial p}{\partial y} \\
 \rho \frac{Dw}{Dt} &= -\frac{\partial p}{\partial z} + \frac{\partial}{\partial y} \left(\mu \frac{\partial w}{\partial y} \right)
 \end{aligned} \tag{A1.7}$$

APPENDIX 2.

THE SIMPLIFICATION OF THE ENERGY EQUATION

The (thermal) energy equation for a perfect gas can be expressed in the following form [Kakaç, et al, 1987] :

$$\rho c_p \frac{DT_s}{dt} = \nabla \cdot (\kappa \nabla T_s) + \frac{Dp}{dt} + \mu \Phi \quad (\text{A2.1})$$

$$\Phi = \left[\left(\frac{\partial u}{\partial x} \right)^2 + \left(\frac{\partial v}{\partial y} \right)^2 + \left(\frac{\partial w}{\partial z} \right)^2 \right] + \left(\frac{\partial u}{\partial z} + \frac{\partial w}{\partial x} \right)^2 + \left(\frac{\partial v}{\partial x} + \frac{\partial u}{\partial y} \right)^2 + \left(\frac{\partial w}{\partial y} + \frac{\partial v}{\partial z} \right)^2 - \frac{2}{3} (\nabla \cdot \mathbf{v})^2 \quad (\text{A2.2})$$

By virtue of the equation of motion and the use of the concept of stagnation temperature (T_0), the energy equation reads

$$\underbrace{\rho c_p \frac{DT_0}{dt}}_{\text{convection}} = \underbrace{\nabla \cdot (\kappa \nabla T_s)}_{\text{conduction}} + \underbrace{\frac{Dp}{dt}}_{\text{dissipation}} + \Xi \quad (\text{A2.3})$$

where

$$T_0 = T_s + (u^2 + v^2 + w^2)/2c_p \quad (\text{A2.4})$$

$$\begin{aligned} \Xi = & 2 \frac{\partial}{\partial x} \left(\mu u \frac{\partial u}{\partial x} \right) + \frac{\partial}{\partial y} \left(\mu v \frac{\partial v}{\partial y} \right) + 2 \frac{\partial}{\partial z} \left(\mu w \frac{\partial w}{\partial z} \right) - \frac{2}{3} \text{grad}(\mu \mathbf{v} \cdot \text{div} \mathbf{v}) \\ & + \frac{\partial}{\partial z} \left[\mu u \left(\frac{\partial u}{\partial z} + \frac{\partial w}{\partial x} \right) \right] + \frac{\partial}{\partial x} \left[\mu w \left(\frac{\partial u}{\partial z} + \frac{\partial w}{\partial x} \right) \right] + \frac{\partial}{\partial x} \left[\mu v \left(\frac{\partial u}{\partial y} + \frac{\partial v}{\partial x} \right) \right] \\ & + \frac{\partial}{\partial y} \left[\mu w \left(\frac{\partial v}{\partial z} + \frac{\partial w}{\partial y} \right) \right] + \frac{\partial}{\partial z} \left[\mu v \left(\frac{\partial v}{\partial z} + \frac{\partial w}{\partial y} \right) \right] + \frac{\partial}{\partial y} \left[\mu u \left(\frac{\partial u}{\partial y} + \frac{\partial v}{\partial x} \right) \right] \end{aligned} \quad (\text{A2.5})$$

- κ : heat conduction coefficient
- T_0 : gas stagnation temperature
- T_s : gas static temperature
- c_p : heat capacity at constant pressure

Noting the relative order, the dissipation term Ξ can be simplified as :

$$\Xi \approx \frac{\partial}{\partial y} \left[\mu u \frac{\partial u}{\partial y} \right] + \frac{\partial}{\partial y} \left[\mu w \frac{\partial w}{\partial y} \right] \quad (\text{A2.6})$$

It is also true for the heat conduction terms in the bearing film, i.e. :

$$\nabla \cdot (\kappa \nabla T_s) = \frac{\partial}{\partial y} \left(\kappa \frac{\partial T_s}{\partial y} \right) \quad (\text{A2.7})$$

APPENDIX 3. THE JOULE-THOMSON COEFFICIENT

When the Joule-Thomson coefficient is considered in the flow process, the energy equation reads :

$$u du = c_p dT - \mu_j dp \quad (A3.1)$$

where μ : the Joule-thomson coefficient in the condition of zero-velocity, for air under 150 bar pressure, it can be expressed as follows [Zhang and Shi, 1978]:

$$\mu_j = (2.73 \times 10^{-3} - 0.0895 \times 10^{-6} p)(273/T)^2 \quad (A3.2)$$

To integrate the equation (A3.1) and take the square root of it yields :

$$u = [2c_p (T_0 - T_d) - \mu_{jm} (P_0 - P_d)]^{1/2} \quad (A3.3)$$

where $\mu_{jm} = (\mu_{j0} + \mu_{jd})/2 \quad (A3.4)$

APPENDIX 4.

THE FEM FORMULATION OF THE REYNOLDS EQUATION

The procedures of the derivation of the FEM formula are illustrated by taking the static part of the Reynolds equation as an example. In order to clarify the derivation, the Reynolds equation is written as a compact form :

$$\begin{aligned} & \operatorname{div}\left\{\frac{h^3}{12\mu} [p^\circ \operatorname{grad} p_0 + p_0 \operatorname{grad} p^\circ] - p_0 h_0 V/2\right\} + p_0 \frac{\partial f^\circ}{\partial p} \\ & = \operatorname{div}\left(\frac{h^3}{12\mu} p^\circ \operatorname{grad} p^\circ\right) - \sum_{i=1}^n \delta (f^\circ(p_i) - p_i^\circ \frac{\partial f^\circ}{\partial p}) \end{aligned} \quad (\text{A4.1})$$

Note that the operations div and grad are only performed for x and z .

In the present formulation of the Reynolds equation, only the Dirichlet boundary condition, Γ_0 , appears, i.e. the peripheries of a bearing pad.

The FEM formulation of the Reynolds equation can be derived by following the standard procedures [Cuvelier et al, 1986], i.e.

- 1). to multiply the equation by a test function ψ which vanishes on the bearing peripheries;
- 2). to integrate the modified form of the Reynolds equation derived from step (1) over bearing area, Ω ;
- 3). to apply Green's formula to the integral form.

Performing the steps (1) and (2) gives :

$$\begin{aligned} & \int (\operatorname{div}\left\{\frac{h^3}{12\mu} [p^\circ \operatorname{grad} p_0 + p_0 \operatorname{grad} p^\circ] - p_0 h_0 V/2\right\} + p_0 \frac{\partial f^\circ}{\partial p}) \psi_k \, d\Omega \\ & = \int \left\{ \operatorname{div}\left(\frac{h^3}{12\mu} p^\circ \operatorname{grad} p^\circ\right) - \sum_{i=1}^n \delta (f^\circ(p_i) - p_i^\circ \frac{\partial f^\circ}{\partial p}) \right\} \psi_k \, d\Omega \end{aligned} \quad (\text{A4.2})$$

After the step (3), the equation becomes :

$$\begin{aligned} & \int \left(\left\{ \frac{h^3}{12\mu} [p^\circ \operatorname{grad} p_0 + p_0 \operatorname{grad} p^\circ] - p_0 h_0 V/2 \right\} \cdot \operatorname{grad} \psi_k \right) d\Omega - \int p_0 \frac{\partial f^\circ}{\partial p} \psi_k \, d\Omega \\ & = \int \left(\frac{h^3}{12\mu} p^\circ \operatorname{grad} p^\circ \right) \operatorname{grad} \psi_k \, d\Omega + \sum_{i=1}^n \delta (f^\circ(p_i) - p_i^\circ \frac{\partial f^\circ}{\partial p}) \psi_k \, d\Omega \end{aligned} \quad (\text{A4.3})$$

Note that $\int (\text{div } \psi_k \{ \frac{h_0^3}{12\mu} [p^o \text{grad } p_0 + p_0 \text{grad } p^o] - p_0 h_0 V/2 \}) d\Omega$ and $\int \text{div}(\frac{h_0^3}{12\mu} \psi_k p^o \text{grad } p^o) d\Omega$ can be converted into linear integral over the boundaries, which are equal to zero, i.e. $\int_{\Gamma_0} d\Gamma = 0$.

The unknown p in the domain Ω can be written as :

$$p_0 = \sum_{j=1}^N P_j \psi_j \tag{A4.6}$$

from which we deduce the following system of linear algebraic equations for pressures in all nodal points, P_1, P_2, \dots, P_n :

$$\begin{aligned} & \sum_{j=1}^n P_j (\int \{ \frac{h_0^3}{12\mu} [p^o \text{grad } \psi_j + \psi_j \text{grad } p^o] - \psi_j h_0 V/2 \} \text{grad } \psi_k) d\Omega - \int P_i \psi_i \frac{\partial f^o}{\partial p} \psi_k d\Omega \\ & = \int (\frac{h_0^3}{12\mu} p^o \text{grad } p^o) \text{grad } \psi_k d\Omega + \sum_{i=1}^n \delta (f^o(p_i) - p_i^o \frac{\partial f^o}{\partial p}) \psi_k d\Omega \end{aligned} \tag{A4.7}$$

As mentioned earlier, the bearing area, Ω , in the finite element approximation is subdivided into a finite number of triangles. Assume that there are N vertices of triangles: $\sigma_1, \sigma_2, \dots, \sigma_n$. For each nodal point, σ_i , a basic function ψ_i is defined with the following properties :

- 1). $\psi_j (\sigma_i) = \delta_{ij} = \begin{cases} 1 & \text{if } i=j \\ 0 & \text{if } i \neq j \end{cases} \quad i, j, = 1, 2, \dots, N$
- 2). ψ_j is linear in each triangle
- 3). ψ_j is continuous on $\bar{\Omega} = \Omega \cup \Gamma_0$,

If the element does not include a part of a restrictor, a component of the coefficient matrix and a component of the right hand side vector are separately expressed as follows :

$$K_{ij} = \frac{h_e^3}{24\mu} \frac{|\Delta|}{\Delta^2} [(B_j \sum P_i B_i + C_j \sum P_i C_i)/3 + P_e^o (B_j B_i + C_j C_i)] - \frac{h_e}{12} \frac{|\Delta|}{\Delta} (U^e B_i + W^e C_i) \tag{A4.8a}$$

$$R_j = \frac{h_e^3}{24\mu} \frac{|\Delta|}{\Delta^2} p_e^o (B_j \sum P_i B_i + C_j \sum P_i C_i) \tag{A4.8b}$$

If the element does enclose a part of a restrictor, a component of the coefficient matrix and a component of the right hand side vector become :

$$K_{ij} = \left\{ \frac{h_e^3}{24\mu} \frac{|\Delta|}{\Delta^2} [(B_j \sum P_i B_i + C_j \sum P_i C_i)/3 + P_e^0 (B_j B_i + C_j C_i)] - \frac{h_e}{12} \frac{|\Delta|}{\Delta} (U^e B_i + W^e C_i) \right\} \left(1 - \frac{|\Delta_r|}{|\Delta|}\right) \quad (A4.9a)$$

$$R_{ij} = \left\{ \frac{h_e^3}{24\mu} \frac{|\Delta|}{\Delta^2} P_e^0 (B_j \sum P_i B_i + C_j \sum P_i C_i) \right\} \left(1 - \frac{|\Delta_r|}{|\Delta|}\right) \quad (A4.9b)$$

where

$$P_e = (P_1 + P_2 + P_3)/3 \quad (\text{Because of the linear interpolation function})$$

$$\int_{\Omega_e} d\Omega = |\Delta|/2, \quad \int_{\Omega_r} d\Omega = |\Delta_r|/2, \quad \int_{\Omega} \psi_j d\Omega = |\Delta|/6$$

$$\frac{\partial p}{\partial \xi} = \sum_{j=1}^N P_j \frac{\partial \psi_j}{\partial \xi}$$

$$N = 3 \text{ for the triangle element,} \quad \xi = x, z$$

$$\psi_j = (A_j + B_j x + C_j z)/\Delta$$

$$\frac{\partial \psi_j}{\partial x} = \frac{B_j}{\Delta}, \quad \frac{\partial \psi_j}{\partial z} = \frac{C_j}{\Delta}$$

$$A_j = x_k z_{k+1} - x_{k+1} z_k, \quad B_j = z_k - z_{k+1}, \quad C_j = x_{k+1} - x_k$$

$$\text{with } k = \text{mod}[(j+1)/3], \quad (\text{mod is operation to find remainder})$$

Note that if the restrictor area is small, the equation (A4.9a) can take the same form as that in the non-restrictor region, i.e. the equation (A4.8a).

If a point in the element is inside of the inlet restrictor region, the components read :

$$K_{ij}|_{\delta=1} = \frac{\partial f^0}{\partial p_i} A_d, \quad R_j = (f^0(p_i) - p_i \frac{\partial f^0}{\partial p_i}) A_d \quad (A4.10)$$

where

$$A_d : \text{restrictor area, } A_d = \pi d^2/4$$

Therefore, the unknowns can be found by solving the set of linear equations, because the matrix and the right-hand side vector are already expressed by the constants.

The FEM formulation for the dynamic equations can be derived by following the same procedures.

APPENDIX 5. ANALYSIS OF BALL-CONICAL SURFACE CONTACT

The most relevant characteristics of ball-conical surfaces (or other surfaces, e.g. spherical surface) are the stiffness in the contact region in form of line contact and the rotation about a very small angle for self-alignment.

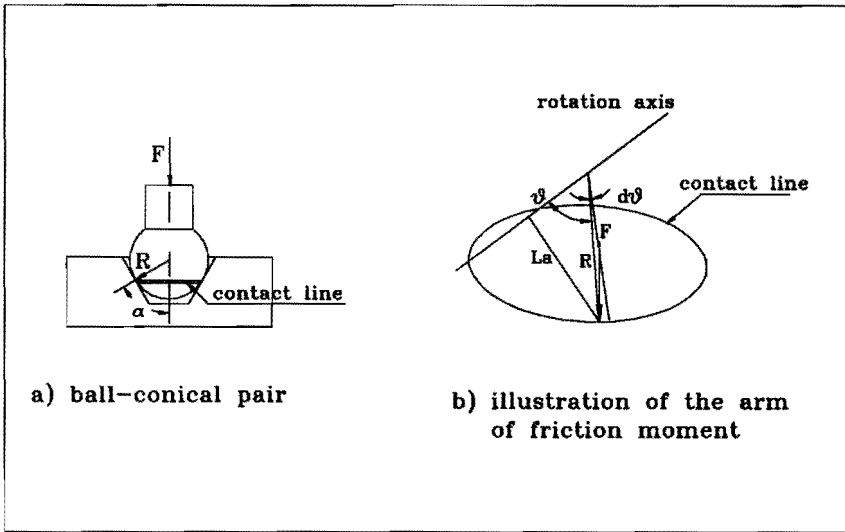


Fig. A5.1. Ball-conical surface contact and its line contact

As shown in Fig. A5.1a, in the ideal condition, the contact between these two surfaces can be considered as a line contact, as illustrated in hatching lines.

The stiffness (deformation) can be estimated by the formula used in the analysis of rolling bearings. One of them is that given by Palmgren [Palmgren, 1964], which reads :

$$\delta = \frac{2.45 F_n^{0.9}}{E_r^{0.9} L_{ef}^{0.8}} \quad (A5.1)$$

where F_n : force perpendicular to contact surface, $F_n = F \cos \alpha$
 L_{ef} : effective length, $2 \pi R \sin \alpha$
 R : ball radius, α : conical angle

E_r : the reduced modulus of elasticity of materials

$$\frac{1}{E_r} = \frac{1}{2} \left[\frac{1 - \nu_1^2}{E_1} + \frac{1 - \nu_2^2}{E_2} \right] \quad (\text{A5.2})$$

$$E_r = 2.29 \times 10^5 \text{ N/mm}^2 \text{ for steel-steel contact}$$

$$E_r = 1.36 \times 10^5 \text{ N/mm}^2 \text{ for steel-brass contact}$$

ν_i : the Poission ratio of material i

E_i : the elasticity modulus of material i

The deformation in the transverse direction has the following relation with the normal deformation, i.e. $\delta_t = \delta \cos \alpha$. Therefore, the deformation in the transverse direction can be written as follows :

$$\delta_t = \frac{0.62 F^{0.9} (\cos \alpha)^{1.9}}{E_r^{0.9} R^{0.8} (\sin \alpha)^{0.8}} \quad (\text{A5.3})$$

The contact stiffness in the transverse direction, K_c , can be expressed as :

$$K_c = dF/d\delta_t = 0.56 E_r^{0.9} R^{0.8} F^{0.1} (\sin \alpha)^{0.85} / (\cos \alpha)^{1.9} \quad (\text{A5.4})$$

From this relation, it is easy to find out that the optimal conical angle α is 30° . After introducing this optimal angle and the reduced elasticity, the contact stiffness can be written :

$$K_c = C_c R^{0.8} F^{0.1} \quad (\text{A5.5})$$

where $C_c = 0.56$ (0.33) for steel-steel (steel-brass)

For the general purpose, a plot of the contact stiffness change with the

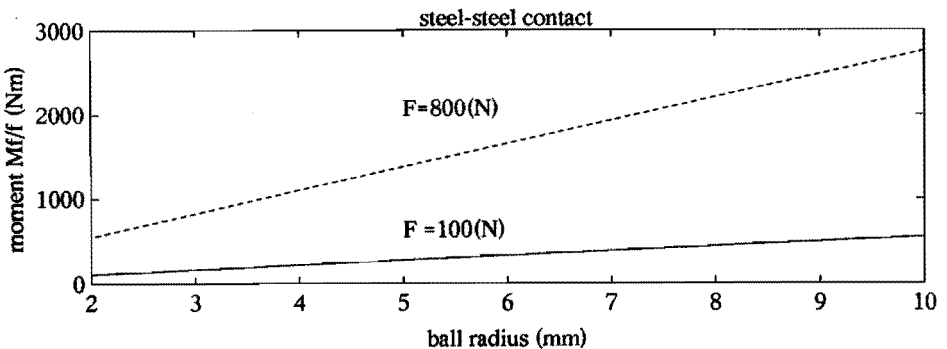


Fig. A5.2. The contact stiffness of ball-conical surface pair

ball radius and loading force is given in Fig. A5.2.

In concerning the self-alignment in ball-cone pairs, it is difficult to say what really happens in the contact. In an ideal condition of contact, one may say the self-alignment depends on the friction behavior at contact.

Due to close contact, the component of loading force in tangential direction is balanced by itself. The rotation axis of the friction moment is a line through the ball centre and parallel to the bearing surface, which implies that the local force on the circle will have different contribution to the total friction moment due to the difference in the arm length. At one point, the local friction force, if we do not consider the material hysteresis, can be expressed as :

$$dF_f = f F \cos \alpha / (2\pi R \sin \alpha) (R d\theta) \tag{A5.6}$$

and the distance of the local friction force to the rotation axis reads :

$$L_a = R \sin \theta \tag{A5.7}$$

Hence, the local friction moment reads :

$$dM_f = (f/2\pi) F R \cos \alpha \sin \theta d\theta \tag{A5.8}$$

and total friction moment becomes :

$$M_f = (2f/\pi) F R \cos \alpha \tag{A5.9}$$

For the general purpose, a plot of the ratio of friction moment over friction coefficient with the ball radius and loading force is given in Fig. A5.3.

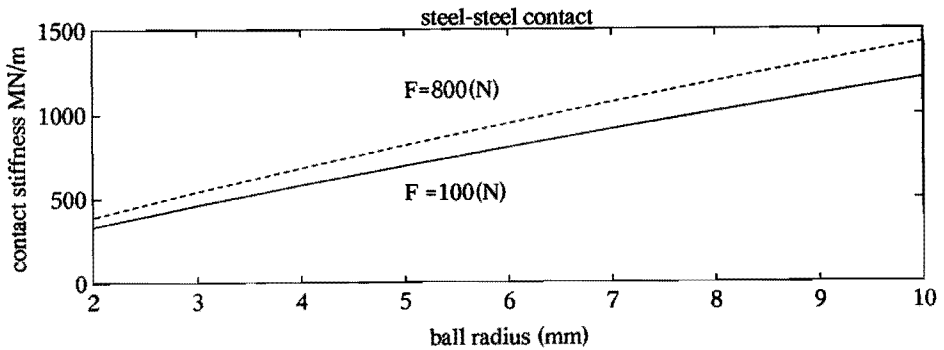


Fig. A5.3. The friction moment of ball-conical surface pair

APPENDIX 6. ANALYSIS OF A PAIR OF RIGID-FLEXIBLE MOUNTING

We concentrate on a pair of the pad connections: one side is rigidly mounted on the slide through the hinge and the other side through a kind of soft spring, which can be schematically shown in Fig. A6.1.

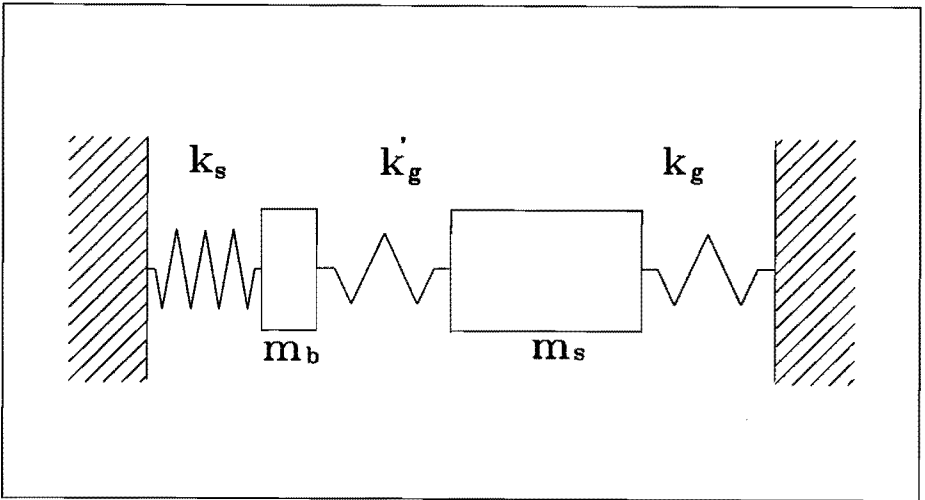


Fig. A6.1. Schematically illustration of a mounting pair

On the side with rigid mounting, the stiffness is equal to the gas film stiffness and on the side with the soft connection the stiffness is the result of two springs in series: gas film stiffness and soft spring stiffness.

$$\frac{1}{k_t} = \frac{1}{k_s} + \frac{1}{k'_g} \quad (\text{A6.1})$$

If the stiffness of the soft connection (k_s) is much lower than the stiffness (k'_g) of gas film of the pad mounting in the same side, the result stiffness will be approximately equal to the soft spring stiffness, $k_t \cong k_s$. In the situation from one equilibrium condition to another, the changes of forces in two sides must be equal. Hence, we have the following relation :

$$k_g \Delta h_w = k_s \Delta l \tag{A6.2}$$

or

$$\Delta h_w = (k_s/k_g) \Delta l \tag{A6.2a}$$

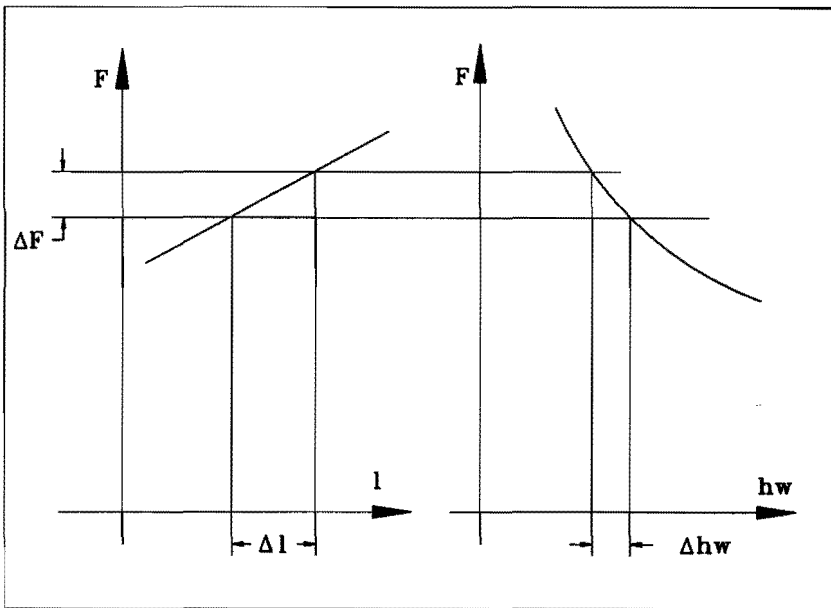
where k_g : the stiffness of the pad mounted in the opposite side of the soft connection

k_s : the stiffness of soft connection

Δh_w : the change of bearing gap height in the rigid connection

Δl : the displacement of the soft spring

From the equation (A6.2a), it can be easily seen that if the stiffness ratio (k_s/k_g) is very small the pad gap change will be very small, which can be illustrated by Fig. A6.2.



$$k_s = \Delta F/\Delta l$$

a) soft spring

$$k_g = \Delta F/\Delta h_w$$

b) gas film

Fig. A6.2. Illustration of the stiffness characteristics of the soft spring and gas film pair

APPENDIX 7.

THE EQUATIONS OF VIBRATION MOTION OF THE SLIDE

In order to present the general forms of the equation of vibration motion, we define the stiffness vector, k , damping vector, D and the bearing position vectors, a_x , a_y , a_z . In the damping factor model, the stiffness vector has the length of the numbers of bearing used in a gas bearing system. In the three element model, the length of the stiffness vector is doubled. If soft springs are introduced, the length of the stiffness vector is extended to the sum of the original length plus the number of the soft springs. However, the length of the damping vector is equal to the number of bearings in most cases in which no additional damping is introduced. For convenience, the orders of the stiffness and damping vectors follow the rule: the closer the stiffness component to the guide, the earlier the number. Therefore, the plate springs were numbered as 7 (6) to 10 (8) in the configuration I (II & III).

With those notations and referring to the coordinates defined in Fig. 5.6, the equations of vibration motion for the three element model read :

The motion in Y-direction :

$$ms \ddot{y} + Sk(3,10) y - Skz(3,10) \alpha + Skx(3,10) \gamma + SD(3,6) \dot{y} + SDz(3,6) \dot{\alpha} - SDx(3,6) \dot{\gamma} - \sum_{i=1}^4 [k(i+6) \xi_i + k(i+2) \zeta_i + d(i+2) \dot{\zeta}_i] = 0$$

The motion in Z-direction :

$$ms \ddot{z} + Sk(1,2) y + Skz(1,2) \alpha - Skx(1,2) \beta + SD(1,2) \dot{z} + SDz(1,2) \dot{\alpha} - Skx(1,2) \dot{\beta} - \sum_{i=1}^2 [k(i) \zeta_i + d(i) \dot{\zeta}_i] = 0$$

The rotation about X-axis :

$$Jx \ddot{\alpha} - Sky(1,2) z + Skz(3,10) y + [Skyy(1,2) + Skzz(3,10)] \alpha - Skxy(1,2) \dot{\alpha} - Skxz(3,10) \dot{\gamma} + SDy(1,2) \dot{z} - SDz(3,6) \dot{y} + - [SDyy(1,2) + SDzz(3,10)] \dot{\alpha} - SDxy(1,2) \dot{\beta} - SDxz(3,10) \dot{\gamma} - - \sum_{i=1}^4 [k(i+4) az(i+4) \xi_i + k(i+4) az(i+4) \zeta_i + d(i+2) az(i+2) \dot{\zeta}_i] + \sum_{i=1}^2 [k(i) ay(i) \zeta_i + d(i) ay(i) \dot{\zeta}_i] = 0$$

The rotation about Y-axis :

$$J_y \ddot{\beta} + S_{kx}(1,2) \dot{z} + S_{kxy}(1,2) \dot{\alpha} + S_{kxx}(1,2) \dot{\beta} - S_{Dx}(1,2) \dot{z} - S_{Dxy}(1,2) \dot{\alpha} - S_{Dxx}(3,10) \dot{\beta} - \sum_{i=1}^2 [k(i+2) \dot{\zeta}_i + d(i+2) \dot{\zeta}_i] = 0$$

The rotation about Z-axis :

$$J_z \ddot{\gamma} - S_{kx}(3,10) \dot{y} + S_{kxz}(3,10) \dot{\alpha} - S_{kxx}(3,10) \dot{\gamma} - S_{Dx}(3,6) \dot{y} - S_{Dxz}(3,10) \dot{\alpha} - S_{Dxx}(3,10) \dot{\gamma} - \sum_{i=1}^4 [k(i+6) \dot{ax}(i+6) \dot{\xi}_i + k(i+2) \dot{ax}(i+2) \dot{\zeta}_i + d(i+2) \dot{ax}(i+2) \dot{\zeta}_i] = 0$$

The motion of plate springs, $j = 1, 4(3), i = 7(6), 10(8)$, for configuration I (II & III) :

$$m_b \ddot{\xi}_j - k(i) \dot{y} + k(i) \dot{az}(i) \dot{\alpha} + k(i) \dot{ax}(i) \dot{\gamma} + [k(i) + k(i+4)] \dot{\xi}_j - k(i) \dot{\zeta}_i + d(i) \dot{\xi}_j - d(i) \dot{\zeta}_i = 0$$

The motion of two top bearings, $i = 1, 2$:

$$-k(i) \dot{z} + k(i) \dot{ay}(i) \dot{\alpha} - k(i) \dot{ax}(i) \dot{\beta} + [k(i) + k(i+14)] \dot{\zeta}_i - d(i) \dot{z} + d(i) \dot{ay}(i) \dot{\alpha} - d(i) \dot{ax}(i) \dot{\beta} + d(i) \dot{\zeta}_i = 0$$

The motion of side bearings, $i = 3, 6 (5)$, for configuration I (II & III) :

$$-k(i) \dot{y} - k(i) \dot{az}(i) \dot{\alpha} + k(i) \dot{ax}(i) \dot{\gamma} + [k(i) + k(i+14)] \dot{\zeta}_i - d(i) \dot{y} - d(i) \dot{az}(i) \dot{\alpha} + d(i) \dot{ax}(i) \dot{\gamma} + d(i) \dot{\zeta}_i = 0$$

The motion of bearings connected to plate springs, $i = 7(6), 10(8), j = 1, 4 (3)$ for configuration I (II & III) :

$$-k(i) \dot{\xi}_j + [k(i+4) + k(i+14)] \dot{\zeta}_i - d(i+4) \dot{\zeta}_i + d(i+4) \dot{\xi}_i = 0$$

The equations of vibration motion for the complex stiffness model read :

The motion in Y-direction :

$$m_s \ddot{y} + S_k(3,10) \dot{y} + S_{kz}(3,10) \dot{\alpha} - S_{kx}(3,10) \dot{\gamma} + j [S_{D}(3,6) \dot{y} + S_{Dz}(3,6) \dot{\alpha} - S_{Dx}(3,6) \dot{\gamma}] - \sum_{i=1}^4 k(i+6) \dot{\xi}_i = 0$$

The motion in Z-direction :

$$m_s \ddot{z} + S_k(1,2) y + S_{kz}(1,2) \alpha - S_{kx}(1,2) \beta + j [SD(1,2) z + SD_z(1,2) \alpha - S_{kx}(1,2) \beta] = 0$$

The rotation about X-axis :

$$J_x \ddot{\alpha} - S_{ky}(1,2) z + S_{kz}(3,10) y + [S_{ky}(1,2) + S_{kzz}(3,10)] \alpha - S_{kxy}(1,2) \beta - S_{kxz}(3,10) \gamma + j \{SD_y(1,2) z - SD_z(3,6) y + [SD_{yy}(1,2) + SD_{zz}(3,10)] \alpha - SD_{xy}(1,2) \beta - SD_{xz}(3,10) \gamma\} - \sum_{i=1}^4 k(i+4) a_z(i+4) \xi_i = 0$$

The rotation about Y- axis :

$$J_y \ddot{\beta} + S_{kx}(1,2) z + S_{kxy}(1,2) \alpha + S_{kxx}(1,2) \beta - j[SD_x(1,2) z + SD_{xy}(1,2) \alpha + SD_{xx}(3,10) \beta] = 0$$

The rotation about Z-axis :

$$J_z \ddot{\gamma} - S_{kx}(3,10) y + S_{kxz}(3,10) \alpha - S_{kxx}(3,10) \gamma - j[SD_x(3,6) y + SD_{xz}(3,10) \alpha - SD_{xx}(3,10) \gamma] - \sum_{i=1}^4 k_1(i+6) a_x(i+6) \xi_i = 0$$

The motion of plate springs, $i = 1, 4$ (3) for configuration I (ii & III) :

$$m_b \ddot{\xi}_i - k(i+6) y + k(i+6) a_z(i) \alpha + k(i+6) a_x(i) \gamma + [k(i+6) + k(i+10)] \xi_i + j d(i+10) \xi_i = 0$$

where

$$S_{mn}(i,j) : \sum_{k=i}^j m(k), \quad S_{mn}(i,j) : \sum_{k=i}^j m(k) a_n(k),$$

$$S_{mnl}(i,j) : \sum_{k=i}^j m(k) a_n(k) a_l(k)$$

$n=x, y, z; m = k, d$

k, d : stiffness and damping vectors

$x, y, z, \alpha, \beta, \gamma$: coordinates for movable frame

ξ_i : coordinates for plate springs

ζ_i : coordinates for bearing zero mass elements

m_s : mass of moving part of the slide

m_b : mass of bearing attaching to the soft spring

According to these equations, one can easily build the detailed matrices for a specific configuration and the selected model.

APPENDIX 8.
TEST RESULTS OF VIBRATION OF THE SLIDE

Fig. A8.1 shows the test results at the reference point to determine the vibration modes in the Z-axis and in the rotations about X- and Y-axes. The vertical axis in the figures is the response of magnitude. The slide was excited with the exciter and the response was measured with an accelerometer. Two natural frequencies with relative high value can be clearly identified, i.e. 50 Hz and 350 Hz. The natural frequencies of slide are located between these two frequencies. Therefore, they present no trouble on the identification of the slide's natural frequencies.

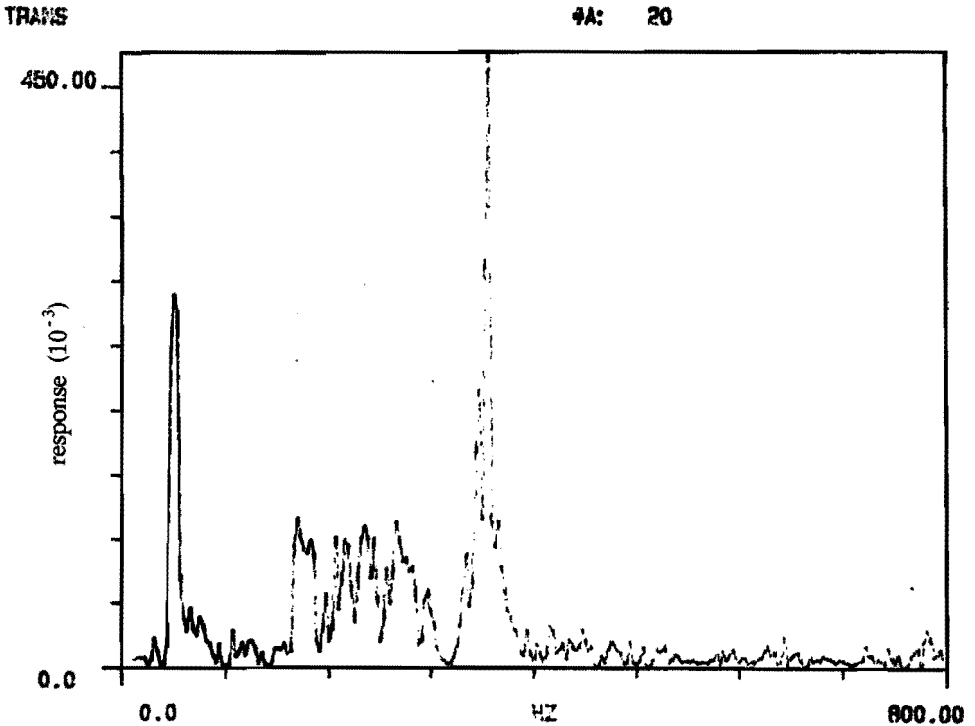


Fig. A8.1. The test result at the reference point on the granite

Fig. A8.2 shows a test result for determining the vibration modes in the

Y-direction. The slide was excited with the hammer and the response was measured with an accelerometer. From the figure, it can be seen that the natural frequency can be readily determined. Two relative low peaks are the vibration of basis and the third one is the rotation about X-axis.

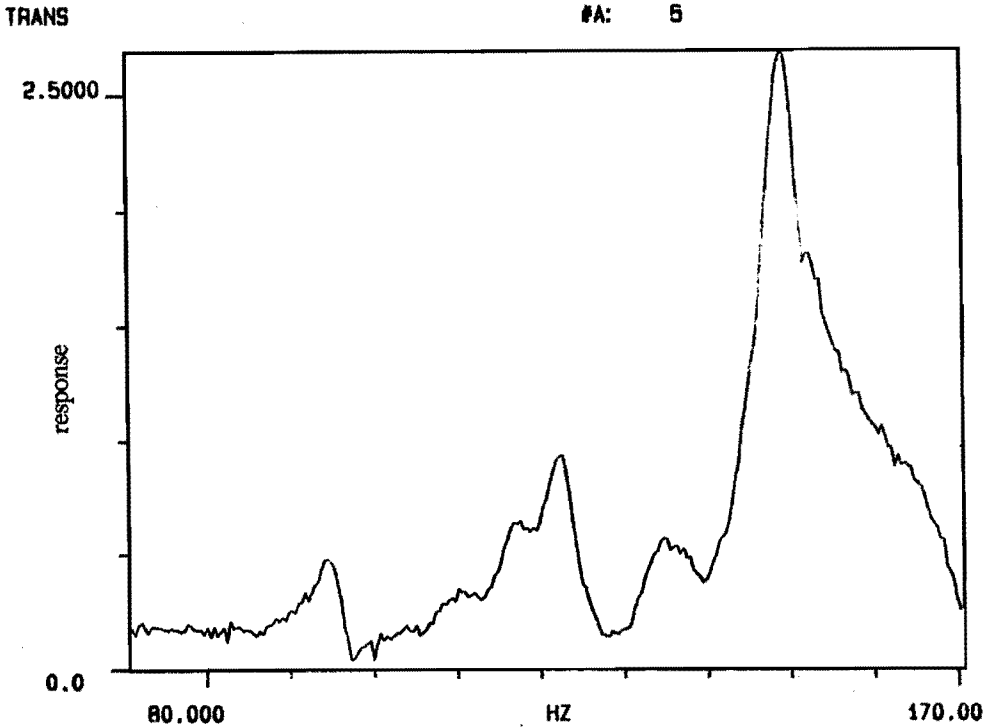


Fig. A8.2. A test result to determine the natural frequencies in Y-direction

Fig. A8.3 shows the test results on checking the rigid body assumption of the frame. The slide was excited with the hammer and the response was measured with an accelerometer. The top figure is the response when the slide was excited on the right-hand side of the slide and the bottom figure is the result excited on the left-hand side of the slide. From Fig. A8.3, it can be seen that two figures have the exact same number of peaks and first one with

the same magnitude. It can be concluded that the slide can be considered as a rigid body. For the additional information, the coherence function of the test results is shown in Fig. A8.4.

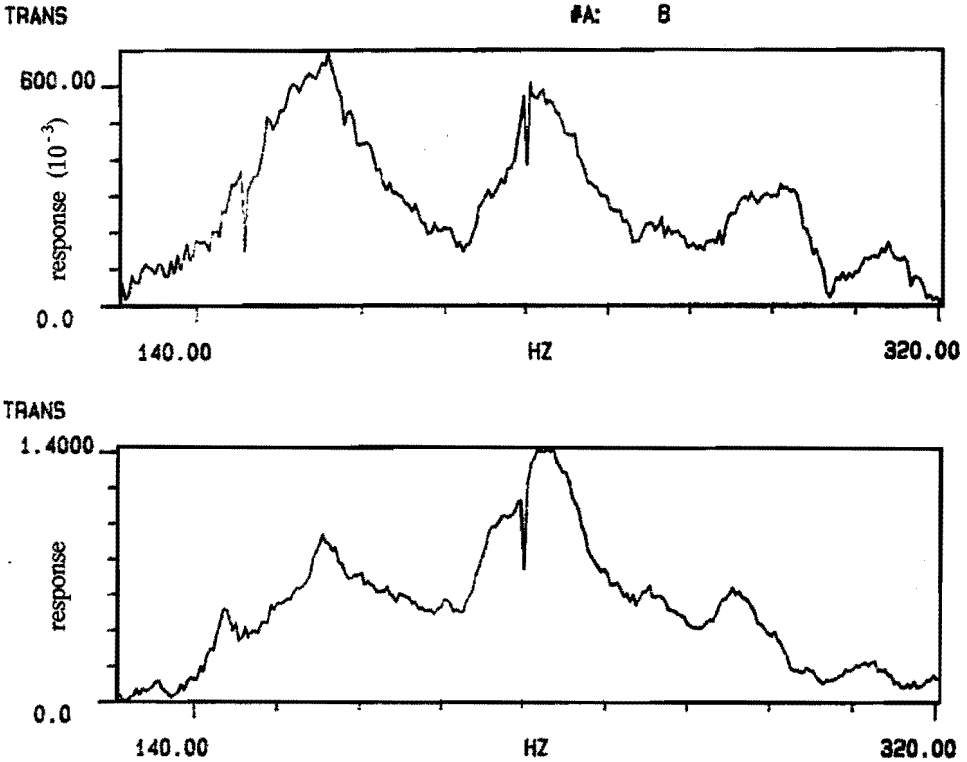


Fig. A8.3. Test results on slide in the different position

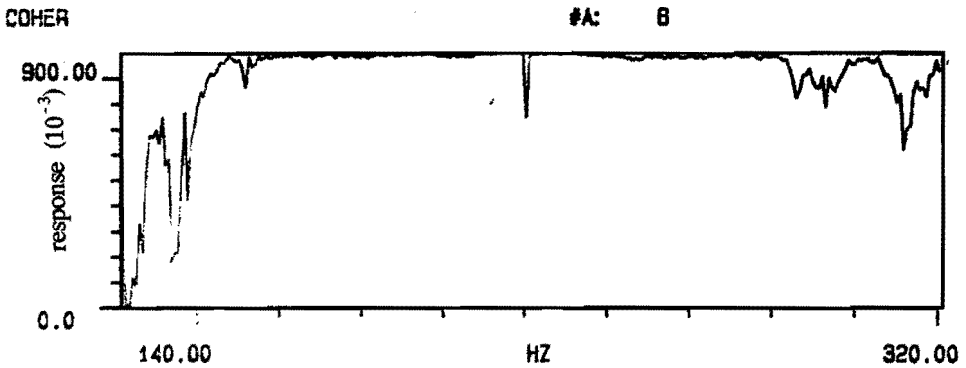


Fig. A8.4. The measured coherence of the test results shown in Fig. A8.3

REFERENCES

1828

- * Willis, R. B. A. "On the pressure produced on a flat plate when opposed to a stream of air issuing from an orifice in a plane surface", Trans. of Camb. Phi. Soc., Vol. 3, no. 1, pp 129 - 141

1854

- * Hirn, G. A. "Sur les principaux phenomenes qui presentent les frottement mediats", Bull. Soc. Ind. Mulhouse, Vol. 26, no. 129

1886

- * Reynolds, O. "On the theory of lubrication and its application to Mr. Beauchamp Tower's experiments, including an experimental determination of the viscosity of olive oil", Phil. Trans. R. Soc. A., Vol. 177

1892

- * Wood, W. H. "Counter balance for journals", U. S. A. Patent 46664531

1949

- * Cope, F. "The hydrodynamic theory of film lubrication", Pro. Roy. Soc. A, Vol. 197, pp 201 - 217

1959

- * Fuller, D. D. editor, 1st International Symposium on Gas-lubricated Bearings, Washington D.C., USA
- * Rothe, H. C. "Air bearings for guidance components of ballistic missiles and their production aspects", Paper in 1st International Symposium on Gas-lubricated Bearings, Washington D.C., USA

1962

- * Dowson, D. "A generalized Reynolds equation for fluid film lubrication", Int. J. Mech. Sci., Vol. 4, pp 159 - 170

1963

- * Kao, H. C. "A theory of self-acting gas lubricated bearings with heat transfer through surface", J. of Basic Eng., pp 324 - 326

1967

- * Wilcock, D. F. "Externally pressurized bearings as servomechanism I — The simple thrust bearing", J. of Lub. Tech., pp 418 - 424

1968

- * Castelli, V., and J. Pirvics "Review of numerical method in gas bearing film analysis", J. Lub. Tech., pp 777 - 792

1969

- * Constantinescu, V. N. "Gas Lubrication", Published by ASME
- * McCabe, J. T., Elord, H. G., Carfago, S. and R. Colsher "Summary of investigations of entrance effects of circular thrust bearings", Paper 17, 5th Gas Bearing Symposium, Southampton, UK
- * Jona, M. G. "Non-linear effects and pneumatic hammer in a recessed thrust bearing", 5th Gas Bearing Symposium, Southampton, UK
- * Vorh, J. H. "A study of inherent restrictor characteristics for hydrostatic gas bearings", Paper 30, 5th Gas Bearing Symposium

1971

- * Stowell, T. B. "Application of control theory to pneumatic hammer in externally pressurized gas-lubricated thrust collar bearings", Paper 2, 6th Gas Bearing Symposium, Southampton, UK

1972

- * Sparrow, E. M., Beavers, G. S. and I. T. Hwang "Effect of velocity slip on porous-walled squeeze films", J. of Lubr. Tech.

1975

- * Stiffler, A. K. and D. M. Smith "Dynamic characteristic of an inherently compensated, square, gas film bearing", J. of Lub. Tech., pp 52 - 62

1976

- * Bennett, J., Hudson, B. G. and H. Marsh "The flow characteristics of small orifices used in externally pressurized gas bearings", Paper E3, 7th Gas Bearing Symposium, Southampton, UK
- * Blondeel, E., Snoeys, R. and L. Devrieze "Externally pressurized bearings with variable gap geometries", Paper E2, the same as above
- * Haycock, R. "Static and dynamic characteristics of a precision gas-lubricated interferometer slide", Paper C1, the same as above

1978

- * Zhang, Z. Y. and B. S. Shi "Refrigeration and low temperature technology", (text book in Chinese), Published by the Machinery Press
- * Kanai, A. and M. Miyashita "Nanometer positioning characteristics of closed looped differential hydro- or aerostatic actuator", Annual of CIRP

1980

- * Blondeel, E., Snoeys, R. and L. Devrieze "Dynamic stability of externally pressurized gas bearings", J. Lub. Tech., Vol. 102, pp 511 - 519

- * Gross, W.A., Matsch, V., Castelli, V., Eshel, A., Vohr, J. H. and M. Wildmann "Fluid Film Lubrication", A Wiley International Publication
- * Pan, C. H. T. "Gas Bearings", Chapter 4. of <<Tribology, Friction, Lubrication and Wear>>, edited by Szeri, A. Z.

1981

- * Mori, A. and H. Mori "Modified Reynolds equation and boundary conditions for analysis of dynamic properties of externally pressurized gas bearings", Paper 16, Gas Bearing Symposium, Lanchiester, U.K.

1982

- * Yahya, S. M. "Fundamentals of compressible flow", Wiley Eastern Limited

1983

- * Li, Y. D. and J. M. Wang "Experimental studies of double semi-spherical aerostatic spindles", (in Chinese), Paper for Second National Conference on Gas Bearing Technology, Changchun, China
- * Liu, D., Liu, Y. H. and X. W. Shi "The finite element methods for externally pressurized gas bearings", (in Chinese), Internal Report, no. 155, Harbin University of Technology, China
- * Wen, Z. Z., Lin, J. and X. C. Qiao "An improvement of the Powell method for design of aerostatic bearings with orifice restrictors", (in Chinese) Internal Report, Xi'an JiaoTong University, China

1984

- * Patir, N. and H. S. Cheng "An average flow flow model for determining the effect of three dimensional isotropic on partial hydrodynamic lubricating films", J. Lubr. Tech., Vol. 100
- * Tønder, K. "A numerical assessment of the effect of striated roughness on gas lubrication", J. of Tribology, Vol. 106, pp 315 - 321

1985

- * Pande, S. S. "Analysis of tapered land aerostatic thrust bearings under conditions of tilt and rotation", Wear, Vol. 104, pp 297 - 308
- * Plessers, P. "Dynamic instability of aerostatic bearings in mechanical systems", Ph. D. Thesis, Catholic University, Leuven, Belgium
- * Roblee, J. W. "Design of externally pressurized gas bearings for dynamic applications", Ph. D. Thesis, California University, USA

1986

- * Cuvlier, C., Segal, A. and A. A. van Steenhoven "Finite Element Method and Nernier-Stocks Equation"

- * Holster, P. L. and J. A. H. Jacobs "Theoretical analysis and experimental verification of the static properties of externally pressurized air-bearing pads with load compensation", 9th Gas Bearing Symposium, USA
- * Roblee, J. W. and C. D. Mote jr. "Vibration damping in externally pressurized gas bearings" Paper for International Conference on Vibration Problem in Engineering, June, 17-20, Xi'an China
- * Shimokohbe, A., Aoyama, H. and I. Watanabe "A high precision straight-motion system", Precision Engineering, Vol. 8, no. 3

1987

- * Fukui, S. and R. Kaneko "Experimental Investigation of Externally Pressurized Gas Bearings Under High Knudsen Number Conditions", ASME Paper 87-trib-15
- * Gans, R. F. "On random Reynolds roughness", J. of Tribology, Vol. 109
- * Kakaç, S., Shah, R. K. and W. Aung "Handbook of single-phase convective heat transfer", John Wiley and Sons, Inc.
- * Li, W. and C. H. T. Pan "A new numerical technique for the analysis of lubrication films", IMechE Paper C225/87
- * Liu, D., Liu, Y.H., Shi, X. W. and J. Y. Li "The finite element and boundary element methods in gas lubrication", IMechE Paper, C240/87
- * Wang, J. M. "On the principle and possible methods to improve aerostatic bearing stiffness", Master Thesis, Eindhoven University of Technology (TUE), The Netherlands

1988

- * Arakere, N. and H. D. Nelson "An interior collection method for static and dynamic analysis of finite length gas journal bearings", J. Tribology, Vol. 110, pp 456 - 461
- * Kato T. and Y. Hori "A fast method for calculating dynamic coefficient of finite width journal bearings with quasi Reynolds boundary condition", J. Tribology, Vol. 110, pp 387 - 393
- * Majumder, M. C. "Study of the pneumatic instability of externally pressurized gas thrust bearings with slip velocity", Wear, Vol. 124
- * Plessers, P. and R. Snoeys "Dynamic stability of mechanical structure containing externally pressurized gas-Lubricated thrust bearings", J. of Trib., Vol. 110, pp271 - 278
- * Wang, J. M., Kodde, L. and M. J. W. Schouten "Approach to the high stiff and stable aerostatic bearings", Proceedings of Conference on High Speed

Technology, Lappeeranda, Finland

1989

- * Mitsuya, Y., Ohkubo, T. and H. Ota "Averaged Reynolds Equation extended to gas lubrication possessing surface roughness in the slip flow regime: approximation method and confirmation experiments", J. of Trib., Vol. 111
- * Newland, D. E. "Mechanical vibration Analysis and computation", Longman Scientific & Technical
- * Raad, P. E. and J. E. White "Entrance and stationary roughness effect on the load carrying capacity of a wide wedge gas bearing", J. of Trib., Vol. 111, pp 41 - 48
- * Teeuwesen, J. W. M. C. "Performance evaluation and a quality control system for three coordinate measuring machines", Ph. D. Thesis, TUE

1990

- * Faires, V. M. and C. M. Simmang "Thermodynamics", Sixth Edition, Collier Macmillan International Editions
- * Lin, J. F., Jou, J. C. and G. S. Lu "Two-dimensional flows in gas hydrostatic bearings in thin films of variable thickness analyzed by finite element method", Tribology Int., Vol. 23, no. 5, pp 351 - 360
- * Scharrer, J. K. and I. Hibbs Jr. "Flow coefficient for the orifice of a hydrostatic bearing", Trib. Trans., Vol. 33, pp 543 - 550
- * Teague, C. and C. Evens "Patterns for precision instrument/machine design (mechanical aspects)", Tutorial in ASPE Annual Meeting
- * Wang, J. M. "Design of externally pressurized gas bearings: Theory and Practice", Internal Report, no. WPA 0921, TUE
- * Wang, J. M. and P. H. J. Schellekens, (a) "Dynamic natural frequency and stability of bearing systems", Presented in the 45th STLE Annual Meeting, Dever, Colorado, USA
- * Wang, J. M. and P. H. J. Schellekens, (b) "Stiffness characteristics of externally pressurized gas bearings", Proceeding of 6th ASPE Annual Meeting, Rochester, New York, USA

1991

- * Holster, P. L., Jacobs J. A. H. and J. Roblee "The measurement and finite element analysis of the dynamic stiffness of nonuniform clearance, gas thrust bearings", J. of Trib., Vol. 113, pp 768-776
- * Hageaves, D. J. "Surface waviness effects on the load-carrying capacity of rectangular hydrostatic pads", Wear, Vol. 145, pp 137 - 151

- * Snip, J. G. "Development of experimental set-up for testing static and dynamic properties of aerostatic bearing pads", (in Dutch), Internal Report, no. WPA 1090, TUE
- * Wang, J. M. and P. H. J. Schellekens "Design of high performance externally pressurized gas bearings", Progress in Precision Engineering, Proceeding of IPES6/UME2, Braunschweig, Germany
- * Yang, J. H. "Modeling of dynamic performance of linear guide with externally pressurized gas bearings", Internal Report, no. WPA 1152, TUE

1992

- * Dricssen, E. G. M. "The modeling and design of air bearing guide for precision applications", (in Dutch), Master Thesis, TUE
- * Soons, J. A., Theuws, F. C. and P. H. J. Schellekens "Modeling the errors of multi-axis machines: a general methodology", Precision Engineering, Vol. 14, no.1
- * Wang, J. M. and P. H. J. "Tri-conical gap shaped externally pressurized gas bearing", to be published in Trans. STLE

SUMMARY

Externally pressurized gas (EPG) bearings are widely used in precision machines. However, in practice, a lot of problems regarding both industrial applications and scientific research have not been fully solved, some of them are even little understood. The motivation and aim of the research are to try to solve some of the problems. Based on providing up-to-date knowledge and efficient tools, especially for precision applications. The research shows that the developed software and experimental system can be effectively used in the design, study and testing of both individual EPG bearings and EPG bearing systems.

In the beginning of this thesis, the basic concepts of gas bearings are presented as the general introduction. These concepts include the working principle, short history, properties and the definition of the current research. The main body of the thesis consists of two parts: Part one presents the design methods of single pads, as well as the numerical and experimental research on some special aspects, including the effects of pad body tilt, surface imperfections, motion velocity and temperature drop. Part two describes the principles in the design of more accurate systems with EPG pads, as well as simulation and experiments on linear motion systems.

Part one presents the theoretical basis and the results of numerical simulation and experimental verification of single EPG bearings, including descriptions of effects of bearing body tilt, surface imperfection, temperature drop in the downstream restrictor and the refinement of the restrictor region in bearings. Based on the theoretical basis the design software was developed with solving two dimensional solutions of the time-dependent Reynolds equation. The detailed studies include optimizations of bearing gap shape, effects of bearing body tilt, surface imperfections, motion velocity and temperature drop. The tri-conical gap shaped pads are superior to the parallel and bi-conical gap shaped pads in all aspects: high load capacity, high stiffness, wide stability region, less sensitive to tilt, surface imperfection and motion velocity, and low temperature drop.

Part two discusses the conceptual arguments and the models to design EPG bearing systems. At first, the design principles such as loop stiffness, symmetry, kinematic mounting and driving and preloading are discussed in detail. Two models were developed to describe the gas film stiffness for modeling the dynamic behavior of a gas bearing system. The solution methods and techniques to use the models were also discussed in this chapter. Thereafter, it presents the detailed study on a large linear guide with a comparable size to a guide used in CMMs, particularly dealing with the constructional details in the design of linear guides and the determinations of the natural frequencies of the gas bearing systems. In this chapter, the comparisons of the experiments and the model predictions were presented in three different configurations of the same linear guide. All the experimental results are well correlated to the model predictions.

SAMENVATTING

Uitwendig van druk voorziene gaslagers, doorgaans aangeduid als luchtlagers, worden momenteel veelvuldig toegepast in precisiemachines. In de praktijk echter zijn vele problemen met betrekking tot de industriële toepassing van en het wetenschappelijk onderzoek naar luchtlagers nog niet volledig opgelost. Over enkele aspecten is er zelfs nauwelijks kennis aanwezig. De motivatie en het doel van dit onderzoek zijn daarom gericht op het oplossen van deze problemen door het verkrijgen van meer inzicht in en het ontwikkelen van efficiëntere gereedschappen voor luchtlagers met name voor precisie toepassingen. Het onderzoek heeft o.a. geleid tot de ontwikkeling van een softwarepakket en een experimentele opstelling waarmee op effectieve wijze zowel individuele luchtlagers als luchtlagersystemen bestudeerd, ontworpen en getest kunnen worden.

In de algemene inleiding van dit proefschrift worden allereerst de basisaspecten van luchtlagers gepresenteerd. Deze aspecten hebben betrekking op het werkingsprincipe, een kort historisch overzicht, luchtlagereigenschappen en de definiëring van het huidige onderzoek. Het hoofdgedeelte van dit proefschrift bestaat uit twee gedeelten: het eerste gedeelte behandelt ontwerp methodieken voor individuele luchtlagers alsmede het numeriek en experimenteel onderzoek naar enkele specifieke aspecten, zoals de invloed van lagerkantelingen, oppervlakte-onnauwkeurigheden, snelheid en temperatuurdalingen. Deel twee beschrijft de ontwerpprincipes voor meer nauwkeurige systemen met luchtlagers en de simulatie en experimenten m.b.t. lineair bewegende systemen.

Deel een geeft de theoretische basis en de resultaten van numerieke simulatie en experimentele verificatie van individuele luchtlagers, inclusief de beschrijving van de invloed van lagerkanteling, oppervlakte-onnauwkeurigheid, temperatuursdaling in de "downstream" restrictie en de verbetering in het restrictie gebied van luchtlagers. Op basis van de theoretische kennis is een softwarepakket ontwikkeld voor het geven van een 2-dimensionale oplossing voor de tijdsafhankelijke Reynolds-vergelijking.

De gedetailleerde studies bevatten o.a. de optimalisatie van de luchtlagerspleet, de invloed van lagerkanteling, oppervlakte onnauwkeurigheid, temperatuurdaling en snelheid. Luchtlagers met een "triconical" lagerspleet blijken in vergelijking tot

luchtlagers met parallelle en "bi-conical" lagerspleten over veel betere eigenschappen te beschikken en wel wat betreft alle aspecten: hoge belastbaarheid, hoge stijfheid, stabiliteit over een groot gebied, minder gevoelig voor kanteling, oppervlakte-onnauwkeurigheden, snelheid en temperatuursdalingen.

Deel twee behandelt de ontwerpregels en de modellen voor het ontwerp van luchtlagersystemen. In de eerste plaats komen ontwerpprincipes met betrekking tot de stijfheid, symetrie, kinematische ophanging, de aandrijving en de voorspanning in detail aan de orde. Twee modellen zijn ontwikkeld voor de beschrijving van de stijfheid van het luchtlager ten behoeve van de modellering van het dynamisch gedrag van luchtlagersystemen. De oplossingsmethodieken en technieken voor deze modellen komen eveneens aan de orde in dit hoofdstuk. Vervolgens wordt een gedetailleerde studie van een grote lineaire geleiding gepresenteerd; welke met name gericht is op de constructieve details in het ontwerp van lineaire geleidingen en op de bepaling van de eigen frequenties van luchtlagersystemen. De betreffende geleiding is wat afmeting betreft, vergelijkbaar met geleidingen welke in coördinaten meetmachines gebruikt worden. In dit hoofdstuk is hierbij een vergelijking gemaakt tussen het experimenteel bepaald gedrag en de door het model voorspelde gedrag van de geleiding en wel voor drie verschillende configuraties van dezelfde geleiding. Alle experimenteel bepaalde gegevens komen goed overeen met de voorspellingen aan de hand van het model.

CURRICULUM VITAE

PERSONAL

Name: Junming, WANG
Born: April 21, 1960 in Acheng, Heilongjiang, China

EMPLOYMENT

4/1990 - 11/1992 BOTECH, Boogers Technology in Precision Instrument and Metrology Systems, Helmond, The Netherlands
3/1988 - 3/1990 IVO, Eindhoven University of Technology, Eindhoven The Netherlands
10/1988- 12/1988 Eindhoven University of Technology, Eindhoven
8/1982 - 10/1986 Research Institute of Optics and Electronics
Chinese Academy of Science, Chengdu, China

EDUCATION

3/1988 - 11/1992 **Ph. D.** in the Section for Precision Engineering
Department of Production Technology & Automation
Faculty of Mechanical Engineering
Eindhoven University of Technology
3/1988 - 3/1990 **Further Education** under Subject of the Computer Aided
(Simultaneously) Design and Manufacturing for Discrete Products
IVO, Eindhoven University of Technology
6/1987 - 1/1988 **ir. (M.Sc.)** in the Section of Power Transmission and
Tribology, Department of Design Engineering
Faculty of Mechanical Engineering
Eindhoven University of Technology
10/1978- 7/1982 **B.S.** in Section of Precision Production Technology
and Manufacturing Process, Mechanical Department I
Harbin University of Science and Technology
Harbin, China

ACTIVITY

Session Chairman in the Session of Gas and Magnetic Bearings
International Conference in High Speed Technology
Finland (1988)

Member of American Society for Precision Engineering (ASPE)

Member of Society of Tribologist and Lubrication Engineers (STLE)

Member of KIVI (Koninklijk Instituut van Ingenieurs)

STATEMENTS

DESIGN OF GAS BEARING SYSTEMS FOR PRECISION APPLICATIONS

J. M. WANG

I

With the ever increasing demands on machine accuracy, also systems using gas bearings have to provide better performance. This can only be achieved by paying more attention to the practical details and the development of efficient tools to design gas bearing systems.

— this thesis

II

In the design of a closed-loop controlled gas bearing system, the ideal position for mounting the actuator is at the joint between the bearing pad and the structure.

— this thesis

III

High film stiffness of a gas bearing is easily lost by a poor design of the joint, which unfortunately occurs in many applications, even in commercial products.

— this thesis

IV

The use of the concept of error correction in machine tools is a fundamental step towards higher precision in production.

— J. A. Soons, F. C. Theuws and P. H. J. Schellekens

<<Precision Engineering>> Vol. 14. No.1 1992

V

A building has to be as comfortable as our skin; it lives, it breathes, it surrounds us without oppressing us. A building has to be as healthy as we want our body to be.

— Ton Alberts <<Healthy Buildings>>
© Longman Group UK Limited 1992

VI

A better strategy to solve the deadlock problem in computer operating systems can only be derived from a fuller understanding of the deadlock problem itself. This also holds true for the problem solving in human activities, as stated in the book <<The Ideal Problem Solver>>, by J.D. Bransford and B. S. Stein.

VII

As the new millennium approaches, the crucial need of the human race is to find a unifying vision of the nature of man and society.

— << Bahá'u'lláh >> Bahá'í International Community,
Office of Public Information, New York, 1991

VIII

What exists serves for possession. What does not exist serves for effectiveness.

— <<Tao De Jing>>

IX

Symmetry is not only a form of natural beauty, but also a fundamental rule to avoid mistakes, e.g. in the design of precision machines.

Eindhoven, 10th October 1992